SYNTHESIS OF OXIDE BASED SYSTEMS: SEARCH FOR NOVEL OPTICAL MATERIALS FOR RADIATION DOSIMETRY

By

SANU S. RAJ

(CHEM01200904003)

BHABHA ATOMIC RESEARCH CENTRE, MUMBAI

A thesis submitted to the

Board of Studies in Chemical Sciences

In partial fulfillment of requirements

For the Degree of

DOCTOR OF PHILOSOPHY

of

HOMI BHABHA NATIONAL INSTITUTE

AUGUST 2016

Homi Bhabha National Institute[1]

Recommendations of the Viva Voce Committee

As members of the Viva Voce Committee, we certify that we have read the dissertation prepared by **Smt. Sanu. S. Raj** entitled **"Synthesis of oxide based systems: Search for novel optical materials for radiation dosimetry"** and recommend that it may be accepted as fulfilling the thesis requirement for the award of Degree of Doctor of Philosophy.

D Das. 19.01.2017
Chairman : **Dr. D. Das** **Date:**

19.01.2017
Guide / Convener: **Dr. A. K. Tyagi** **Date:**

Co-guide - (if any) **Date:**

19/1/17
Examiner : **Prof. Amreesh Chandra** **Date:**

19/1/2017
Member : **Dr. M. S. Kulkarni** **Date:**

Sudarsan. V 19/1/2017
Member : **Dr. V. Sudarsan** **Date:**

19-01-2017
Member : **Dr. Vinita G. Gupta** **Date:**

Final approval and acceptance of this thesis is contingent upon the candidate's submission of the final copies of the thesis to HBNI.

I/We hereby certify that I/we have read this thesis prepared under my/our direction and recommend that it may be accepted as fulfilling the thesis requirement.

Date: 19.01.2017

Place: BARC

(Signature)

Guide

---

[1] This page is to be included only for final submission after successful completion of viva voce.

STATEMENT BY AUTHOR

This dissertation has been submitted in partial fulfilment of requirements for an advanced degree at Homi Bhabha National Institute (HBNI) and is deposited in the Library to be made available to borrowers under rules of the HBNI.

Brief quotations from this dissertation are allowable without special permission, provided that accurate acknowledgement of source is made. Requests for permission for extended quotation from or reproduction of this manuscript in whole or in part may be granted by the Competent Authority of HBNI when in his or her judgment the proposed use of the materialis in the interests of scholarship. In all other instances, however, permission must be obtained from the author.

(Sanu S. Raj)

DECLARATION

I, hereby declare that the investigations presented in the thesis have been carried out by me. The work is original and has not been submitted earlier as a whole or in part for a degree / diploma at this or any other Institution / University.

(Sanu S. Raj)

List of Publications arising from the thesis

Journals

1. $MgAl_2O_4$ spinel: Synthesis, carbon incorporation and defect-induced luminescence, **Sanu S. Raj**, S. K. Gupta, V. Grover, K. P. Muthe, V. Natarajan, A. K. Tyagi, *J. Mol. Struc.,* **2015**, *1089*, 81-85.
2. TL and OSL studies of carbon doped magnesium aluminate ($MgAl_2O_4$:C), **Sanu S. Raj**, D. R. Mishra, A. Soni, V. Grover, G. S. Polymeris, K. P. Muthe, S. K. Jha, A. K. Tyagi. *J. Radi. Phys. Chem.,* **2016**, *127*, 78-84.
3. Origin of visible photoluminescence in combustion synthesized α-Al_2O_3: Effect of thermal treatment, **Sanu S. Raj**, S. K. Gupta, N. Pathak, V. Grover, A. K. Tyagi, *J. Adv.Powder Tecnol.* (minor revision submitted).

Conference proceedings

1. Nature of multiple TL defects in ($MgAl_2O_4$:C) spinel; **Sanu S. Raj**, D. R. Mishra, A. Soni, N. S. Rawat, K. P. Muthe, S. K. Gupta, M. S. Kulkarni, V. Grover and A. K. Tyagi. Proceedings of the International Conference on Luminescence and its Applications (ICLA- 2012) 7-10th Feb, 2012, Hydrabad, India.
2. Nonlinear-OSL phenomenon defects having closely spaced photoinsation cross-sections in $MgAl_2O_4$:C spinel : D. R. Mishra, **Sanu S. Raj**, A. Soni, K. P. Muthe, S. K. Gupta, M. S. Kulkarni, V. Grover, A. K. Tyagi, Proceedings of the International Conference on Luminescence and its Applications (ICLA- 2012) 7-10th Feb, 2012, Hyderabad, India.

(Sanu S. Raj)

Dedicated to
My

Parents
&
Grandparents

ACKNOWLEDGEMENTS

With great pleasure presenting my thesis and expressing my deepest regards, deep sense of gratitude and sincere thanks to my research guide Dr. A. K. Tyagi, Head, Nuclear and Energy Materials Section, Chemistry Division, B A R C, for his valuable guidance, constant encouragement, keen interest and good wishes throughout the research work. In the present situation of my life, it would have been impossible for me to accomplish this without his firm and optimistic approach.

I would like to express my deepest gratitude to Dr. Devesh Mishra, Dr. K. P. Muthe, Dr. Vinita G. Gupta and Dr. S. K. Gupta without their guidance, help and support the completion of the thesis would have been difficult.

It is also my great pleasure to thank Dr. S. K. Jha, Head, ERMS (HPD) and Dr.Hemalatha Padmanabhan for their support in carrying out the research work. My sincere thanks are due to Dr. P. K. Sarkar (Ex - Head, HPD) for granting me permission for doing this work and Dr. R. K. Singhal for his encouragement. Special thanks to my friend Dr. Himanshi N. Mishra for her continuous support as a good friend and helping me with the facilities which she could provide. It is with immense gratitude that I acknowledge the comments, suggestions and encouragement rendered by my Doctoral Committee members, Dr. D. Das, Dr. M. S. Kulkarni, Dr. V. Natrajan, Dr. V. Sudarsan and Dr. Vinita G. Gupta. I would like to thank Dr.Pramilla D. Sawant, Dr. Vandana Pulhani, Dr. Remya Devi, Ms. Madhuparna Dutta, Mr. Santosh Kamble, Ms. Farheen and Ms. Nilashri for their support.

I thank all those who have helped me directly or indirectly in the successful completion of my thesis. There are no words to thank my entire family for their love and continuous support. Last but not least I would like to specially thank my husband K. S. Jayandhan and my lovely kids Thakarshi and Medha.

CONTENTS

SYNOPSIS

Al_2O_3:C is one of the most stable and sensitive phosphors used in both thermoluminescence (TL) and optically stimulated luminescence (OSL) mode. Due to its promising optical properties, high thermo-chemical stability and relatively low effective atomic number (Z_{eff} ~10.2), it has been successfully used in personnel radiation dosimetry **[1]**. Carbon doping enhances concentration of the F/F^+ centres (identified as basic luminescence recombination centres) along with the dosimetric metastable charge traps leading to high TL/OSL sensitivity of Al_2O_3:C **[1-4]**. Extensive research on development of new oxide based OSL material with good optical/chemical stability along with better radiation damage resistance has been carried out on a wide variety of materials (YAG:C, $LiMgPO_4$: Tb, B [lithium magnesium phosphate (LMP)], $BaSO_4:Eu^{2+}$) **[5-8]**. $MgAl_2O_4$ has been used as an optical and insulating material in the radiation field due to its radiation resistance **[9]**, chemical inertness, high melting point and good mechanical strength **[10-15]**. In $MgAl_2O_4$, cation antisite defects are produced by Al^{3+} and Mg^{2+} inversion **[16]** where Al^{3+} acts as an electron trap due to its extra positive charge and Mg^{2+}acts as a hole trap due to less positive charge. The incorporation of cations of various size/charge (ionic potential) into $MgAl_2O_4$ spinel leads to various kinds of defects **[17-19]** which leads to interesting optical behaviour. In phosphor materials, after exposing to ionizing radiation, the radiation induced free charge carriers get trapped at pre-existing metastable defect sites. The subsequent optical/thermal stimulation of these radiation induced trapped charges (i.e. de-trapping) results in radiative recombination as luminescence. In case of optical stimulation, this luminescence is termed as optically stimulated luminescence (OSL) and in case of thermal stimulation as thermoluminescence (TL). After irradiation with neutrons, X-rays and the UV-light, optical absorption of magnesium aluminate spinel single crystals of different compositions MgO.nAl_2O_3 (n=1.0 and 2.5) were investigated to elucidate the existence of specific absorption bands related to lattice defects **[20]**.

A comparative investigations of Radioluminescence (RL) and TL has been performed in spinels obtained at different processing conditions and different crystalline forms to reveal the role of crystalline imperfections in the radiation-induced processes **[20]**. High purity, stoichiometric, polycrystalline $MgAl_2O_4$ spinel samples were studied for their TL and OSL properties by Yoshimura **[9]** where as three-dimensional thermoluminescence (TL) spectra and two dimensional contour maps resulting from $MgAl_2O_4$ crystals irradiated with X-rays were studied by Kim et al. **[21]**. $MgAl_2O_4:Tb^{3+}$ was prepared by combustion synthesis and its defect centers were studied by correlating various techniques such as Electron Spin Resonance (ESR), TL and OSL by Alagu Raja et al. **[22]**. Incorporation of carbon in yttrium aluminum garnet (YAG) has shown remarkable improvement in its dosimetric properties **[5]**. Radiation resistance, chemical inertness, high melting point and good mechanical strength are some of the important prerequisites required for a promising phosphor. As $MgAl_2O_4$ fulfils all of them, this material is among the promising candidates for developing new phosphors for TL/OSL radiation dosimetry. Carbon doped $MgAl_2O_4$ and its dosimetric response have not been studied so far. Therefore, it would of great interest to explore the dosimetric properties of carbon doped $MgAl_2O_4$. In the present research work, carbon was introduced in $MgAl_2O_4$ lattice using two different methods and the detailed TL and OSL studies on the developed carbon doped $MgAl_2O_4$ was carried out. These results will help in the development of $MgAl_2O_4$ based new TL/OSL sensitive phosphors. In order to investigate new candidates for optical materials for dosimetry, nano-alumina powders were annealed at various temperatures and have been extensively investigated for their photoluminescence (PL) behaviour and the defects responsible for them. These studies will provide insights in mechanism of Al_2O_3 based dosimetry materials.

Chapter 1: Introduction

This chapter explains the history, development and types of two main techniques used for radiation dosimetry such as thermoluminescence (TL) and optically stimulated luminescence (OSL). Detailed discussion has been provided on the mechanism of formation of defects in these materials, about the storage of absorbed dose and the annihilation after the stimulation as heat or light is given.

In thermally stimulated luminescence (TL), a discussion on glow curve, effects of doping, different types of commercially used TL phosphors and their sensitivity to radiation dose has been provided.

According to the modes of stimulation and detection of light signals, various terminologies like luminescence, DOSL for delayed optically stimulated luminescence, LM-OSL for linearly modulated optically stimulated luminescence, POSL for pulsed optically stimulated luminescence, PTOSL for photo-transferred optically stimulated luminescence and COSL for cooled optically stimulated luminescenceare discussed in detail. Different OSL materials, their merits and demerits, current research on the development of new OSL materials etc. has also been discussed.

Chapter 2: Experimental

A concise description of different routes for synthesis employed, the techniques used for the characterization, methods adopted for carbon doping and TL, OSL, PL studies have been explained in this chapter. The main route adopted for synthesis was gel combustion method. Powder XRD was used for structural characterisation.

Two methods were adopted for carbon doping. The first method employed was electron gun evaporation system. It is normally used for vacuum evaporation of thin films, as a means to attain temperature high enough to melt $MgAl_2O_4$ in the presence of graphite. The second method employed graphite furnace. In this method the furnace is made up of graphite crucible kept in core of Cu coil for inductive heating. The temperature of furnace was monitored by pyrometer based temperature measurement system. TL and OSL studies of the carbon doped samples were performed after irradiating the sample using $^{90}Sr/^{90}Y$ beta source.

PL data were recorded on an Edinburgh CD-920 unit equipped with Xe flash lamp as the excitation source. The data acquisition and analysis were carried out by F-900 software provided by Edinburgh Analytical Instruments, UK.

Chapter 3: TL and SL studies of carbon doped magnesium aluminate ($MgAl_2O_4$:C)

$MgAl_2O_4$:C phosphor samples prepared by the two different methods were studied for their TL and OSL response. The OSL signal was found to decrease with increase in temperature on account of TL traps getting empty. This gives the direct correlation between the two signals. All the TL traps in both the samples were OSL sensitive and contributing actively to OSL signal. They have similar types of the TL/OSL defects with multiple overlapping TL glow peaks ranging from 100 °C to 400 °C. In order to measure TL parameters such as thermal trap depth, frequency factor and order of kinetic associated with charge transfer process in TL phenomenon, the computerized curve de-convolution analysis (CCDA) has been used. Two methods of incorporating carbon in $MgAl_2O_4$ could generate the defects of similar types in $MgAl_2O_4$:C lattice. However, the $MgAl_2O_4$:C synthesized by electron gun shows relatively larger concentration of the TL/OSL defects as compared to $MgAl_2O_4$:C synthesized using vacuum assisted melting method. The photo-ionization cross-section (PIC) associated with fastest OSL component of $MgAl_2O_4$:C is found to be 50% times than that of fastest OSL component of commercially available dosimetric grade α-Al_2O_3:C. This is an encouraging result. The $MgAl_2O_4$:C thus developed shows good dynamic OSL dose linearity. This work established that $MgAl_2O_4$:C could be developed as potential tissue equivalent OSL/TL material.

Chapter 4: $MgAl_2O_4$:C defect-induced luminescence

This chapter is devoted to the effect of carbon doping on the photophysical properties of $MgAl_2O_4$. Photoluminescence study of $MgAl_2O_4$:C by electron gun denoted as A and by graphite furnace denoted as B was carried out. The photoluminescence spectroscopy exhibited defect-induced emissions with enhanced intensity and a significant blue shift in the emission band was also observed in the case of sample B. The photoluminescence decay studies indicated that multiple trapping and de-trapping events were experienced before the radiative recombination process. Average lifetime was observed to be 4.83ls which is typical of defect-related emission. The results were complemented by electronparamagnetic resonance (EPR) technique. The CIE coordinates for sample B were found to be x = 0.231and y = 0.227 which establish it as a blue-emitter.

Chapter 5: Preparation and optical properties of nano Al_2O_3

The Al_2O_3 nano-powders were synthesized by a fuel-deficient gel combustion synthesis employing glycine as a fuel. The samples were annealed at different temperatures (1200ºC, 1300ºC, 1450ºC) with the aim of introducing different defect nature/concentration and their effect on luminescence. Powder XRD studies revealed the formation of nano α-Al_2O_3 and appreciable crystallinity was obtained at all the three temperatures. The emission spectra of all the three samples showed broad bands albeit with different shapes which on deconvolution yielded three components. This indicated the presence of three types of defects which were also characterised by time resolved emission studies. The lifetimes of different traps have been correlated to the transitions involved. This work contributes to understanding of nature of the defects occurring in Al_2O_3 as the manifestation of variation in annealing temperatures and in turn provides insights into TL/OSL properties of alumina based dosimetry materials.

Chapter 6: Summary and future scope

The doping of the carbon has been achieved in two ways – by using electron gun and by heating the parent oxide in graphite furnace. The TL/OSL sensitivity greatly enhanced for electron gun synthesized $MgAl_2O_4$:C. The carbon doped $MgAl_2O_4$:C exhibited impressive OSL properties to further develop this phosphor for radiation dosimetry. However, there is a need of further study, to optimize the synthesis parameters of carbon doping in $MgAl_2O_4$ in order to enhance its suitability for various fields of radiation dosimetry. The scaling up of synthesis also needs attention. Attempts will be made in future to incorporate nitrogen in $MgAl_2O_4$.

References:

1. M. S. Akselrod, V. S. Kortov, D. J. Kravetsky, V. I. Gotlib, *Radiat. Prot. Dosim.* 1990, 47, 159-164.
2. M. S. Kulkarni, D. R. Mishra, K. P. Muthe, A. Singh, R. M. Gupta, S. K. Kannan, *Radiat. Meas*. 2005, 39, 277-282.
3. K. H. Lee, Jr. J. H. Crawford, *Appl. Phys. Lett.*1978, 33, 273.
4. V. S. Kortov, I. I. Milman, V. I. Kirpa, J. Lesz, *Radiat. Prot. Dosim.*1994, 55, 279-283.

5. M. S. Kulkarni, K. P. Muthe, N. S. Rawat, D. R. Mishra, M. B. Kakade, S. Ramanathan, S. K. Gupta, B. C. Bhatt, J. V. Yakhmi, D. N. Sharma, *Radiat Meas.*, 2008, 43, 492-496.
6. X. Yang, J. Xu, H. Li, H. Tang, Q. Bi, Y. Cheng, Q. Tang., *J. Phys. D: Appl. Phys.* 2009, 42, 145411.
7. B. Dhabekar , S. N. Menon, E. A. Raja, A. K. Bakshi, A. K. Singh, M. P. Chougaonkar, Y.S. Mayya, *Nucl. Instrum. Method. Phys. Res. B* 2011, 269, 1844-1848.
8. B. C. Bhatt, A. Soni, G. S. Polymeris, D. K. Koul, D. K. Patel, S. K. Gupta, D. R. Mishra, M. S. Kulkarni. *Radiat. Meas.* 2014, 64, 35-43.
9. E. M. Yoshimura, E. G. Yukihara, *Radiat. Meas*. 2006, 41, 163-169.
10. J. E. Sheehan, J. Sigalovsty, J. S. Haggerdy, J. R. Porter, *Ceram. Eng. Sci. Proc*. 14, 1993, 660-670.
11. G. Baudim, R. Martinez, P. Pene, *J. Am. Ceram. Soc.,* 1995, 78, 1857–1862.
12. H. S. Tripathi, B. Mukherjee, S. Das, M. K. Haldar, S. K. Das, A. Ghosh, *Ceram. Int.,* 2003, 29, 915-918.
13. V. Paris, S. Hayan, M. P. Dariel, N. Frange, E. Zaretsky, *AIP conference proceedings*. 2009, 1195, 1003-1006.
14. D. Mohapatra, D. Sarkar, *J. Mater. Sci*. 2007, 42, 7286-7293.
15. C. Kinoshita, H. Abe, S. Maeda, K. Fukumoto, *J. Nucl. Mater.*, 1995, 219,152-160.
16. V. T. Gritsyna, Y. G. Kazarinov, V. A. Kobyakov, I. E. Reimanis, *Nul. Inst. Method in Phys. Res. B*, 2006, 250, 342-348.
17. K. E. Sickafus, J. M. Wills, N. W. Grimes, *J. Am. Ceram. Soc.,* 1999, 82, 3279.
18. S. A. T. Redfern, R. J. Harrison, H. St. C. O’Neill, D. R. R. Wood, *Am. Mineral,* 1999, 84, 299-310.

19. D. B. Uberuaga, R. Smith, J. A. Ball, R. W. Grimes, *Phys. Rev. B*, 2007,104116.

20. V. T. Gritsyna, I. V. Afanasyev-Charkin, Yu. G. Kazarinov, K. E. Sickafus, *Nucl. Instr. Meth.*, 2004, 218, 264-270.

21. T. K. Kim, H. S. Choe, J. I. Lee, C. N. Whang, J. Korean Phys. Soc., 1997, 30, 347-351.

22. E. A. Raja, S. N. Menon, B. Dhabekar, N. S. Rawat, T. K. Gundu Rao, *Indian J. Pure Appl. Phys.*, 2009, 47, 420-425.

LIST OF FIGURES

LIST OF TABLES

Chapter 1

Introduction

1.1 Luminescence

Luminescence refers to emission of radiation in visible or near visible region subsequent to absorption of energy (excitation) by a substance **[1]**. It can occur in a wide variety of compounds such as inorganic, organic and semi-conductors, under different conditions. The light emission can be stimulated by some internal or external process, and it is the characteristic of the compound. It has been used since the middle of 20th century in the determination of the integrated radiation dose exposed to humans, or dating archaeological specimens and geological sediments. For the assessment of the integrated radiation dose or the event, zeroing of the latent luminescence at some time in the past is required. This zeroing occurs through heating of materials such as commonly used radiation dosimeters, archaeological pottery, bricks and porcelain or by exposure to daylight for geological sediments. Luminescence signal builds up again through exposure to either radiation from man-made sources or from the weak natural environmental background radiation and gets annihilated either by thermal or optical stimulation. During exposure, radiation energy is accumulated and stored in the crystal lattice in the form of electrons or holes trapped at defect sites. During stimulation, the trapped charges are released and annihilated to give luminescence **[2]**.

This chapter will describe thermo-luminescence and optically stimulated luminescence as they are the mainstay of this thesis.

1.2 Thermally stimulated luminescence (TSL)

Thermoluminescence dosimetry is a well-established dosimetric technique with application in areas such as personnel, environmental, medical, industrial and space dosimetry. Radiation monitoring has been conveniently carried out using thermally stimulated luminescence (TSL) technique. The phenomenon of thermo luminescence

(TL) has been known since 1663, when Robert Boyle observed the emission of light by diamond when it was heated in the dark **[3]**.

In thermo-luminescence dosimetric technique, the metastable energy levels called trapping centers created by pre-existing defects in the material, trap some of the electrons and holes created by ionizing radiation. During radiation measurement, heating of the material facilitates the trapped carriers to get excited to conduction band in the case of electrons and to valence band in the case of holes. These mobile charge carriers are captured by other types of energy levels created by defects called luminescence centers. A photomultiplier tube is used to measure the light emitted by luminescence centers during electron or hole capture. The integrated intensity of emitted light is proportional to the absorbed dose by the material **[4]**.

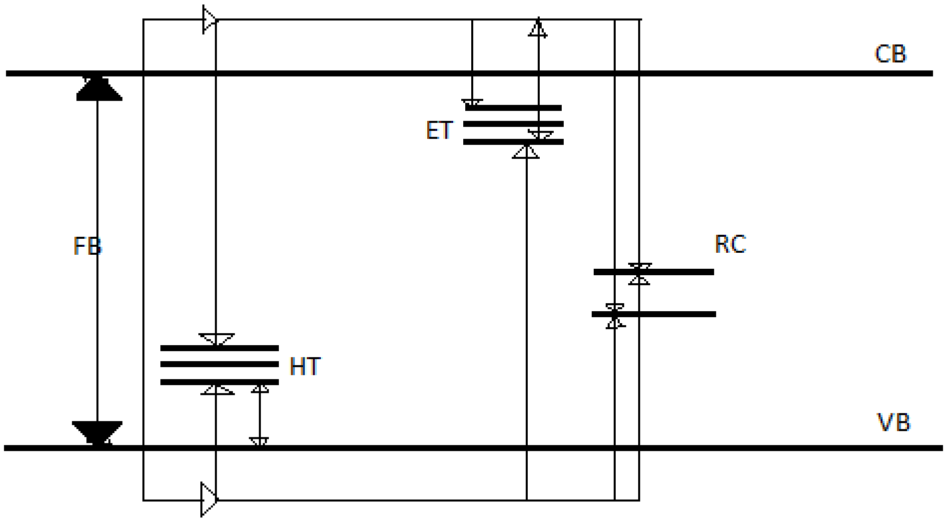

Fig 1.1 Band structure schematic of semiconductor

It can be understood in terms of the band structure model of semiconductor. In a semiconductor there are two relevant energy bands: (i) an almost completely filled valence band (VB) and (ii) an almost empty conduction band (CB). The two energy bands are separated by a forbidden band gap (FB), which means that between these two bands there are no electronic energy levels. Transitions of electrons between the valence band and the conduction band are allowed and they produce free electrons in the conduction band and free holes in the valence band. However, defects create other types of energy levels which trap electrons (ET) near conduction band, hole are trapped (HT) near valence band and luminescence centers (RC) where the recombination of trapped electrons and holes occurs **[5]**.

Depending up on the symmetry properties of the ground and excited states, optical transitions between energy levels located in the forbidden band gap are allowed according to selection rules. Transitions between the energy levels in the gap and the conduction band results in empty electron traps in the band gap. Electrons from conduction band or electrons from other centers can be trapped in these localized defects in the crystal lattice. Trapped electrons can be released thermally or optically. The partially filled valence band implies that free holes can exist in this band. It is possible to consider centers with energy levels in the forbidden band gap, which are capable of trapping free holes, which are available in the valence band similar to the description for electronic levels in the band gap. Trapped holes can also be released thermally or optically like the trapped electrons. A hole trap is generated after releasing the trapped hole **[6]**.

Due to ionizing radiation, electrons are excited from the valence band to the conduction band leading to the presence of significant concentrations of free electrons in the conduction band and free holes in the valence band. Quite often in ionic materials, the primary radiolytic reactions resulting from interactions between radiation and the crystal take place at anions. In case of chlorides, the Cl^- and for oxides, O^{--} ions, interact with radiation. Due to these processes, excitations with binding energies slightly smaller than the forbidden band gap take place and these excitations are called excitons [**7, 8**]. Usually, the subsequent de-excitation processes are sufficiently energetic and effective to induce atomic/ionic displacements in the crystal lattice, which leads to the formation of radiation induced defects**.** The simplest example is NaCl. Here, the lattice takes on a regular, repeating shape (Fig1.2).

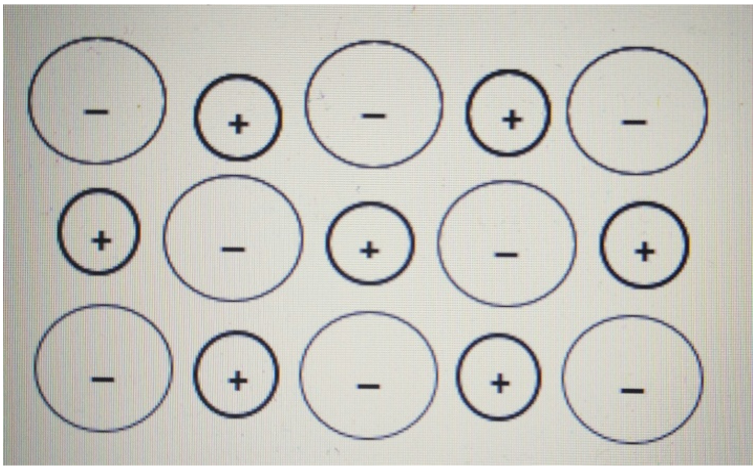

Fig. 1.2 Structure of NaCl

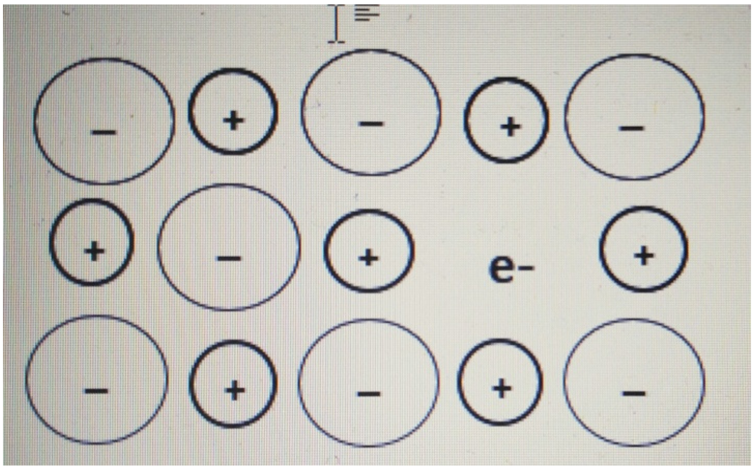

Fig. 1.3 Structure of NaCl after irradiation

After irradiation with X-rays, gamma rays, or beta radiation, the resulting crystal looks like as shown in Fig.1.3. Single electrons occupy the vacant anion lattice.

Well-known examples of radiation-induced defect centers are the F-centers and V-centers. F-center is an anion vacancy in the crystal lattice with a trapped electron. ‘F’ in the name ‘F-center’ had come from the German word ‘Farbe’, which means color. Due to F-centers, the crystal absorbs sufficient light in a limited frequency range and as a result, the crystal becomes colored. For each electron, which is trapped at the electron trap a hole is produced which gets trapped at a hole trap, so as to maintain electro-neutrality of the crystal. The other group of defects, V-centers absorb light in the violet part of the visible spectrum. Impurities such as transition metal ions, create another class of imperfections, which are quite often the reason why certain minerals show a characteristic color. This is due to absorption bands caused by electronic transitions between energy levels in the band gap. The energy levels in the band gap depend on the nature of the imperfection, lattice defect or impurity. It can be located at any energy position varying from just below the bottom of the conduction band to just above the top of the valence band. A variety of defects belonging to the above-mentioned two classes of centers, which are associated with energy levels in the forbidden band gap, are also produced during exposure to the ionizing radiation.

1.2.1. Glow curves

Thermally stimulated luminescence, or thermoluminescence (TL), is the luminescence emitted as a function of temperature, is observed by heating an irradiated sample at a constant rate to about 500°C. The TL signal is characterised by a “glow curve”, with distinct peaks occurring at different temperatures, which relate to the electron traps present in the sample due to the defects in the lattice structure. Once trapped, the electron can be evicted by thermal vibrations of the lattice. These vibrations become stronger due to the increase in the temperature, and the probability of release increases so rapidly that within a narrow temperature range, trapped electrons are quickly liberated. Some of these electrons recombine with trapped holes resulting in emission of light (TL). Depending on the depth of defects or traps, the lifetime of trapped electrons varies. Low-temperature traps (shallow traps) are thermally drained more quickly even at room temperature than the deep traps [**9**].

1.2.2 Doping

Defects can lead to dramatic performance improvements over the "ideal" material, but it can limit some other functions of materials. Pure corundum (alumina) has its application as a hard grinding material, but it is the presence of trace metal impurities such as iron or chromium ions that produces the electronic transitions which create the beautiful colors of ruby and sapphire **[10]**. Few materials have band gaps, which corresponds to the visible spectrum. By the addition of different atoms into the crystal, materials with a relatively wide band gap can be designed to luminesce in the visible region. The additional atoms are called dopants and have a different electronic orbital structure compared to the host crystal lattice. Therefore, in regions of the crystal around the dopant atom, within the forbidden band gap additional energy levels become available. These energy levels can accommodate electrons or holes. If these levels are close to the conduction band, the dopant is called a donor, and if close to the valence band, it is called an acceptor. Transitions between these levels can give rise to visible luminescence. In such case, the dopant is known as an activator. In most cases, the activator is present in extremely small concentrations, ranging from hundreds to tens of ppm level. Sometimes the excited electron can find other path ways to dissipate its energy by non-radiative recombination mechanisms. These are introduced by impurities called inhibitors, usually associated with defects in the crystal, or levels in the middle of the band gap, called deep levels. The defects in the crystal can result in shallow levels which are close to the edge of either the valence or conduction bands. Shallow levels in the band gap can trap the excited electrons and prevent the electron from decaying immediately back to the valence band. Instead the decay may occur only after a long time. The mechanism behind the technique of thermo luminescence is the dislodging of the trapped electrons back into the conduction band by a small amount of heat and from there it can readily decay to the valence band.

1.2.3 Thermoluminescence: Current status

There have been tremendous research efforts both experimental and theoretical, directed towards TL and developing new phosphors **[1]**. The important features for a compound to be used as a dosimeter are its radiation sensitivity, dose linearity, radiation resistance, fading, repeatability and simple response so that it is easy to use as a TL/OSL reader **[5]**. Several groups of materials such as alkali and alkaline-earth halides, whose typical representatives are LiF and CaF_2, sulfates ($MgSO_4$, $CaSO_4$), sulfides MS (M = Mg, Sr, Ca, Ba), oxides Al_2O_3, BeO and SiO_2 are studied with respect to the TL dosimetry requirements. The first basic TL material LiF:Ti, Mg (TLD-100), having tissue equivalence (Zeff = 8.04), which is an important factor for personnel dosimetry is still extensively used **[11]**. Studies on TL properties of carbon doped Al_2O_3 (TLD-500) were carried out by Akselrod et al. **[12]**, which is a very sensitive material to radiation exposure, with a linear dose response from 0.05 μGy to 10 Gy and fading rate of 3% by year (when kept in the dark). The search for materials with a high TL yield is still going on. Studies on TL properties of the AlN ceramic, which represents a new class of compounds, are of contemporary relevance. At equal doses, the TL yield of this ceramic is much larger than that of the most sensitive Al_2O_3:C dosimeter **[13]**. However, so far, an extremely high fading prevented the development of AlN-based dosimeters suitable for practical applications.

Some of the widely practiced phosphors in TL dosimetry are briefly discussed below and shown in Table 1.1.

(i) Lithium fluoride

LiF:Mg, Ti (TLD-100) is the most extensively used phosphor in the TL dosimetry. This detector is available according to isotopic compositions, e.g. ^{6}Li enriched TLD-600 and ^{7}Li enriched TLD-700 and TLD-100 with the natural abundance. Their gamma dose sensitivities are almost the same but they have significantly different sensitivities for neutrons. Therefore, they are valuable as detectors in mixed neutron-gamma fields. The TL spectrum of LiF: Mg, Ti (i.e. TLD 100) is characterized by the appearance of a dominant glow peak at ~ 235 °C which is the 5th peak out of the twelve peaks that populate the TL spectrum of this phosphor **[14]**.

(ii) LiF:Mg, Cu, P (Li-MCP)

This phosphor is commercially synthesized and available in different forms such as powder, hot pressed polycrystalline chips, ^{6}Li and ^{7}Li analogues including thin films. They have various brand names viz. GR 200 (China), TLD 100H, TLD 600H, TLD 700H (USA), TLD 370 (Russia), MCP- N (Poland). They are used in the dose interval of 1-10 Gy particularly in clinical dosimetry for therapeutic applications. They show less fading at room temperature which is an advantage **[15]**.

(iii) Calcium fluoride (CaF_2)

CaF_2:Mn, (i.e. TLD 400) is a useful dosimetric phosphor having enhanced sensitivity as compared to TLD 100 and has a simpler structure of its TL curve **[16]**. Due to the lack of tissue equivalence, this material cannot be used in personnel dosimetry. However, it has found application in environmental dosimetry. It has a single TL glow peak at ~ 310 °C **[17]**.

Table 1.1 Characteristics of some TL materials [11, 18]

Materials	**Type of dosimeter**	**Useful range**	**Thermal fading**
LiF:Mg,Ti	TLD-100	10µGy-10Gy	5-10% per year
LiF:Mg,Cu,P	TLD-100H	1Gy-20Gy	3% per year
^{6}LiF:Mg,Ti	TLD-600	10µGy-20Gy (Neutron sensitive)	Negligible
^{6}LiF:Mg,Cu,P	TLD-600H	1µGy-20Gy (Neutron sensitive)	Negligible
^{7}LiF:Mg,Cu,P	TLD-700H	1µGy-10Gy	Negligible
CaF_2 :Dy	TLD-200	0.1µGy-10Gy	16% total in two weeks
CaF_2 :Mn	TLD-400	0.1µGy-100Gy	15% total in 3 months
Al_2O_3:C	TLD-500	0.05µGy-10Gy	3% per year
$Li_2B_4O_7$:Mn	TLD-800	5µGy-105Gy	5% in three months
$CaSO_4$:Dy	TLD-900	1µGy-100Gy	8% in 6 months

(iv) Al_2O_3:C

The sensitivity of Al_2O_3: C (TLD-500K) is 40 to 60 times better than that of TLD 100. It has a very low zero dose value (i.e.TL background readout of sample which has not been irradiated) and ensures radiation detection threshold level as low as 0.05 μGy. It shows low fading (less than 5% per year) and has an emission spectrum which has a maximum around 420 nm, a region where photo multiplier tubes are most efficient. Its effective atomic number (10.2) is reasonably small. Its usable dose range extends from 0.05 μGy to 10 Gy **[12]**.

1.3 Optically stimulated luminescence

In optically stimulated luminescence (OSL), light of appropriate wavelength and intensity is used to stimulate the charge carriers trapped in metastable defect states. When the material is subjected to light stimulation, charge carriers are optically released from the traps and emit a light signal proportional to the absorbed dose. Albrecht and Mandeville **[19]** were the first to demonstrate that photo-stimulation by visible light results in an ultraviolet emission in X-ray exposed BeO samples which was due to the presence of doubly occupied electron traps. Later, Braunlich *et al.* and Sanborn et al.**[20, 21]** had studied the dose-dependence of TLDs using an infrared stimulation of Ce, Sm, and Eu-doped MgS, CaS, and SrS. However, the mode of simultaneous stimulation and detection of an emitted light signal did not attract much attention until 1985, when Huntley *et al.* **[22]** demonstrated optical dating of sediments and started using in the field of dating. Later Markey *et al.* resolved optically stimulated luminescence in a highly sensitive α-Al_2O_3:C TLD material **[23]**. However, in some other TLD materials like BeO, **[24, 25]** CaF_2:Mn, **[26]** and $CaSO_4$:Dy **[27-29]**, the phosphorescence caused by an optical stimulation was shown to be useful for radiation dosimetry. This use of optically enhanced phosphorescence achieved only a limited success due to its low sensitivity. There are different kinds of dosimeters available for personnel as well as industrial applications such as doped LiF, $CaSO_4$, CaF_2, and $Li_2B_4O_7$ which have been developed and studied in the past few decades. In LiF:Mg,Ti, the most commonly used TL material, the trapped charges cannot be easily optically stimulated. OSL in LiF:Mg,Ti can be observed, but the minimum detectable dose is high **[30]**. As a result, TL and OSL dosimetry are usually based on different materials. OSL is simple and the readout is completely optical and plastics can be used in the manufacturing of the OSL dosimeter. Unlike TL, there are no high energy consuming heaters, no thermocouples, no need to establish good thermal contact between the dosimeter material and the heater. In addition by eliminating the step of heat stimulation, the changes in the defect structure of the material due to thermally stimulated diffusion **[5]** are prevented and thermal quenching effects are avoided **[31]**. In principle, optical stimulation is gentle on the detector material as it involves only electrons or holes. It requires simple instrumentation and components that are easy to integrate. In addition to the dosimeter, a light source such as light emitting diodes (LEDs), laser, or filtered lamp is needed. Each one has its own advantages, disadvantages and costs. For general applications, high power LEDs are most reliable, being used in both commercial and research instruments **[32, 33]**.

A major commercial dosimetry service provider had adopted optically stimulated luminescence (OSL) almost 20 years back and this technique is being used by millions of radiation workers worldwide. Now it has been adopted in a variety of places, from hospitals to International Space Station. OSL is used to monitor doses to astronauts by the U. S. National Aeronautics and Space Administration (NASA) **[34]**, and in space experiments by the European Space Agency **[35]**. Medical physicists are investigating the use of OSL dosimeters in hospitals as a part of quality control programs **[36]**. It has been estimated that more than 25% of about 5 million badges in use world over are in fact OSL dosimeters **[37]**. Institutions participating in clinical trials in radiotherapy in United States employ OSL technique (for example, by the Radiation Physics Centre, University of Texas, M. D. Anderson Cancer Center) **[38]**. In USA, some leading and nationally accredited service providers replaced TLD with Al_2O_3:C–based OSL dosimetric systems for personnel dosimetry **[36]**. Many other countries have also introduced Al_2O_3:C for personnel dosimetry **[39]**. Al_2O_3:C OSL dosimeters have also been accepted by the National Council on Radiation Protection and Measurements (NCRP) **[40]**. For the past few years, OSL has emerged as a real time in-vivo dosimetry technique for radiotherapy beams. This is because of Al_2O_3:C which possess most of the important characteristics required for personnel dosimeters such as high sensitivity, high resolution, capability of measurements of absorbed dose for both photon and electron beams, availability in different sizes and shapes and non dependency on beam parameters.

In medical dosimetry, adoption of OSL for a variety of tasks has been increasing. In other applications, like accident dosimetry using the OSL from tooth enamel has proven to be challenging. The increase in the number of publications on OSL continues and it reflects the growing interest and “popularization” of the technique. Both TL and OSL detectors work as passive, integrating radiation detectors. At room temperature, the population of charges trapped due to the exposure to ionizing radiation can be stable for thousands of years. Thus, until readout is performed, the information related to the radiation exposure, i.e. the trapped charge concentrations remains recorded in the crystal lattice. Readout of this information is carried out by stimulating the detector by providing sufficient optical energy to these trapped charges to escape, recombine the carriers and emit light. For the OSL readout, the detectors are illuminated. In an OSL material it is desirable to characterize the high photoionization cross-section, i.e., to have trapping centers whose trapped charges can be easily stimulated with light; this is not the case for all TL materials. The traps associated with the TL peaks may or may not be the same as for OSL. Due to the irradiation of the material, the traps get populated with electrons and hence the OSL intensity is related to the absorbed radiation dose. The spectral regions of emitted OSL during recombination of the detrapped charges and that of stimulating photons are different. The OSL signal during exposure to the stimulation light is observed to decrease to a low level as the trapped charge is depleted (decay curve). The physical principles of OSL and TL are thus closely related. OSL measures only the component of the trapped electron population that is most sensitive to light and measured at or close to room temperature and thus results in less alteration of the crystal **[41]**. OSL, however, differs from other optical processes such as (i) Radio-luminescence or scintillation in which the emission of light signal continues as long as ionizing radiation remains incident on the sample and the intensity is proportional to the dose rate, (ii) Photoluminescence or fluorescence in which the emission of light signal continues as long as a light beam is incident on a sample and the signal may or may not be influenced by the radiation and (iii) radio-photo-luminescence in which on subsequent illuminations by an appropriate light, the emission of a light signal proportional to the amount of pre-irradiation takes place during an illumination due to the excitation and de-excitation of stable color centres. The same signal can be recorded any number of times from an irradiated sample whereas the resetting is done by a pre-established heat treatment. The correlation between the wavelengths of stimulating light and the emitted light is not there in OSL; the emitted light could be of longer or shorter wavelengths as compared to those of the stimulating light. To optimize an OSL reader for any specific material and application, one must know the material's OSL emission spectrum and excitation spectrum. For this reason, most of the literature on new OSL materials is dedicated to these aspects **[42]**.

General features of OSL are as follows:

(i) The sample can be read multiple times as only partial depopulation of the traps occurs with shorter optical stimulations.

(ii) This technique is amenable for use of different types and modes of light beams for optical stimulation and measurements.

(iii) Using very narrow stimulating beams (a few tens of nm) a high spatial resolution of a dose distribution in an OSL material can be studied.

(iv) Since no heating is involved for the readout of OSL, the thermal changes influencing the sensitivity and thermal quenching of a luminescence signal (usually dominant in some TLDs due to heating) are avoided.

1.3.1 Concepts of OSL

The OSL phenomenon, like thermoluminescence, can be understood in terms of the energy band model constituted by the valence band (VB) and the conduction band (CB) which are separated by a forbidden gap. In a perfect crystal, there are no electronic states in the forbidden gap. However, introduction of impurities created either during synthesis or deliberately introduced via doping can lead to the occurance of localized metastable states in the forbidden gap which may act as traps for the charge carriers (electrons and holes) produced upon interaction of the material with radiation. The charge carriers may radiatively recombine to yield luminescence either by (i) recombining at the recombination centre to yield instantaneous luminescence also known as radioluminescence (RL) (ii) recombining via metastable states after getting trapped which may stay there for longer durations till sufficiently stimulated. This trapped electron can be released by means of thermal stimulation in TL and by optical stimulation on OSL. This may travel freely in the conduction band till it recombines with a hole and yields luminescence. However, in TL, once the pre-irradiated sample is heated to fixed temperature, the consequent emission of a light signal is proportional to the amount of ionizing radiation. And following the TL read out, the sample is reset for further use. But in OSL, all the trapped charge carriers in a pre-irradiated sample cannot be sufficiently stimulated by a single illumination by low-intensity source **[43]**. Thus it provides an option of multiple readouts of an irradiated sample. The sample can be reset for further use either by an intense optical bleaching carried out for longer duration employing light of suitable wavelength/energy or by providing established heat treatments. The OSL signal is recorded by integrating the light emission for a fixed interval of time following stimulation.

Depending upon the mode of stimulation and detection, various OSL technologies are being employed **[44]**. These are briefly described as follows.

1.3.2 Continuous-wave optically stimulated luminescence (CW-OSL)

This mode is the simplest technique based on OSL **[23]**. Here, the most important requirement is that the stimulating and the emitted wavelength should be as far apart as possible. The pre-irradiated sample is stimulated with a constant intensity of light and the traps are emptied using a fixed wavelength of light and intensity. As mentioned earlier, the emitted luminescence has different wavelength as compared to stimulating light. The detector is optimised to register only the emitted luminescence in order to minimize any interference from the stimulating light. This is done by employing various appropriate narrow band filters for both. The intensity of the emitted light decreases in an exponential manner with time and most of the OSL emission occurs very fast. This results in a fast read-out (~seconds).

1.3.3 Delayed optically stimulated luminescence (DOSL)

In this technique, the stimulating and emitted radiations are separated in time domain. Thus, the pre-irrdiated material is stimulated and during stimulation the detector does not record any signal. The luminescence is measured after the stimulation. DOSL could be either phosphorescence **[24-29]** or luminescence which is delayed due to the extended lifetime of the luminescent centers **[23, 31]**. In this, the charge carriers liberated from the stable traps (stable at normal temperatures) by optical stimulation are re-trapped at the shallower traps, and a slow release of these charge carriers results in enhancement of phosphorescence which yields the delayed luminescence response (~ tens of minutes). In delayed luminescence, the charge carriers released by stimulation reach the luminescence center and the resultant emission gets delayed for durations of the order of a few tens of milliseconds. This helps in complete separation and discrimination between the stimulated light and the emitted light **[45]**. The advantage of this technique is there is no limitation on the energy and the intensity of stimulation.

1.3.4 Linearly modulated optically stimulated luminescence (LM-OSL)

The LM-OSL technique employs stimulation of the optically active material by linearly increasing the intensity of stimulating light beam rather than a constant intensity source (CW-OSL) and the resulting emitted signal is measured **[46]**. Due to the presence of a distribution of traps in the material, the photo-ionization cross section also varies with the intensity of stimulation. As a result, in time domain the luminescence signals of the traps get separated such that the larger photo-ionization cross section would lead to quicker electron release from that trap. Thus the traps get emptied (release their charge) depending on the magnitude of photo-ionization cross section, starting from the traps that have highest cross section followed by the ones whose cross-section magnitude is lesser, till all the traps are emptied. The output in LW-OSL is therefore in the form of distinct peaks as a function of read-out time. It also helps to deconvolute the overlapping peaks from different OSL traps in the sample **[47]**.

1.3.5. Pulsed optically stimulated luminescence (POSL)

This technique is based on DOSL, wherein the stimulation is provided by light of short pulses (order of hundreds of nanoseconds) with the frequency of thousands of Hertz. The pulses are produced by repeatedly switching on and off the stimulation source. The pulse width and the frequency are chosen according to the lifetime of the luminescence. Generally, the pulse widths are much less than lifetime of OSL emission. The OSL emission is usually measured between the stimulation pulses. The detector is blocked during the stimulation and hence the detection of the emitted OSL signal and the stimulation are separated by time discrimination. POSL technique has been successfully demonstrated for the use of α-Al_2O_3:C in radiation dosimetry **[12]**.

1.3.6 Photo-transferred optically stimulated luminescence (PTOSL)

PTOSL is a technique employed to utilise stable deeper traps for radiation dosimetry. In this technique, the charge carriers are transferred from deeper traps to obtain a luminescence signal **[48, 49]**. This involves first emptying up the main OSL traps in the pre-irradiated sample. This is followed by illumination by a proper wavelength light to evict the charges from deeper traps to produce a light signal. This can either occur by direct radiative recombination or via shallower traps as intermediates.

1.3.7 Cooled optically stimulated luminescence (COSL)

This was introduced by Miller *et al.* **[50]**. COSL is a material specific technique and cannot be generalised **[51]**. The sample kept at very low temperatures (e.g., liquid N_2 temperature) is heated to room temperature. This is followed by irradiating the sample to a known dose. The optical stimulation is then carried out at a low temperature. The low temperature optical stimulation populates the empty shallow traps by charge transfer from the traps which was already filled due to irradiation. These shallow traps release the charge carriers while attaining room temperature and their recombination produce a dose-dependent light signal called COSL. It is vital technique that can be employed for TLD readout without heating a TLD.

1.3.8 OSL materials for radiation dosimetry

The basic criteria for materials selection for OSL application are more or less same as that of TL. There are OSL materials for personnel as well as industrial radiation dosimetery. The concept of tissue equivalence is relevant in case of personnel dosimetry using OSL also. The OSL materials can be further subdivided into two categories viz., (i) synthetic and (ii) natural. Carbon-doped alumina is a synthetic OSL material, which has found wide speard accetance as it satisfies most of the prerequisites for personnel radiation dosimetry. The following section presents a brief discussion on the merits and demerits of different types of OSL materials used for radiation dosimetry.

(i) Al_2O_3

As it was mentioned earlier, nature has bestowed Al_2O_3 (alumina) with unprecedented properties such as high chemical and radiation stability (high melting point), and wide forbidden gap (9.5 eV). The wide band gap supports the formation of different types of point defects which facilitate trapping of charges leading to color centres. These are important properties for exploring its potential towards dosimetry applications. In addition, it has high abundance also. These attributes have prompted researchers to develop a variety of OSL dosimeters based on Al_2O_3 and its substituted derivatives. Out of several alumina based materials, Al_2O_3:C has been demomonstrated as an ultra-sensitive TLD material, but it suffered a setback as it is susceptible to daylight leading to erasing of the radiation-induced information in the lattice. However, this problem can be circumvented to a great extent by a controlled high temperature quenching which leads to sharp reduction in its daylight sensitivity. There are other options also like using high heating rates while performing TL readout measurements, and UV-induced TL sensitivity **[52]**. The erasing of the dosimetric TL glow peak of the irradiated Al_2O_3:C on exposure to light provides insights into mechanism of TL peak and an OSL signal with acceptable fading. It was observed that the main luminescence produced by the F centers has a lifetime of about few tens of ms **[23]**, and this facilitated the extension of this material for POSL technique **[45]**. It is evident from literature that Al_2O_3:C attracted attention all over the world, which resulted in development of different cost-effective synthesis protocols. These efforts led to facile availability of this material **[53, 54]**. In addition to carbon doping, several other dopants such as Si, Ti, etc. in Al_2O_3 could also be incorporated. However, OSL results were not encouraging **[55, 56]**.

In view of aforementioned sensitivity of Al_2O_3:C towards daylight, it is required to fabricate a light-tight packing of dosimeter based on this material. This further necessitates readout and handling of Al_2O_3:C based dosimeter in faint light to avoid uncontrolled erasing of stored information. As reported by West *et al.***[57]**, there are two antagonistic effects of exposure of Al_2O_3:C based dosimeter to sunlight namely (i) erasing of the radiation-induced stored dosimetric information and (ii) generation of optical signal induced by sunlight exposure. If enough precautions are not taken, it may lead to a compromise on quality of the information generated using Al_2O_3:C based dosimeter. It has also been observed that there is slight irreproducibility in the properties of Al_2O_3:C prepared batch to batch from a single crystal of Al_2O_3:C, which can plausibly be attributed to different carbon contents in Al_2O_3 **[58]**.

OSL response varies as an inverse function of LET of radiation, which is correlated to the charge, mass and energy of a high-energy charged particle (HCP). Commonly a decrease in efficiency of OSL process is attributed to inhomogenous profile of the physical events created by the charged particles' path which produces various radiation induced effects in a material along the vicinity of a track formed by interaction of charged particle **[59, 60]**.

(ii) BeO

BeO consists of low atomic number elements and hence satisfies the tissue equivalence condition and in turn a promising OSL material. Its low cost and abundance are other attractive features. However, BeO is still not as popular as Al_2O_3 based materials for OSL applications due to its relatively poor sensitivity and chemical toxicity. Despite these odds, BeO has been in use as a personnel TL dosimeter **[61]** in Italy. It is well known that the chemical toxicity of any material, in fine powder or dust form, can be considerably reduced by compaction followed by sintering. The apprehension of BeO toxicity was also overcome by using well-sintered discs of BeO which can be easily handled with almost no health hazards. BeO has a unique combination of properties such as high electrical insulation and high thermal conductivity, exceptional thermal stability etc. **[62]**. It has been found that there is no correlation between intense TL glow peaks and the OSL signal which implies that the origin of TL and OSL in BeO is different **[48]**.

In BeO, the main dosimetry TL glow peak is at 220°C whereas the OSL signal is characterized by a blue-green (420-550 nm) light stimulation, which remains unchanged irrespevtive of the presence or absence of TL peak **[48]**. Impure samples of BeO were found to exhibit a much superior sensitivity as compared to the pure samples **[25]**, which implies that the inadvertent impurities act as activators. Thus there is a need to engineer incorporation of suitable impurities in BeO lattice.

(iii) Other OSL sensitive materials

In addition to Al_2O_3 and BeO, there are several other OSL materials such as MgO, Mg_2SiO_4:Tb, $LiAlO_2$:Tb, and several other activated silicates **[63].** Similar to Al_2O_3 and BeO, MgO has very high thermal stability and near tissue equivalence. Tb-doped MgO has shown OSL signal on irradiation to ionizing radiation **[64]**. In view of its near tissue-equivalence, MgO:Tb has the potential for OSL dosimetry and continued research efforts are need of the hour to exploit this material. Masson *et al.* **[65]** have reported the OSL sensitivity of Tb-activated silicates and aluminates.

Several inorganic fluorides are also being contemplated for OSL applications. The OSL sensitivity of $KMgF_3$:Ce **[66, 67]** was found to be about one order higher than that of commercial Al_2O_3:C. However, this materials has inherent disadvantages such as high self-dose (~1.5 μGy/h), attributed to the natural abundance of the ^{40}K isotope, and non–tissue equivalence ($Z_{Eff.} = 14.7$). $NaMgF_3$:Ce has shown OSL sensitivity comparable to that of Al_2O_3:C for its UV (280 nm) emission for a stimulation by blue LED. However, this material suffers from fading during post-irradiation storage or transport **[66]**.

Among the ABF_3 fluorides, a new development of $NaMgF_3:Eu^{2+}$ has been reported by Dotzer *et al.*, **[68]**. The replacement of activator Ce^{3+} by Eu^{2+} (0.2%) appears to have considerably improved the characteristics of the $NaMgF_3$. It exhibited a linear dose response with the lowest detection limit of 130 nGy. Its post-irradiation fading during storage could be minimized by optimizing post-synthesis thermal treatments (sintering and quenching temperatures).

Ammonium salts such as thallium-doped NH_4Br and $(NH_4)_2SiF_6$ have been found to exhibit significant OSL with detectable signals for doses as small as 5 μGy, **[69]**, however the OSL signals of these materials fade very fast during storage even at room temperature. Among alkali halides, the OSL of KCl and KBr have made some noticeable impact. KBr:Eu was found to exhibit about ten times higher OSL sensitivity and smaller fading than KCl:Eu **[70]**. But both KCl:Eu and KBr:Eu suffer from self-irradiation due to the natural abundance of ^{40}K, which limits their applications.

Yttrium aluminum garnet, $Y_3Al_5O_{12}$, (YAG) is a well known laser material **[71]**. By doping carbon to YAG, Kulkarni *et al.* **[72]** had developed an OSL material ($Y_3Al_5O_{12}$:C). The samples prepared in the presence of a graphite liner (under high vacuum) exhibited intense OSL. A linear dose response in the range 10 mGy to 100Gy was observed in YAG:C sample. The most attractive feature of $Y_3Al_5O_{12}$:C is absence of fading even after two months of post-irradiation storage. However, YAG does not satisfy the tissue equivalence criterion.

1.3.9. Radiation dosimetry under accidental conditions

Radiation dosimetry under accidental conditions does not rely on regular dosimetery materials. In several radiation accidents, including Hiroshima and Nagasaki and Chernobyl, common materials like bricks and other building materials have been used for dose assignment. There has been growing concern for the estimation of radiation doses for members of public in the event of a radiological accident. It is difficult to meet such unforeseen requirments by regular radiation dosimeters, which are suitable only for normal situations. Evaluation of the doses under the accident conditions is carried out by using common objects made of ceramics. To measure much smaller doses as quickly as possible, work was initiated to exploit some of the commonly used items for establishing their OSL sensitivity **[73]**. Several OSL sensitive electronic components have been reported which facilitate faster measurements. Of late, mobile phone components and electronic components of ID cards have been evaluated for this purpose as these are carried by most individuals all the time **[74]**. In the event of unforeseen situations, the OSL measurements and dose assignment can be arrived at using the electronic components of gadgets of everyday use.

1.4. Plan of the present work

Significant progress has been made in the field of optically stimulated luminescence and thermoluminescence not only in understanding the phenomenon but also in developing new techniques and materials. Since the Photomultiplier tubes can efficiently detect even very feeble light signals, it is possible to monitor TL process in all its finest details. As a result TL has become a technique of choice for detection of radiation as well as for characterization of defects **[19]**.

In the case of OSL, its applications are no more limited to a particular area like archaeological and geological dating. Commercially available OSL systems have already become very popular for personnel dosimetry, environmental monitoring, space dosimetry, and medical physics. Compared to the other available systems such as plastic scintillation dosimeters, diode detectors etc., OSL has specific advantages in various clinical applications. At this point of time, Al_2O_3:C is widely used in all OSL applications, mainly because of its very high sensitivity; but research is still going on for the development of new materials with better characteristics.

The present thesis has its focus on creation and management of defects in hitherto unexplored materials like $MgAl_2O_4$:C to see their PL, OSL and TL sensitivity and the defects responsible for these phenomena, so that they can be developed as potential dosimetric materials. Detailed studies also undertaken to understand the deep insight into defects present in Al_2O_3.

Chapter 2

Experimental

2.1 Introduction

$MgAl_2O_4$ possesses a rare combination of valuable properties such as high strength at elevated and normal temperatures, thermal shock resistance, high chemical inertness. Hence it has been considered as an important material in various fields **[75]**. The crystal structure is face centred cubic lattice of oxygen with Mg^{2+} ions in tetrahedral sites and Al^{3+} ions in octahedral sites. Eight molecules form the unit cell with 64 tetrahedral and 32 octahedral sites. One eighth of tetrahedral sites are occupied by Mg^{2+} ions and half of octahedral sites are occupied by Al^{3+} ions. But synthetic $MgAl_2O_4$ shows 30% antisite defects which is due to interchange of divalent and trivalent ions on octahedral and tetrahedral lattice positions **[76, 77]** which lead to creation of defect centres. Hence electrons and holes produced by radiation can get trapped in these defects and show luminescent properties. The chemical and thermal stability of $MgAl_2O_4$ is as good as that of the promising thermoluminescent material Al_2O_3. The development of Al_2O_3: C has become the turning point in the history of radiation dosimetry and triggered the evolution of mindset of the dosimetry community from TL to OSL **[18]**. When anion deficient Al_2O_3 was grown in presence of carbon, the TL and OSL response was very good even with very low doses. The presence of defect helps the use of compound for a particular application. Studies can identify a set of optimized synthesis parameters which would realize expected performance. These insights can also suggest alternate synthesis pathways for engineering the defects of interest and therefore are an integral part of development of any dosimetric phosphor. The crystal structure consists of oxygen as FCC with Al in octahedral sites and some in tetrahedral sites (antisite defect). This structural similarity encouraged us to try carbon doping in $MgAl_2O_4$ for developing a new phosphor for radiation dosimetry which has been already proved for Al_2O_3.

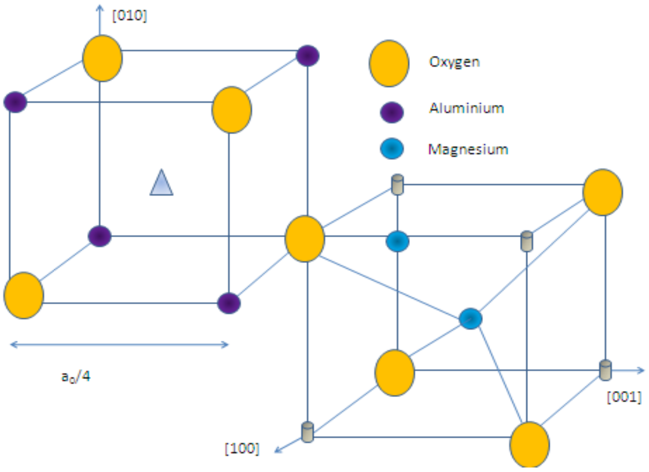

Fig. 2.1 Structure of $MgAl_2O_4$. Mg ions occupy tetrahedral sites while Al ions occupy octahedral sites.The unoccupied tetrahedral sites are represented by (blue) triangles and octahedral sites are shown by the (grey) cylinders.

This chapter deals with the synthesis methodologies, characterization technique and luminescence studies mainly photoluminescence, thermoluminescence, optically stimulated luminescence of $MgAl_2O_4$. An explanation of the nature of defects that are produced and their evolution when plain magnesium aluminate crystals are subjected to a variety of thermal treatments in a strongly reducing composite ambience of vacuum and carbon along with their dosimetric consequences is given. As the major preparation route followed was gel combustion method, the basic principles involved and experimental details are explained briefly.

2.2 Combustion synthesis

In combustion process, redox reaction between an oxidant and a fuel occurs. Generally metal nitrates are used as oxidants and glycine, citric acid etc as fuel. The final product obtained has high phase purity with improved powder characteristics like narrow distribution of particle size, high surface area and better sinterability **[78-81]**. The combustion process occurs in two steps (i) gel formation and (ii) gel combustion. The basic parameters relevant to the combustion process are briefly discussed as follows.

2.2.1 Fuel selection in the combustion process

Any substance which on its consumption provides heat or power is termed as a fuel. The fuel in the combustion process should be able to maintain the compositional homogeneity among the constituents and should undergo combustion with an oxidizer (i.e., nitrates) at low ignition temperature. A large variety of organic materials mainly carboxylic acids can serve as fuel for the combustion process such as citric acid, ascorbic acid, glycine etc. Materials like urea, hydrazine, hexa methylene tetra amine (HMTA) can also be used. One of the most common fuels glycine (NH_2CH_2COOH) is a cheap amino acid, has been used in the present work. It is known to act as a complexing agent for a number of metal ions, as it has a carboxylic acid group at one end and amino group at the other **[82]**. The zwitterionic glycine molecule can effectively complex metal ions of varying ionic sizes and charges. This helps in preventing selective precipitation to maintain compositional homogeneity among the constituents.

2.2.2 Gel formation and combustion

The first step is gel formation in the combustion process which controls the phase purity of the final product, hence very important. In this step, the nitrate salts of the metals of interest are mixed together in required stoichiometry in aqueous media as nitrates fulfil the requirement of oxidant by providing the oxygen for combustion of the fuel. To this solution a suitable fuel is then added in an appropriate amount. The fuel serves the dual purpose of not only providing the heat of reaction during the redox combustion process, but also binding the reacting metal ions so as to bring them in close proximity to one another. This transparent aqueous solution is heated at about 80°C on a hot plate to remove the excess solvent by thermal dehydration because any excess water left behind would lead to a sluggish combustion, deteriorating the phase purity and powder quality. The viscous liquid formed after thermal dehydration is termed as gel and it maintains an intimate blending between fuel and an oxidant necessary for the combustion process.

The gel thus obtained is then subjected to a higher temperature (~ 250°C for glycine) for triggering the combustion reaction, which is self-propagating. As a result of exothermic decomposition of fuel-oxidant precursor, a voluminous powder is formed with a simultaneous evolution of large volume of gaseous products. Depending on the nature and amount of the fuel used in the process, the voluminous product thus obtained may be the desired phase, or a semi-decomposed precursor with a considerable carbonaceous residue. The process of very high exothermicity generation during the combustion in the form of flame or fire is termed as auto-ignition. Since the time for which the auto-ignition exists is rather short (< 10 seconds), the powder is further calcined at temperatures around 600°C to remove the traces of any undecomposed fuel, nitrates and their decomposition products, if any. Hence chemically pure and crystalline product is obtained.

The processes of gel formation and gel combustion can be visualized in a better way in Fig. 2.1 given below. The solution in the beaker after the process of thermal dehydration forms the gel. The gel thus formed, on further heating on the hot plate undergoes auto-ignition characterized by a bright flame which once initiated, rapidly propagates throughout the gel. It is persistent only for a short duration of about 4-5 seconds and the reaction can raise local temperatures upto 1500°C. Within this short duration the product formation as a large voluminous powder takes place.

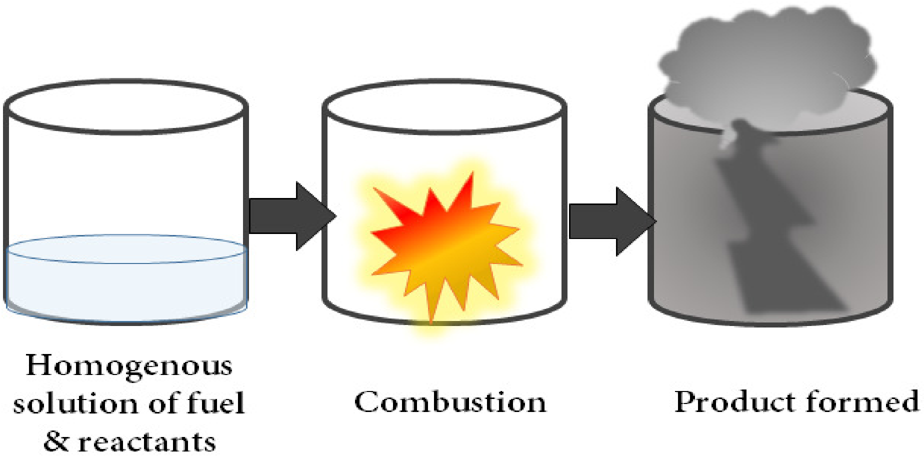

Fig. 2.2 Pictorial representation of gel combustion

2.2.3 Calculation of oxidant-to-fuel ratio based on stoichiometry

The extent of exothermicity associated with the combustion process is governed by the ratio of oxidant-to-fuel used. The oxidant-to-fuel molar ratio has a significant bearing on the product phase as well as the product powder properties. On the basis of stoichiometry, for achieving maximum exothermicity the ratio of oxidizing and reducing valencies should be unity **[78, 83]**. The calculation of these valencies and the ratio satisfying this concept is explained by means of a typical example of $MgAl_2O_4$. The oxidizing valencies calculated for oxidants in this case viz., Magnesium nitrate, $Mg(NO_3)_2.6H_2O$ and aluminum nitrate $Al(NO_3)_3.9H_2O$ are 10- and 15- respectively,whereas the reducing valency of the fuel glycine is 9+.

The oxidizing and reducing valencies were calculated as follows:

i). $Mg(NO_3)_2.6H_2O$: (oxidizing valency of Mg = 2^+, N = 0)

(reducing valency of O = 2^-)

Thus the net oxidizing valency = 10^-

ii). $Al(NO_3)_3.9H_2O$: (oxidizing valency of Al = 3^+, N = 0)

(reducing valency of O = 2^-)

Thus the net oxidizing valency of two molecules of $Al(NO_3)_3.9H_2O$ = (2 x 15^-)30^-

iii). NH_2CH_2COOH : (oxidizing valency of N = 0, H = 1^+, C = 4^+)

Thus the net reducing valency = 9^+

As C and N are lost as CO_2 and N_2, respectively, during the combustion process the valencies of C and N are taken as 4+ and 0 **[82]**. The propellant chemistry ratio of oxidizing-to-reducing valencies 1:1.66. The oxidant-to-fuel ratio less than that of 1.66, is termed as the fuel-deficient ratio and any ratio greater than 1.66 is termed as fuel-rich ratio.

2.2.4 Advantages of the gel combustion process

The preparation of the precursor is advantageous since it prevents the random redox reaction between a fuel and oxidizer and thus reduce the possibility of local variations in the characteristics of the combustion-synthesized powder. Also, the gel precursor provides short diffusion paths due to the atomistic level blending of the constituent elements in the required stoichiometric ratio and facilitates the required phase formation during combustion.

In the second step of the combustion technique, the exothermic decomposition of the gel precursor occurs. Here, due to the auto-decomposition of the fuel and oxidant, the final product is mostly free of reactants. Hence, the process does not need any further processing of the precursor. Auto-ignition exists only for a few seconds, and in most of the cases, the required phase is produced within this time as the heat of combustion generated is sufficient. Hence, the combustion technique can be considered as time saving, low temperature method of synthesis.

2.2.5 Precautions to be taken during combustion

As combustion is a spontaneous and vigorous process, a large amount of heat is released in a very short duration and hence a few precautionary measures are necessary while performing the process.

(i). The large swelling of viscous precursor, the large volume of gaseous products eliminated and the high exothermicity can cause explosion if the reaction takes place in a narrow opening container instead of a wide mouthed apparatus.

(ii). It is better to conduct the combustion reaction in a fume hood as it gives safe ventilation of the gaseous products and hence any kind of damage to the surrounding environment or the experimenter can be avoided.

(iii). The combustion synthesized powders are very reactive, due to their high surface area. To avoid any attack of atmospheric gases and moisture, the right conditions of calcinations (e.g. time and temperature) and proper storage are necessary.

2.3 Synthesis of $MgAl_2O_4$

Synthesis of $MgAl_2O_4$ was carried out by gel combustion process **[76, 84, 85]**. The starting materials were magnesium nitrate, $Mg(NO_3)_2.6H_2O$ and aluminum nitrate $Al(NO_3)_3.9H_2O$. In minimum amount of nitric acid,the stoichiometric amounts of reactants such as $Mg(NO_3)_2.6H_2O$ and aluminum nitrate $Al(NO_3)_3.9H_2O$ were weighed and dissolved one by one. The fuel used was glycine, NH_2CH_2COOH. An appropriate amount of glycine corresponding to 40% of that required for stoichiometric combustion was taken. It was weighed and dissolved in the same solution by slow heating. The solution was evaporated continuously and slowly till a gel was obtained. At this point, the temperature of hot plate was suddenly raised leading to auto-ignition. Due to ignition an exothermic self-propagating reaction occurred and voluminous powder was obtained as product. During combustion the beaker was covered with an aluminum foil and the reactants were mixed thoroughly using a glass rod for complete reaction of the fuel and the reactants.Finally, the product was taken in motor and pestle and dry ball milled for 1 h.

The chemical equation of synthesis can be expressed as:

$$\mathbf{2NH_2CH_2COOH + Mg(NO_3)_2{\cdot}6H_2O + 2\ Al(NO_3)_3{\cdot}9H_2O \rightarrow MgAl_2O_4 + 29H_2O\uparrow + 5N_2\uparrow + 4\ CO_2\uparrow + O_2\uparrow}$$

The powder thus prepared was calcined at 600°C for 4 h in order to remove carbonaceous impurities. The product was then sintered at 1100^{o}C for 10 h to obtain the desired well crystalline product and to remove any impurities. These impurities have detrimental effect on residual TL/OSL signal **[75]**, and hence need to be removed.

2.4 X-ray diffraction (XRD)

X-Ray Diffraction (XRD) is a tool used for qualitative analysis and structure determination of crystalline materials, in which the crystalline atoms cause a beam of incident X-rays to diffract into many specific directions. Diffraction is the slight bending of light as it passes around the edge of an object or through a slit. Depending on their phase difference, the diffracted beams can interfere with each other giving bright or dark fringes in the shadow region. As the crystal lattice consists of parallel rows of atoms equivalent to the parallel lines of the diffraction grating, the inter-planar spacing could be successfully determined from the separations of bright fringes of the diffraction pattern formed due to constructive interference, using the classical Bragg equation.

$$n\lambda = 2d\sin\theta \qquad \text{……………………………………}\mathbf{[2.1]}$$

where λ = wavelength of x-rays

θ = glancing angle (called as Bragg angle)

d = inter planar separation

n = order of diffraction

Cu Kα X-rays, are the most frequently used source in XRD studies. When the K shell of Cu is filled by transition of electron from the L shell characteristic X-ray is emitted. Being electromagnetic waves, X-rays interact with the electron cloud of the atom. Due to the interaction with the fluctuating electric field of x-rays, the electrons of the atoms vibrate in the same frequency and emit radiation of the same frequency. Thus, the incident radiation appears to be scattered by the atoms in all the directions.

The X-ray diffraction experiments can be carried out either from single crystals or from polycrystalline samples. The polycrystalline samples synthesised by gel combustion method were characterised using powder x-ray diffractometer. The instruments and procedures of the common powder diffractometers are explained in the following sections.

2.4.1 Powder XRD instrumental details

A block sketch of the typical powder diffractometer which consists of a source of x-rays and the detector for the detection of diffracted x-rays is shown in Fig. 2.2. Among the different varieties, the most common laboratory diffractometers use sealed tube x-ray source. The x-rays are produced by bombarding high-speed electrons on a metal target, where a part of the electron energy is used in producing the x-ray beam. Hence produced x-ray beam is a combination of a continuous radiation with several intense spikes, which are characteristics of the target elements (called characteristic radiation). The sharp fixed wavelength radiations are most commonly used in the diffraction instruments (angle dispersive). Out of the total electron energy, a very small fraction is used for the production of x-rays and the rest is lost in heating the target element. Thus, the target element has to be cooled continuously during the operation. Using a Be window, the x-rays emitted in all the directions are allowed to escape from a particular direction. β-filter helps to filter the background and β-radiation. After passing through the soller and divergence slits, the x-rays are allowed to fall on the sample.

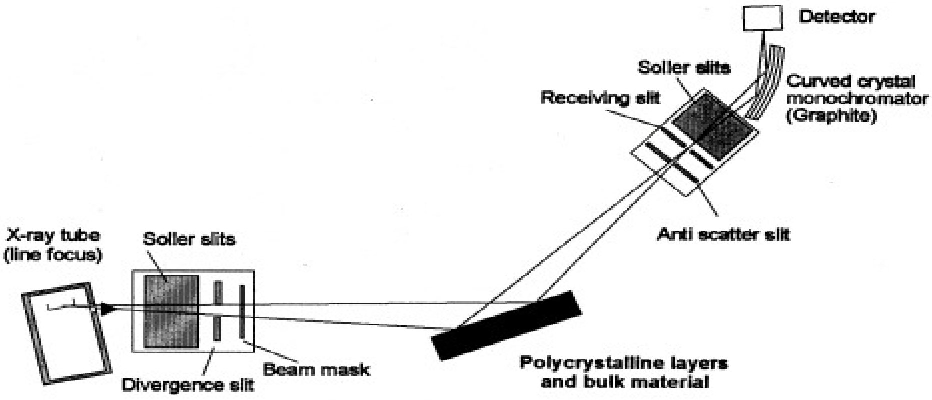

Fig. 2.3 Ray diagram of a typical reflection mode diffractometer **[86]**

The fine grains of sample are generally spread uniformly over a rectangular area of a glass slide using binders like collodion or grease or wax. The amount of sample used for exposure is decided by the scattering power of the elements, absorption coefficient and the amount available. Good scattering and sharp diffraction lines are usually shown by crystalline sample.

The x-rays scattered (diffracted) from the sample are collected either on a film or counters such as gas filled tube or scintillation counters. The gas filled tubes can be a proportional counter or Geiger-Muller counter. The gas which is filled in the tube gets ionized on interaction with radiation. The ions are collected by applying a potential difference between the two electrodes and the current obtained is proportional to the number of photons reaching the detector.

By sweeping the detector from one angle to the other, the diffracted rays are scanned and at the angle where the Bragg's law is satisfied, a constructive interference among the diffracted x-rays occur which results in the sharp rise in the intensity (peak). The counts of the x-ray photon are measured at different angles and a plot of the intensity of diffracted x-rays versus angle is obtained as output.

The peak positions are related with the unit cell parameters of the lattice which gives a set of d-values obtained due to constructive interference. Hence the d-values can be calculated as the inter-planar spacing d_{hkl} between the set of parallel planes which represents the peak position. A particular sample gives a characteristic set of d-values and hence they can be used for identification of the materials. The absolute intensities of the reflections depend on the nature and kind of distribution of atoms in the unit cell as well as on the source intensity and counting time.

2.5 Creation of defects

The entry of extraneous atoms into the crystal structure of the host material creates point defects. In alkali-halides and alkaline earth oxides, F centres are produced by heating the material in the vapour of its metal constituents. Due to the high defect creation energy, low mobility of oxygen vacancies and inadequate Al vapour pressure, this technique of creation of defects however did not produce expected results in case of Al_2O_3. Lee and Crawford heated Al_2O_3 crystals in a graphite tube to a temperature as high as 2000°C in flowing Argon. Heating was carried out in vapour of aluminum and they found that presence of Al did not affect the intensity of 6.1eV whatsoever **[87]**. From this they concluded that 6.1 eV band was not because of the presence of aluminum, but due to the presence of oxygen vacancies. According to them oxygen vacancies were generated because of the extraction oxygen by reducing environment provided by graphite tube and flowing Argon used during heating of alumina crystals. This process later on was renamed as subtractive coloration. This work **[87]** revealed that unlike the oxygen vacancies created by high energy particle bombardment, these thermo-chemically created ones were very stable against thermal annealing. Another very important observation of this paper is that this method is quite precise about the nature of defects it produces. According to the authors (Lee and Crawford) it creates deep traps only in small concentration. Except F, F^+ and F type clusters do not produce other complicated defects like interstitial oxygen clusters. These results implied that creation of thermally stable oxygen vacancies is possible if alumina crystals are annealed in graphite at 2000°C. These results also conveyed the message that reducing environment is an effective tool to create oxygen vacancies into the crystals of alumina. Later it was experimentally confirmed that annealing of Al_2O_3 crystals even at low temperatures in vacuum can cause formation of oxygen vacancies. Kulkarni et.al have developed a new method for the synthesis of Al_2O_3:C which devised a synergetic combination of vacuum and graphite ambience. This newly developed method is called Vacuum Assisted Post growth Thermal Impurification (VAPTI) **[53]**.

2.6 Carbon as a dopant

It is an accepted fact that, the intentionally provided strongly reducing ambience of carbon during growth of alumina crystals causes formation of a large number of oxygen vacancies in the structure of alumina. F centres are formed when these vacancies are occupied by two electrons. Along with extraction of oxygen it is understood that Al^{3+} is substituted by C^{2+} which is accompanied by formation of compensating F^+ centres **[12]**. F^+centres are vacancies occupied by a single electron and they act as recombination centres. This is the reason for the high sensitivity of α-Al_2O_3: C. On the basis of this hypothesis, the experimentally observed emission at 420 nm can be explained. Thermally or optically released electron with F^+ centre can form an excited F centre which under goes radiative relaxation at 420 nm. Or otherwise, the F centres may recombine with thermally released holes resulting in the formation of F^+ centres, which during the process of relaxation emit at 330 nm or transfer energy to F centres causing emission at 420 nm **[88-90]**. The structural similarity of magnesium aluminate with alumina gave us the idea to follow the same methodology for developing a new dosimetric material by carbon doping.

2.6.1 Doping of carbon by electron gun method

An electron gun of an evaporation system, shown in Fig.2.3, which is normally used for vacuum evaporation of thin films, was employed, as a means to attain temperatures high enough that would melt $MgAl_2O_4$ in the presence of graphite.

For this purpose, the $MgAl_2O_4$ powder pressed into pellets has been used. The pellets were sintered at 1100°C for 10h. Subsequently, the pellets were placed in graphite crucible of ~20 mm diameter and 11.5 mm height, of an electron gun system (Hind High Vacuum make Model:EBG-PS-3 K). The pellets were slowly heated with electron beam till it gave hot white glow. Approximately 10 minutes of continuous irradiation raises the temperature near the melting point of the sample and this helps the incorporation of carbon impurity in host lattice. Subsequently, the material was cooled to room temperature in 5 min. The material so obtained was characterized for its optical and dosimetric properties. The material prepared without the use of graphite liner did not show good response in either TL or OSL modes. This type of samples in further discussion will be referred as sample (A).

Fig. 2.4 Electron gun evaporation system **[18]**

Fig. 2.5 Photograph of carbon doped $MgAl_2O_4$ sample

2.6.2 Doping of carbon by using graphite furnace

In this method, a stack of sintered pellets of polycrystalline magnesium aluminate powder weighing ~50 g was placed in a graphite crucible and then melted in high temperature vacuum induction furnace depicted in Fig. 2.5. The furnace is made up of graphite crucible kept in a core of Cu coil for inductive heating. The continuous monitoring of temperature change in the furnace was done by pyrometer based temperature measurement system. The $MgAl_2O_4$ pellets were heated up to 2100°C with 20°C/min and maintained at 2100°C for 50 minutes and then cooled to room temperature with same rate. This results in increase of conductivity of material and thus allows the carbon impurity pathway incorporation in host material. In this thermo-chemical synthesis process, the oxygen vacancies are created in strong reducing graphite environment. Here also, the X-ray diffraction studies of thus developed $MgAl_2O_4$:C show no significant difference from pure $MgAl_2O_4$. The samples thus obtained will be referred as sample B in further discussion.

Fig. 2.6 Inductively heated vacuum melting system **[18]**

The processed $MgAl_2O_4$ phosphor was characterized using thermoluminescence (TL) and optically stimulated luminescence (OSL) techniques. The fading studies on the processed $MgAl_2O_4$ material showed negligible fading in both TL and OSL domain for a period of 3 weeks when compared to its TL and OSL output after 24 hours of exposure. The processed material showed very good linearity in the range 20 mGy to 100Gy.

Quantitative carbon analysis using CHN analyser was done for both the samples and was found in ppm level (~500ppm).

2.7 Thermoluminescence and optically luminescence studies

Dosimetric properties of the samples by the two methods were studied using thermoluminescence (TL) and optically stimulated luminescence (OSL) techniques. In order to record the TL response, the samples were irradiated using a calibrated ^{60}Co gamma source. Using a programmable TL reader system, heater assembly TL was recorded at a constant heating rate of 4°C/s **[91]**. Laboratory made OSL reader system **[92]** based on diode pump solid state laser light stimulation (470 nm) was used for recording continuous wave OSL (CW-OSL) on the samples. The laser power delivered at the sample position was adjusted to~50 mW/cm^2 by measuring the light intensity at the sample position using commercially available laser power meter (Make: Ophir). Any prior irradiation all samples were optically bleached for with 470 nm light intensity ~100 mW/cm^2 for 30 minutes. The developed phosphor samples were separated according to their particle size. After separation, it was fixed on stainless steel (SS) disc (8 mm dia. 0.6m thick) with non-reacting silicon adhesive with measured mass. The silicon adhesive was tested for possible TL/OSL sensitivity. They have not shown any TL/OSL response for any applied radiation doses. Therefore, possibility of TL/OSL interference from the adhesive is being completely overruled in further studies.

2.8 Photoluminescence

Photoluminescence is the phenomenon of generation of luminescence by excitation of a molecule using ultraviolet or visible light photons. Depending upon the electronic configuration of the excited state and the emission pathway it is divided into two categories as fluorescence and phosphorescence. Atoms and molecules after absorbing light at a particular wavelength subsequently emit light of longer wavelength after a brief interval called fluorescence. Phosphorescence occurs in a manner similar to fluorescence, but with a much longer excited state lifetime.

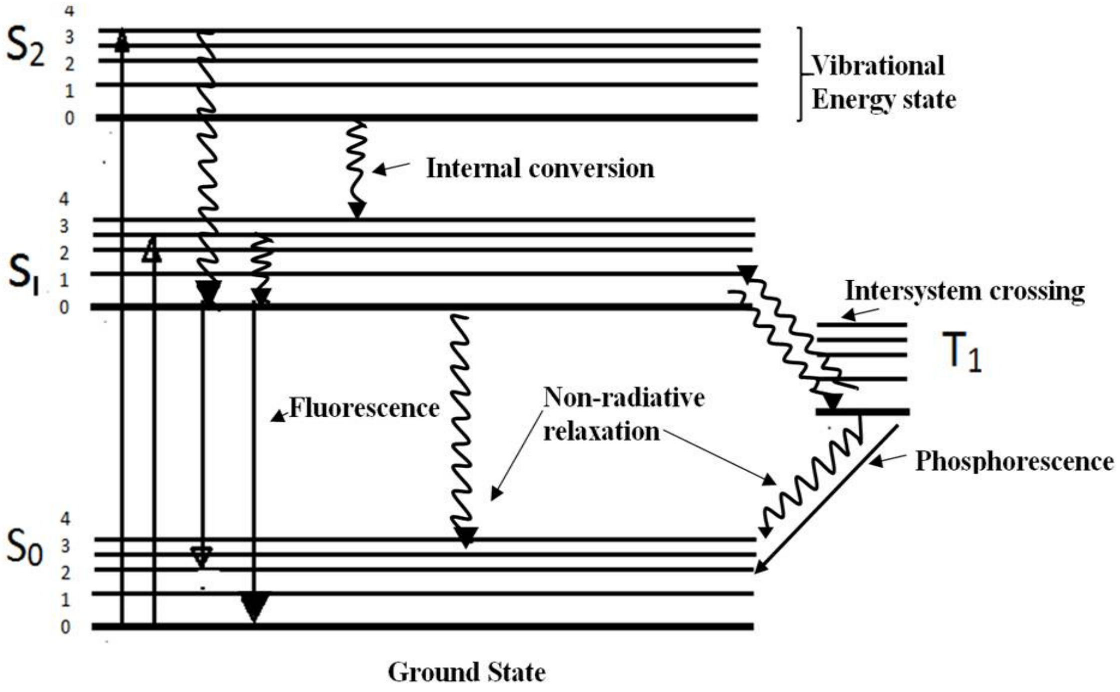

Fig. 2.7 Jablonski diagram

The various energy levels involved in the absorption and emission of light are presented by a Jablonski energy diagram (Fig.2.7).The singlet ground (**S_0**) state, the first (**S_1**) and second (**S_2**) excited singlet states and the triplet (**T_1**) state have been shown as a stack of horizontal lines. The thicker lines in the figure represent electronic energy levels, while the thinner lines denote the various vibrational energy states. Transition associated with absorption or emission of a photon is illustrated using straight arrow and molecular internal conversion or non-radiative relaxation process using wavy arrows.

2.8.1 Photoluminescence spectroscopy

Photoluminescence spectroscopy is an analytical technique used to determine emission and excitation spectra and luminescence lifetimes. When the sample is excited by photons in UV range, it releases its excess energy by the emission of light. Using this technique, detection and recording of emission of light by the sample can be done using different modes such as excitation, emission and luminescence decay lifetime. If there is an emission after absorption, the compound will show excitation spectrum which is actually fluorescence detected absorption with the peak intensity directly proportional to the number of photons absorbed. Excitation spectrum is recorded by scanning the excitation wavelength at a single emission wavelength. In the same way for emission spectrum, emission wavelength is scanned at a single constant excitation wavelength. Both, excitation and emission spectra were recorded using spectrofluorometer. The luminescence lifetime decay was recorded using spectrofluorometer with a pulsed excitation source having pulse duration shorter than that of the excitedstate lifetime of molecule and a fast detector.

2.8.2 Instrumentation: Excitation and emission spectroscopy

Sources used for producing light photons include lasers, photodiodes, and lamps. For selectively transmitting light in a narrow range around the specified excitation wavelength, photons were passed through the excitation monochromator. To control intensity and resolution, the transmitted light was again passeed through adjustable slits before passing into the sample. The emitted light enters the emission monochromator after passing through a filter and prevents the excitation light entering the detector and causing second order peaks. For eliminating background signal and minimizing noise due to light, emitted photons from the sample are detected at a 90º angle from the path of excitation light. Before reaching the photomultiplier tube (PMT), the emitted light transmitted again in a narrow range centred on the specified emission wavelength and adjustable slits for optimum intensity and resolution of the spectra. The instrument used for the present studies has a xenon lamp as an excitation source because of its high intensity at all wavelengths ranging upward from 250 nm. The detected fluorescence with photomultiplier tubes is quantified with appropriate electronic devices and output is stored digitally in graphical form. Schematic diagram and photograph of spectrofluorometer are illustrated in Fig.2.7 (a&b).

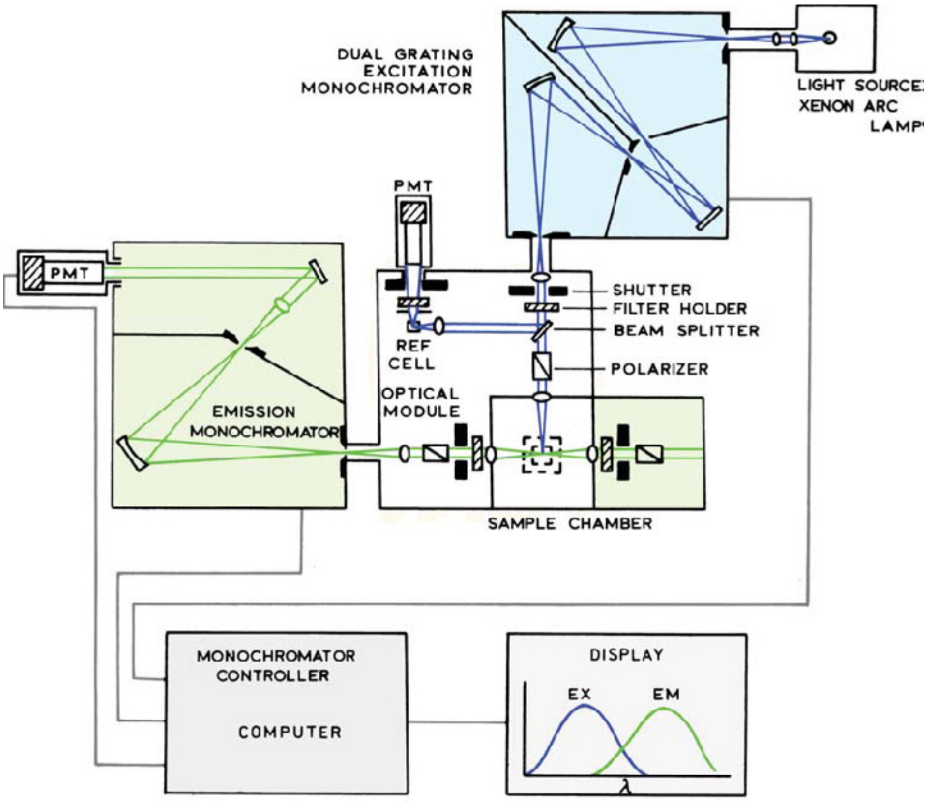

Fig. 2.8 (a) Block diagram of spectrofluorometer **[93]**

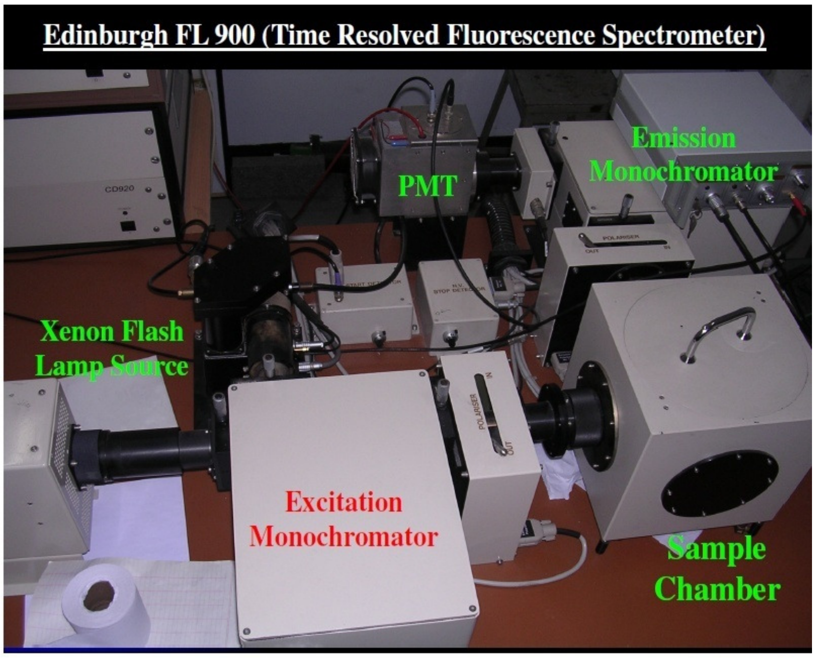

Fig. 2.8 (b) Photograph of the time resolved fluorescence spectrometer **[93]**

2.8.2.1 Excitation spectrum

The excitation spectra of undoped and carbon doped $MgAl_2O_4$ were taken for understanding the defects created in the compound. Two peaks were obtained at 225 nm and 245 nm and could be attributed to the oxygen vacancies (F and F^+ centres) **[94, 95]**. As far as excitation spectra is concerned, both carbon doped samples relative to undoped sample, behaved almost the same.

2.8.2.2 Emission spectrum

The wavelength of maximum absorption is used to excite the compound in order to determine the emission spectrum. The relative intensity of the fluorescence is measured at various wavelengths to plot the emission spectrum.

The emission spectra of undoped and carbon doped $MgAl_2O_4$ powder sample are basically identical to each other irrespective of the excitation energy (225 or 245 nm), showing the common PL peak energy at 460 nm (2.7 eV). This leads to the conclusion that the photoexcitation of the F and F^+ centers results in the same radiative relaxation channel. For confirming the presence of oxygen vacancies, these samples are post-annealed in air at 1200 °C for 15 h and the emission spectrum showed a drastic decrease in the intensity. Doping carbon thermo-chemically using a graphite furnace leads to creation of more anion vacancies which are responsible for enhanced PL emission with a blue shift in Graphite Furnce sample.

2.8.3 Luminescence lifetime

Time-correlated single-photon counting (TCSPC) is a common and well stablished technique for fluorescence lifetime measurements.

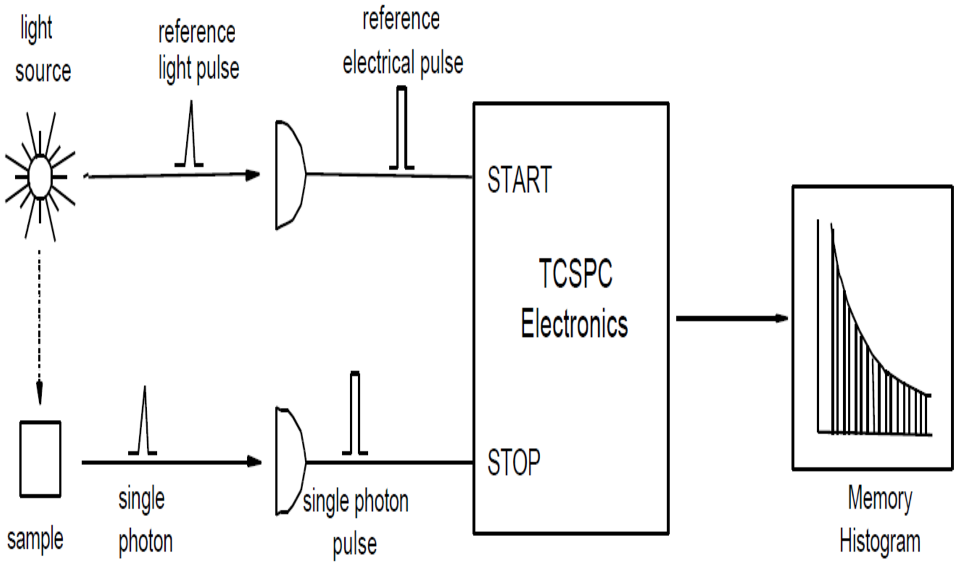

Fig. 2.9 Time-correlated single-photon counting (TCSPC) **[93]**

In TCSPC, using a light source as reference signal, the detection and the arrival time of single photons are measured. TCSPC system is connected and synchronised with detector and light source. Pulsed laser system gives the start signal to TCSPC and the detector gives the stop signal. Illuminated sample sends the fluorescence photon to single photon counting detector. Immediately after detecting the fluorescence photon after excitation, the TCSPC compiles the data and sends to computer. Fluorescence life time measurement was done by noting the time between pulsed excitation and the appearance of first photon. By several time repetition of the excitation emission process a histogram with count versus time is plotted. Most of the photons reaches the detector soon after the excitation pulse hence intensity is high at shorter time interval. As the time increases, there is a drastic decrease in number of photons.

Luminescence lifetime study of carbon doped $MgAl_2O_4$ as well as sintered Al_2O_3 at different temperatures were done and discussed in detail in the coming chapters.

2.9 Conclusions

In this chapter synthesis of polycrystalline samples by gel combustion method was discussed. Doping of carbon by two methods such as electron gun and graphite furnace were discussed briefly. Various characterisation techniques like x-ray diffraction, thermoluminescence, optically stimulated luminescence, photoluminescence were discussed.

Chapter 3

TL and OSL studies of carbon doped magnesium aluminate ($MgAl_2O_4$:C)

3.1. Introduction

Promising optical properties and high thermo-chemical stability have made alumina as a choice of good laser host material. However, relatively low effective atomic number (Z_{eff} ~ 10.2) has generated enough interest for exploring thermo-luminescence (TL) properties of α-Al_2O_3 for potential use in passive radiation dosimetry **[96]**. A significant increase in TL and optically stimulated luminescence (OSL) radiation sensitivity of carbon doped alumina could be observed by some researchers **[53]**. This observed high TL/OSL sensitivity has been attributed to enhanced concentration of F/F^+ centres (identified as basic luminescence recombination centres) along with dosimetric meta-stable charge traps **[97, 53, 88, 98]**. Since then, momentous research has been diverted to the development of new oxide based OSL materials such as YAG:C, $LiMgPO_4$: Tb, B [Lithium Magnesium Phosphate (LMP)], $BaSO_4$:Eu^{2+}etc. **[75, 98-100]**. All these materials have been selected for their good optical/chemical stability along with better radiation damage resistance. $MgAl_2O_4$ is one such material which has considerable radiation resistance **[101]**, chemical inertness, high melting point and good mechanical strength. These properties have led to explore utility of $MgAl_2O_4$ as an optical and insulating material in the radiation field **[102-107]**. In $MgAl_2O_4$, cation antisite defects were produced by Al^{3+} and Mg^{2+} inversion **[108]**. Therefore, Al^{3+} in tetrahedral site can act as an electron trap due to its extra positive charge and Mg^{2+} at octahedral site can act as a hole trap due to lack of one positive charge. When this material is exposed to ionizing radiation, the radiation induced free charge carriers get trapped at pre-existing meta-stable defects site in $MgAl_2O_4$ lattice. The subsequent optical/thermal stimulation of these radiation induced trapped charges (i.e. de-trapping) results in radiative recombination of some charges of the opposite polarity giving rise to luminescence. In case of optical stimulation this luminescence is termed as OSL and in case of thermal stimulation as TL.

Optical absorption of magnesium aluminate spinel single crystals of different compositions $MgO.nAl_2O_3$ (n=1.0 and 2.5) has been investigated after irradiation with neutrons, X-rays and the UV light to elucidate existence of specific absorption bands related to lattice defects **[109]**. The TL and OSL properties of pure $MgAl_2O_4$ were studied by Yoshimura **[101]** along with highlighting the correlation between observed TL/OSL phenomenon in pure $MgAl_2O_4$. In order to investigate TL emission spectrum, the three dimensional TL spectra of $MgAl_2O_4$ exposed to UV light were generated **[110]**. Defect centres responsible for the TL/OSL in $MgAl_2O_4:Tb^{3+}$ have also been investigated by E. Alagu Raja et al. **[76]**. Incorporation of carbon in similar material like alumina has shown remarkable improvement in its dosimetric properties. However, carbon can be incorporated by variety of ways in alumina **[54]**. One of the simplest ways to incorporate carbon is by melting the polycrystalline alumina powder in graphite environment **[54]**. To the best of our knowledge carbon doped $MgAl_2O_4$ and its dosimetric response have not been studied so far. Therefore, it would be of interest to explore the dosimetric properties of carbon-doped $MgAl_2O_4$. Apart from this, $MgAl_2O_4$ also has low effective atomic number (Z_{eff} ~ 11.2) and thus this material is a promising candidate for developing phosphor for TL/OSL radiation dosimetry.

Hence, in the present research work carbon was incorporated in $MgAl_2O_4$ lattice using two different methods. Further the detailed TL and OSL studies on the developed carbon doped $MgAl_2O_4$ have been carried out. These studies will greatly help in the development of $MgAl_2O_4$ based new TL/OSL sensitive phosphors.

3.2. Materials and methods

Synthesis of $MgAl_2O_4$ was carried out by gel combustion process as described in section 2.3. The phase purity of $MgAl_2O_4$ was studied by X-ray diffraction using monochromatized Cu K_α radiation on Panalytical Xpert Pro. The XRD pattern of polycrystalline $MgAl_2O_4$ matches well with that reported in literature (JCPDS Card No. 77-0437). X-ray diffraction pattern of $MgAl_2O_4$ synthesized in the present study is shown in Fig. 3.1.

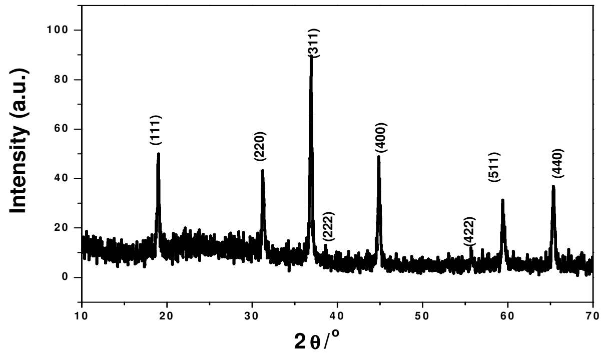

Fig. 3.1 XRD pattern of developed un-doped $MgAl_2O_4$ sample.

For incorporation of carbon, the $MgAl_2O_4$ powders were pressed into pellets and used for further processing. The carbon-incorporation may lead to increase/modification of metastable TL/OSL defects. Doping of carbon by Electron Gun method and by graphite furnace was done as described in section 2.6.1 and 2.6.2 respectively. The processed $MgAl_2O_4$ phosphor was characterized using thermoluminescence (TL) and optically stimulated luminescence (OSL) techniques as described in Section 2.7.

3.3. Results and discussion

The TL/OSL studies are tools detecting meta-stable charge trap defects in semiconductor insulator materials. Each TL peak in TL glow curve is associated with individual meta-stable trap defects. Therefore, presence of multiple TL glow peaks is an evidence of presence of the multiple charge traps levels in materials. On other hand, the study of OSL active traps gives photo-ionization cross-section (PIC) associated with meta-stable traps. Hence, it is important to study the TL/OSL characteristic of developed un-doped/doped $MgAl_2O_4$ for generating useful initial TL/OSL parameter data. This will help in further improvement of the radiation dosimetric characteristic properties of $MgAl_2O_4$:C.

3.3.1. Thermoluminescence (TL) studies of pure and carbon doped $MgAl_2O_4$

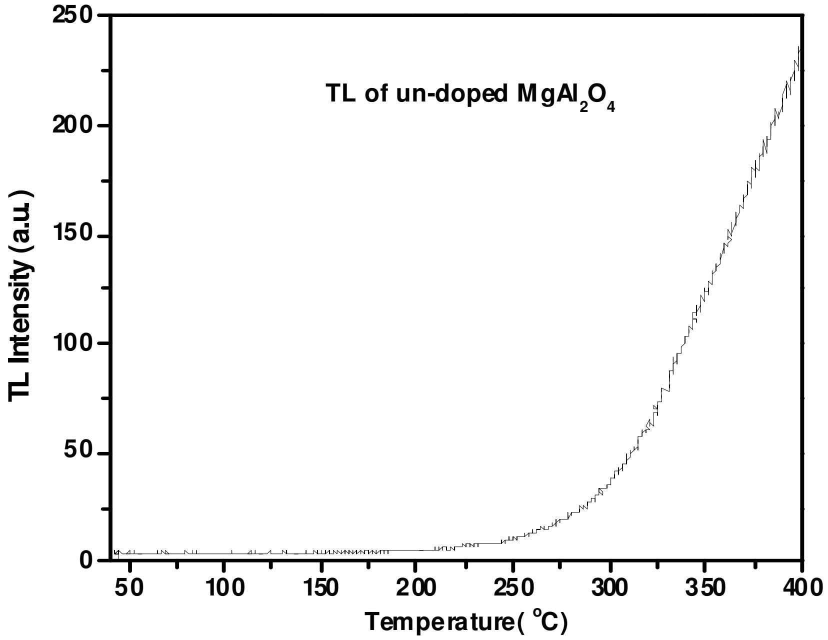

Fig. 3.2 TL glow curve of un-doped $MgAl_2O_4$ for 10Gy absorbed dose and 4K/s heating rate.

Fig.3.2 shows the TL intensity of undoped polycrystalline $MgAl_2O_4$ taken for 10Gy absorbed dose. The infrared/blackbody radiation background from heated sample is being appropriately subtracted from recorded TL signal. The TL glow curve generated was found to increase in the TL intensity from 150°C to 400°C. But this increase in the TL intensity with temperature fails to give any distinguished prominent TL glow peak structure. This TL like observation may be due to high temperature (> 400°C) overlapping TL glow peaks (which cannot be recorded on present TL/OSL reader). Doping of impurity introduces a new set of defects or simply alters the pre-existing defects. Considering these facts along with the TL defects observations from carbon doped meta-stable trap defects in pure Al_2O_3, an attempt was made to incorporate carbon as an impurity in $MgAl_2O_4$.

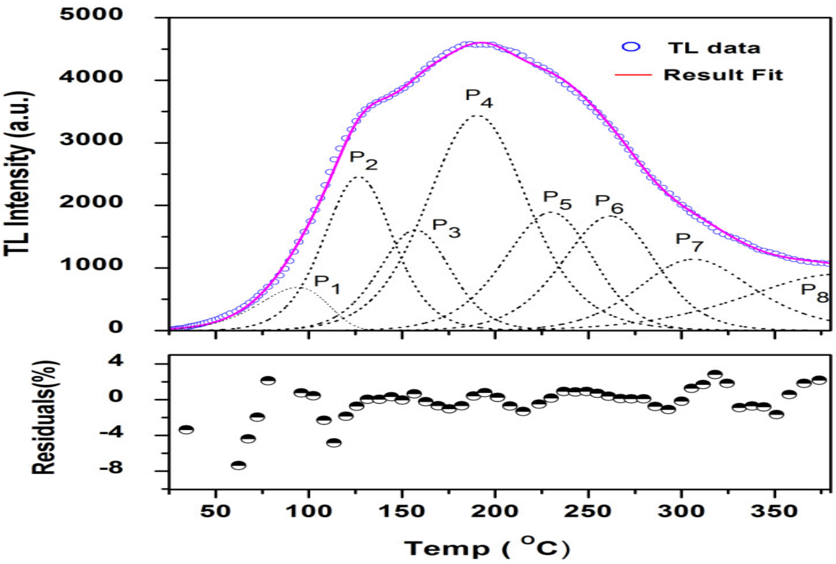

Fig. 3.3 Typical TL glow curve recorded of carbon doped electron gun sample A for 600 mGy absorbed dose at 4K/s heating rate. The simplified Gaussian individual TL peaks fitted to experimental data and red line is resultant fit.

Carbon may be suitably incorporated in host lattice of $MgAl_2O_4$, due to its favourable oxidation state and ionic size considerations. The carbon doping indeed has helped to produce relatively shallow traps as compared to un-doped $MgAl_2O_4$. This has got reflected by TL peaks position in temperature domain as shown in Fig.3.3 and Fig.3.4.

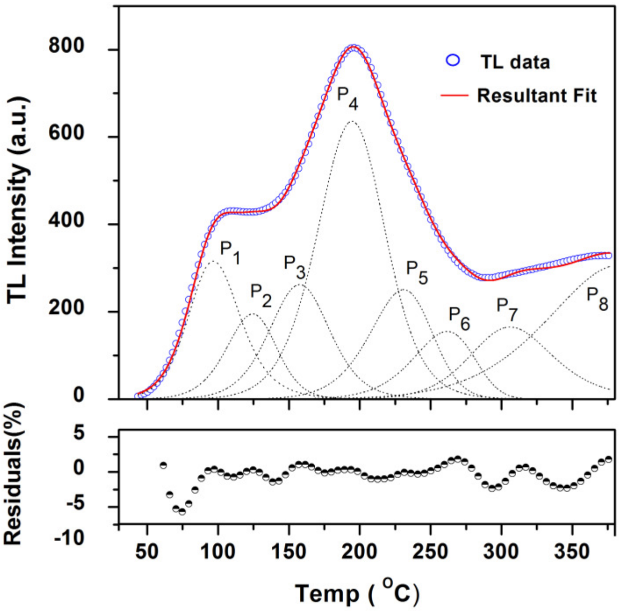

Fig. 3.4 Typical TL glow curve of carbon doped graphite furnace sample B for 18Gy absorbed dose at 4K/s heating rate. The individual TL peaks are shown in dashed curve and resultant fit is by red curve**.**

The TL glow curve of $MgAl_2O_4$:C was recorded using heating rate of 4 K/s for sample A at absorbed dose of 600 mGy and sample B for a dose of 18Gy, respectively.

The meta-stable life time (τ) of trapped charges at given temperature T with trapped depth (E_a) can be expressed by Arrhenius equation as

$$\frac{1}{\tau} = s\, e^{-E_a / kT} \qquad (3.1)$$

Here, S is pre-exponential factor also termed as frequency factor having unit sec^{-1}. The rate of thermal de-trapping of charge concentration ‘n’ at any given time under 1st order kinetics can be expressed as

$$\frac{dn}{dt} = -n\, s\, e^{-E_a/kT} \tag{3.2}$$

There are various methods available to estimate 'E_a' and 'S' and general order of kinetics associated with charge transfer phenomenon in TL processes **[111]**. In present study the TL glowcurve parameters were resolved using a computerized curve de-convolution Analysis (CCDA) for all TL peaks observed in both types of samples. The single glow-peak equation of general order kinetics was used in the case of discrete trap distributions:

$$I(T) = I_m \cdot b^{\frac{b}{b-1}} \exp\left(\frac{E_a}{kT}\frac{T-T_m}{T_m}\right) \cdot \left[(b-1)(1-\Delta)\frac{T^2}{T_m^2}\exp\left(\frac{E_a}{kT}\frac{T-T_m}{T_m}\right) + Z_m\right]^{-\frac{b}{b-1}} \tag{3.3}$$

Where,

$\Delta=2kT/E_a$, $\Delta_m=2kT_m/E_a$ and $Z_m=1+(b-1)\,\Delta_m$. (3.4)

And the frequency factor'S' under 1st order of kinetics can be determined as

$$s = \frac{\beta\, E_a}{kT_M} e^{E_a/kT_M} \tag{3.5}$$

On the other hand, for general order kinetics

$$s = \frac{\beta E_a}{kT_m}\frac{1}{Z_m} e^{E_a/kT_m} \tag{3.6}$$

Equation (3.3), suggested by Kitis et al. **[112]**, is an analytical expression that could be used for CCDA in the case of single-value energy trap depth associated with the localized states, with each crystalline phase of a TL material, corresponding to a discrete trap distribution. All curve fittings were performed using the software package Microsoft Excel, with the solver utility **[113]**, while the goodness of fit was tested using the Figure of Merit (FOM) of Balian and Eddy **[114]**. The obtained FOM values were better than 1.5%. The Fig.3.3 and Fig.3.4 show CCDA and experimental TL glow curve for sample A and sample B respectively, along with the corresponding plot of residuals in each case.

The TL glow curve consists of an eight individual TL peaks (up to temperature 380^{0}C) in both the samples. Table 3.1 shows the TL parameters of sample A extracted by CCDA from experimentally observed individual TL peaks shown in Fig.3.3.

Table 3.1 Numerically estimated TL parameters of sample A

TL Peaks								
TL parameters	**P_1**	**P_2**	**P_3**	**P_4**	**P_5**	**P_6**	**P_7**	**P_8**
I_{max}(a.u.)	**0.69**	**2.46**	**2.62**	**1.60**	**3.43**	**1.89**	**1.14**	**0.9**
T_{max}(°C)	**93.5**	**126.5**	**157.3**	**189.9**	**229.6**	**261.5**	**306**	**382**
E_a(eV)	**0.6**	**0.95**	**1.03**	**0.87**	**1.06**	**1.2**	**1.31**	**0.8**
b	**1.0**	**1.7**	**1.6**	**1.7**	**1.4**	**1.5**	**2.0**	**1.0**
S (s-1)	**1.83×10^6**	**1.26×10^{10}**	**1.44×10^{10}**	**2.62×10^7**	**4.56×10^8**	**2.14×10^9**	**2.23×10^9**	**6.13×10^3**
TL peak area	**0.15**	**0.53**	**0.34**	**1.0**	**0.47**	**0.50**	**0.37**	**0.31**
$\tau_{1/2}$	**1.6h**	**8.4d**	**168d**	**178d**	**47.1y**	**2.38 x10^{3}y**	**1.68 x10^{3}y**	**135y**

The high temperature > 400°C TL glow peak fit is only for fitness, since full TL glow peak above 400°C could not be recorded on present reader system. The frequency factor S has been determined using Equations (5)and (6).The TL glow peak half life ($\tau_{1/2}$) at room temperature has been calculate using following expression

$$t_{1/2} = \frac{\ln 2}{s\ e^{-E_a/kT}} \qquad (3.7)$$

Here, for the simplicity we have assumed 1st order of kinetics to estimate the half-life ($\tau_{1/2}$) of TL peak at room temperature. Since, the general-second order of kinetics half-life ($\tau_{1/2}$) depends on initial number of charge traps in i.e. on absorbed dose. It is found that in sample A TL glow peak P_4 which occurs at 189^{o}C is the most prominent TL peak in terms of integral TL area under TL peak. The other TL peaks like P_1, P_2, P_3,P_5, P_6, P_7, P_8 are relatively less intense as comparable to P_4 in their integrated TL intensity as shown in Table 3.1. The thermal trapped depths (E_a) of these TL peaks are found to vary following an increasing trend from 0.6 to 1.2 eV and most of these TL peaks having order of kinetics more than one. The half-lives ($\tau_{1/2}$) of these individual peaks at 25^{o}C for sample A are listed in Table 3.1.

The TL peaks P_1 and P_2 are having half-lives less than ten days, hence these TL peaks are expected to show post irradiation fading at room temperature. However, the TL peaks above 157^{o}C i.e., P_3-P_8 are having half-lives more than 158 days (some TL peaks has shown half-lives of several years in Table 3.1). Therefore, these TL peaks are thermally stable at room temperature during post irradiation storage. Thus, these peaks can be used as stable TL dosimetric peaks for radiation dosimetric applications. Fig.3.4 shows the CCDA and experimental TL glow curve for sample B. Here as well, the TL glow curve consists of eight individual TL peaks spreading from 95^{o}C to 382^{o}C. The measured TL parameters by CCDA for sample B are listed in Table 3.2.

Table 3. 2 Numerically estimated TL parameters of sample B

TL Peaks								
TL parameters	**P_1**	**P_2**	**P_3**	**P_4**	**P_5**	**P_6**	**P_7**	**P_8**
I_{max}(a.u.)	**3.15**	**1.95**	**2.62**	**6.35**	**2.50**	**1.55**	**1.65**	**3.06**
T_{max}(°C)	**96.50**	**124.20**	**157.30**	**194.20**	**203.60**	**261.50**	**305.7**	**381.0**
E_a(eV)	**0.90**	**0.93**	**0.96**	**0.97**	**1.10**	**1.20**	**1.38**	**0.8**
b	**2.00**	**1.50**	**1.70**	**1.60**	**1.10**	**1.14**	**2.00**	**1.0**
S (s-1) x 10^{10}	**53.60**	**16.50**	**3.98**	**0.62**	**2.93**	**4.41**	**19.50**	**6.34e3**
TL peak area	**0.26**	**0.22**	**0.18**	**1.00**	**0.35**	**0.21**	**0.29**	**0.43**
$\tau_{1/2}$	**4.05min**	**7.08h**	**3.95d**	**3.69d**	**3.46y**	**116y**	**2.9 x10^4y**	**131y**

From both the Table 3.1 and Table 3.2 it is observed that, all TL peaks from P_1 to P_8 in samples A and B are within ± 5°C agreement to each other, indicating similar type of thermal trap depth in both types of the samples. However, in sample B, the peaks P_1, P_2, P_3, P_5, P_6, P_7, P_8 are not as intense compared to P_4. This is also getting reflected under TL peak area values of Table 3.2 and Fig.3.5 (The line is drawn as a guide to eye and no physical law was used to fit the line). The thermal trap depths (E_a) of these individual peaks are found to spread from 0.9 to 1.38 eV, also following an increasing trend, with these individual TL glow peaks showing order of kinetics more than one. The estimated half-lives ($\tau_{1/2}$) at 25°C of TL peaks P_1, P_2, P_3 and P_4 of sample B are in the range of few days (Table 3.2). Hence, these TL peaks are bound to show post irradiation fading. It should be emphasized that a fit with good quality could not be achieved by using lower number of TL peaks in either case. Nevertheless, both these carbon doped samples show the TL glow peak position at almost at same temperature with similar TL sensitivity (i.e. integrated area under TL glow curve for given absorbed dose). However, observed TL sensitivity in electron gun sample A is more than 20 times that of graphite furnace synthesized sample B. The TL glow peaks are relatively better resolved in sample B compared to electron gun sample A. This is possibly due to the slow isothermal diffusion of carbon impurity in graphite furnace synthesis method as compared to prompt adiabatic heating of electron gun sample A and thus the defects did get sufficient time to stabilize and lower their potential energy before cooling of the sample. This leads to freezing of defects at different ensemble energy states in the lattice. Therefore, the defects are not well separated and distributed in sample A as compared to sample B. The TL CCDA results of both samples depict that the two different methods of incorporating carbon in host material $MgAl_2O_4$ have given almost similar types of TL defects which is also reflected in measurement of TL parameters shown in Table 3.1 and 3.2. However, the relative concentration of TL defects gets affected by method of incorporating carbon in $MgAl_2O_4$ i.e. the relative concentration of TL peaks in sample A are comparable to each other. On other hand, for sample B, apart from P_4 TL peak the concentration of peaks P_1, P_2, P_3, P_5, P_6, P_7, P_8 are relatively suppressed as shown in Table 3.2. Defect centre corresponding to P_4 peak position was preferentially incorporated in $MgAl_2O_4$:C by both methods. However, for sample A, the concentration of all TL defects are enhanced as compared to sample B (Table 3.2).

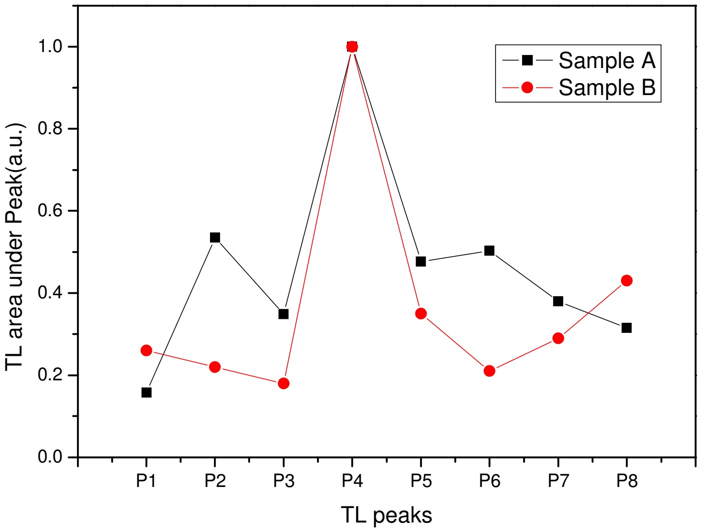

Fig. 3. 5 Comparisons of TL peak integrated area (TL intensity) samples A and B

Hence, the electron gun method of incorporating carbon as an impurity in $MgAl_2O_4$ leads to more hazy defects introduction as compared to slow heating of sample $MgAl_2O_4$ in graphite furnace with considerable increase in TL defects concentrations. However, the thermal trap depths (E_a) of all TL glow peaks of sample A are relatively shallower in terms of energy as compared to sample B. The correlation of the observed enhanced TL sensitivity in sample A and its relative shifts in thermal trap depths (E_a)

(towards lower values) for all TL glow peaks as compared to sample B is another investigating work to be taken up by researcher which is beyond the scope of present thesis .

3.3.2. Optically stimulated luminescence

The CW-OSL response of un-doped $MgAl_2O_4$ has been recorded at 50 mW/cm^2 stimulation intensity at room temperature after irradiation, as shown in Fig.3.6.

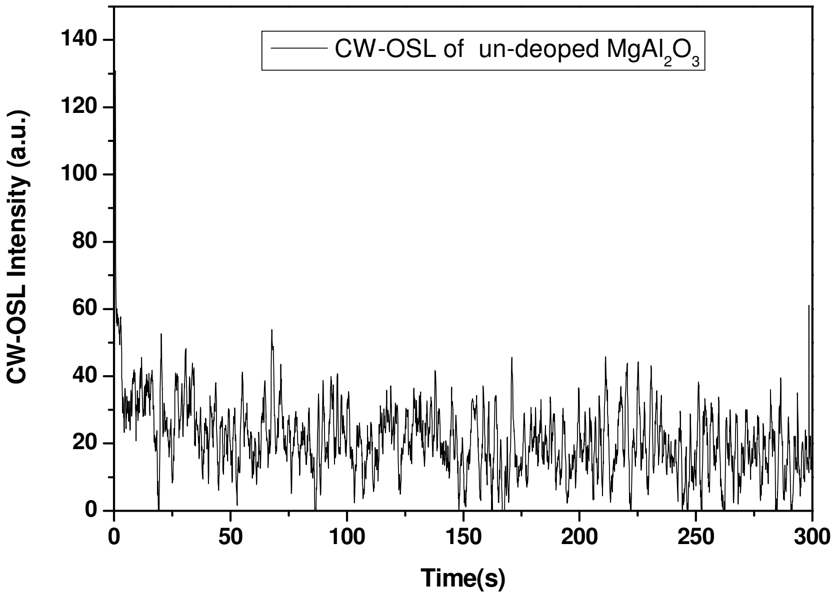

Fig. 3.6 The CW-OSL response of un-doped $MgAl_2O_4$ for 10Gy absorbed dose

No considerable OSL response could be observed for un-doped $MgAl_2O_4$ sample even at 10Gy absorbed dose. However, both carbon doped samples, A and B, show OSL response, with sample B being approximately 22 times less OSL sensitive than sample A in terms of total integral OSL area under curve. The radiation dosimetric consideration of any phosphor requires high TL/OSL sensitivity. Therefore, in further discussion we will focus on the detailed study of OSL characteristics of sample A.

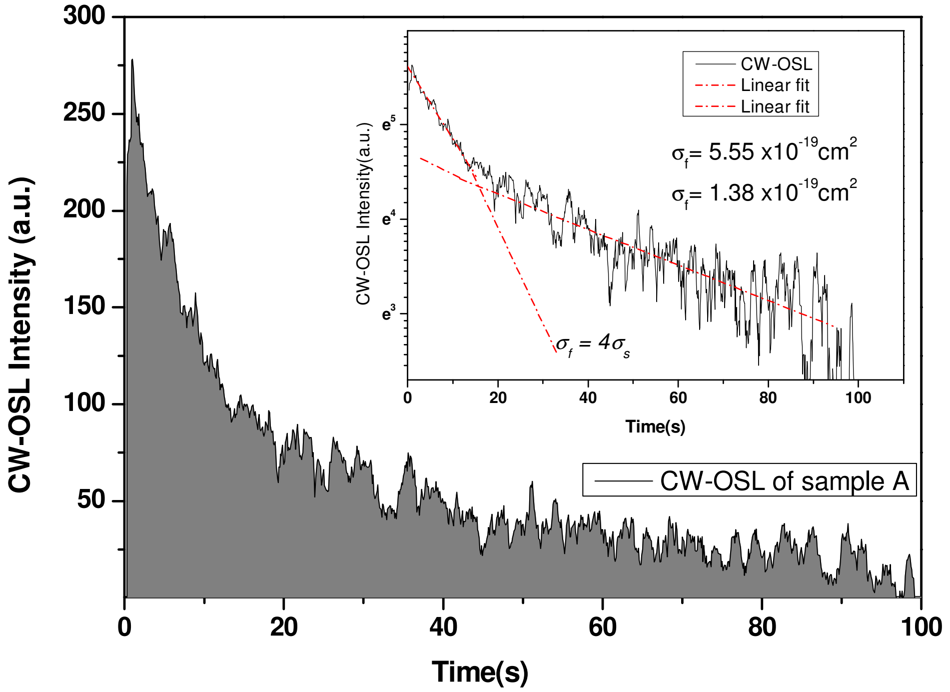

Fig. 3.7 CW-OSL curve of sample A for 40 mGy absorbed dose. The inset fig is linear fit to same curve on natural logarithm scale giving slope as value of PICs for 50 mW/cm^2 stimulation intensity

Fig. 3.7 shows the CW-OSL curve of sample A exposed to 40 mGy absorbed dose. The 2nd order exponential decay fit to CW-OSL curve of sample A shows two well defined decay constants giving values of photo-ionization cross-sections (PIC) $\sigma_f \approx 5.55\text{x}\ 10^{-19}\text{cm}^2$ and relatively slow PIC $\sigma_s \approx 1.38\text{x}\ 10^{-19}\ \text{cm}^2$ for 470 nm of stimulation light. The faster PIC σ_f is found to be 0.4 times higher than that of PIC of the commercially available α-Al_2O_3:C **[115]** for same stimulation wavelength. However, this value of σ_f from $MgAl_2O_4$:C sample A is still good enough to have particle OSL readout. The correlation of OSL vs TL has been investigated by using method of pulse OSL stimulation **[5, 6]** during TL readout. In this method, the pre-irradiated phosphor material is heated linearly along with low intensity (1mW/cm^2) optical stimulation short pulse

(~0.4s) at every fix temperature interval (5-10 °C). This results in superposition of series of the OSL signals over convention TL glow curve. The superimposed POSL signal integral area over TL glow curve is directly proportional to OSL yield at that temperature. The plot of this OSL yield v/s temperature along with conventional glow curve is shown in Fig.3.8 (a & b) for sample A and B, respectively.

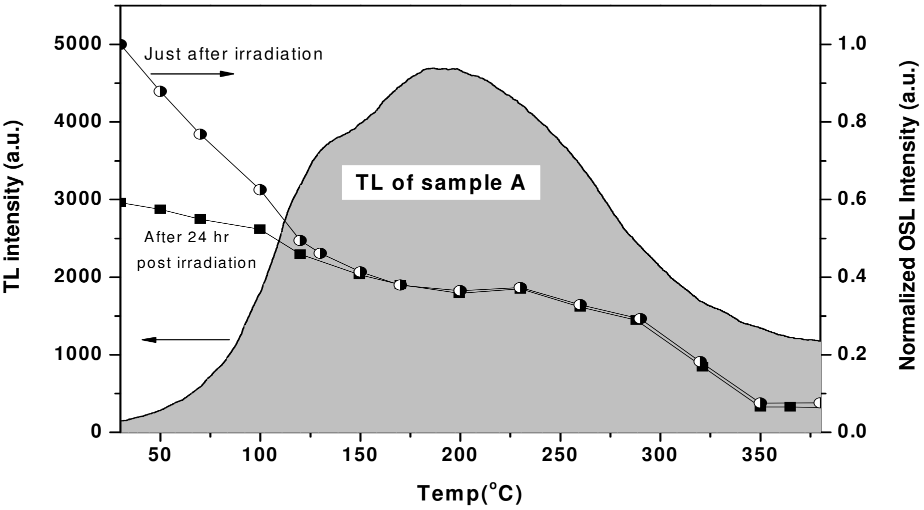

Fig. 3.8 (a) Correlation of TL and OSL signal in sample A

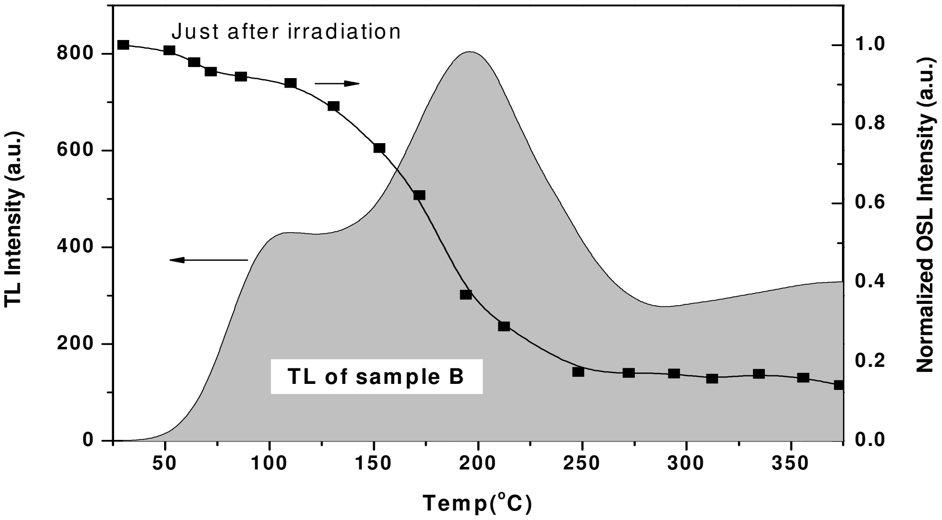

Fig. 3.8 (b) Correlation of TL and OSL signal in sample B

It is evident from Fig.3.7 that all TL traps in both the samples are OSL sensitive and contributing actively to OSL signal. The OSL signal decreases with increase in temperature as TL traps are getting empty which shows direct correlation between two signals. The near 100°C TL peak, meta-stable life time at room temperature is relatively shorter as compared to TL peak 200°C. Therefore, post irradiation dark storage fading of OSL signal from near 100°C TL peak is expected in $MgAl_2O_4$:C. Fig.3.8 (a) shows the OSL yield measured from sample A after 24 hour post irradiation storage in dark and just after irradiation. The OSL signal after 24 hours storage is found to decrease by ~30% than its value just after irradiation. The major decrease in OSL signal is observed due to fading of 100°C TL peak as shown in Fig.3.8 (a). Therefore the dominating post storage OSL fading is due to shallow TL trap defects in sample A. The variation of OSL sensitivity with particle size of the type sample A has also been investigated as shown in Fig. 3.9.

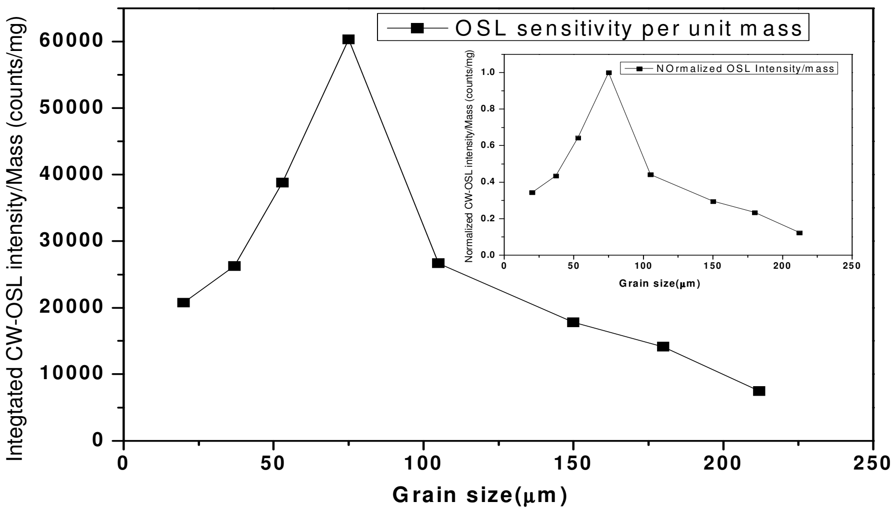

Fig. 3.9 Variation of OSL sensitivity with particle size of sample A for 200 mGy absorbed dose normalized with mass.

The highest OSL sensitivity was observed for 70 μm size of the particles in sample A. Such variation in OSL sensitivity can be understood in terms of **Surface-to-Volume Defects Concentration** (SVDC) ratio which is an inverse function of particle size. With increase in particle size from > 30 μm volume defects dominate over surface defects. As the OSL/TL are predominantly contributed from volume defects, the OSL/TL sensitivity increases with increase in particle size. However, at a particular particle size, for sample A (70 μm) this SVDC ratio is optimum. The decrease in TL/OSL sensitivity with increase in particle size beyond optimum value is partially contributed due to loss of emitted OSL signal due to multiple scattering within the sample material. Therefore, with further increase in particle size, OSL yield decreases as shown in Fig.3.9. The dose linearity of sample A was also studied by plotting the integrated OSL intensity against absorbed dose from 20 mGy to 100 Gy as shown in Fig.3.10. The OSL response has been found to show 16% sub-linearity over this studied dynamic dose range as shown in Fig.3.10.

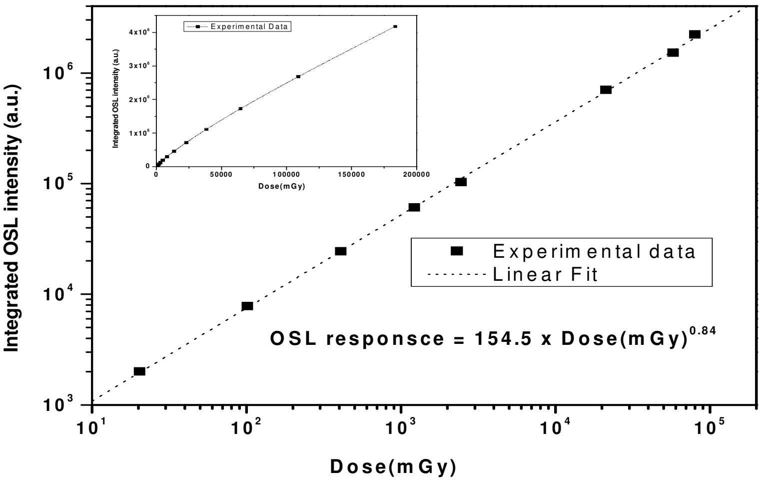

Fig. 3.10 OSL vs. absorbed dose linearity of sample A. The inset graph shows linear scale plot of dose vs OSL response of sample A.

3.4. Conclusions

The undoped $MgAl_2O_4$ synthesized by gel combustion method did not show any TL/OSL sensitivity though there was a partial evidence of relatively high temperature deeper traps. However, significant increase in TL/OSL intensity has been observed on carbon doping in $MgAl_2O_4$ under the reducing atmosphere. The doping of the carbon has been achieved in two ways, – by using electron gun and by heating in graphite furnace. The TL/OSL sensitivity is greatly enhanced for electron gun synthesized $MgAl_2O_4$:C. The carbon doped $MgAl_2O_4$:C has excellent OSL properties to further develop this phosphor for radiation dosimetry. However, there is no significant difference observed in X-ray diffraction studies of both types of carbon doped samples as compared to undoped $MgAl_2O_{4.}$ Thus the difference in carbon concentration profile as a function of depth (from surface) in these two types of samples can be ascertained by techniques like Electron Energy Loss Spectroscopy (EELS) or Focused Ion Beam. These studies will bring immense information for engineering the dosimetric TL/OSL defects in $MgAl_2O_4$:C. Therefore, there exists a great scope of further studies, to optimize the synthesis parameters of carbon doping in $MgAl_2O_4$ in order to enhance its suitability for various field of radiation dosimetry.

Chapter 4

Defect related photoluminescence spectroscopy and EPR studies on pure and carbon doped $MgAl_2O_4$ spinel

4.1. Introduction

Magnesium aluminate spinel ($MgAl_2O_4$) is a refractory oxide material with high toughness and chemical stability, low electrical conductivity and low density (3.6 g/cc) and high melting temperature (2150℃), and is transparent in the visible and infrared wavelength regions **[116-121]**. The bulk properties like chemical resistance, electrical conductivity and melting point are inherent to the material. It possesses a unique combination of valuable properties that makes it a preferred material for many structural, chemical, optical and electrical applications. It is one of the proposed structural materials in fusion reactors **[122, 123]** and prospective biomaterial for aesthetical orthodontics brackets **[124]**. Due to its high temperature properties and relatively good resistance to irradiation, magnesium aluminate spinel ($MgAl_2O_4$) is also considered as a possible matrix for the minor actinides transmutation **[125]**. However, to achieve optical properties (visible and infrared transparency) relative densities above 99% with small pore sizes are required **[126]**.

It is well known that the presence of defects in oxide-based inorganic materials can strongly influence its optical, magnetic, structural, electronic and dielectric properties **[127]**. In order to obtain high quality crystals, it is attempted to minimize the amount of defects. However, the presence of defects sometimes leads to some other important functional properties also. The presence of oxygen vacancies and other oxygen-related defects are known to induce significant luminescence behaviour. The presence of oxygen vacancies in ThO_2 nanorods and zinc pyrophosphate have been reported to give rise to blue emission which can be tuned to white LEDs by choosing suitable dopant ions **[128, 129]**. Similarly, presence of oxygen related defects in $SrZrO_3$ distorted perovskite was shown to exhibit multicolor emission in visible region **[130]**. The development of advanced semiconductor materials with wide band gap (2-5 eV) may give rise to new optoelectronic device, particularly for blue LEDs. In optoelectronic devices, disordered insulators can replace single crystal semiconductors where cost is an important factor.

Recently, oxygen vacancy induced emission in MgO and Al_2O_3 has been extensively explored for dosimetry **[131, 132]** and broadband laser applications **[133-135]**. In contrast to magnesia and alumina, $MgAl_2O_4$, however, is a relatively unexplored matrix. There are few reports which show very low oxygen vacancy induced emission **[136, 137]** from this matrix.

The ability of $MgAl_2O_4$ spinel to incorporate cations of various size/charge and to tolerate cation disorder leads to various kinds of defects **[138-140]** which may lead to interesting optical behaviour. $MgAl_2O_4$ is a highly rugged matrix from the point of view of structural, thermal, chemical and radiation stability. If it is possible to circumvent the problem of low emission efficiency of oxygen vacancies in $MgAl_2O_4$, it could be a promising candidate for physically robust light-emitting material without any requirement of activator ions.

In this study, carbon doping in magnesium aluminate was carried out to investigate its effect on the luminescence behaviour and its correlation with defects. There has been a considerable research on pure and cation doped $MgAl_2O_4$. However, the anion doped $MgAl_2O_4$ is not well studied. Hence, it would be of great interest to explore carbon doped $MgAl_2O_4$ for luminescence studies.

4.2. Experimental

Synthesis, characterization and carbon incorporation using Electron Gun and graphite furnace were done as described in sections 2.3, 3.2, 2.6.1 and 2.6.2, respectively. Photoluminescence data were recorded on an Edinburgh CD-920 unit equipped with Xe flash lamp as the excitation source. The data acquisition and analysis were done by F-900 software provided by Edinburgh Analytical Instruments, UK.

4.3. Results and discussion

4.3.1. Excitation spectroscopy

Excitation spectrum is the spectrum of the excitation light when the emission at a fixed wavelength is detected while the excitation wavelength is scanned. An excitation spectrum determines the wavelengths of light necessary to produce emission or fluorescence from the molecule/compound, as monitored at a particular wavelength. The spectrum is obtained by fixing the emission wavelength and by running the excitation monochromator **[141]**. It characterizes the electron distribution of the molecule in the ground state. Excitation is, in principle equivalent to absorption. An excitation spectrum can be considered as "fluorescence detected absorption' and the intensity of peaks seen in the excitation spectrum is directly proportional to the number of photons absorbed.

Figure 4.1 shows the excitation spectrum of undoped $MgAl_2O_4$. The presence of two peaks at 225 nm and 245 nm could be attributed to the oxygen vacancies in the magnesium aluminate lattice. The peak at 225 nm is attributed to the presence of neutrally charged oxygen vacancy (the F center, the oxygen vacancy with two electrons) and 245 nm to positively charged oxygen vacancy (the F^+ center, the oxygen vacancy with one electron) **[142, 26]**. As far as excitation spectra are concerned there is not much change in both the carbon doped samples (A and B) relative to undoped sample. Schematic of excitation process taking place in magnesium aluminate crystal is also shown in Fig. 4.2.

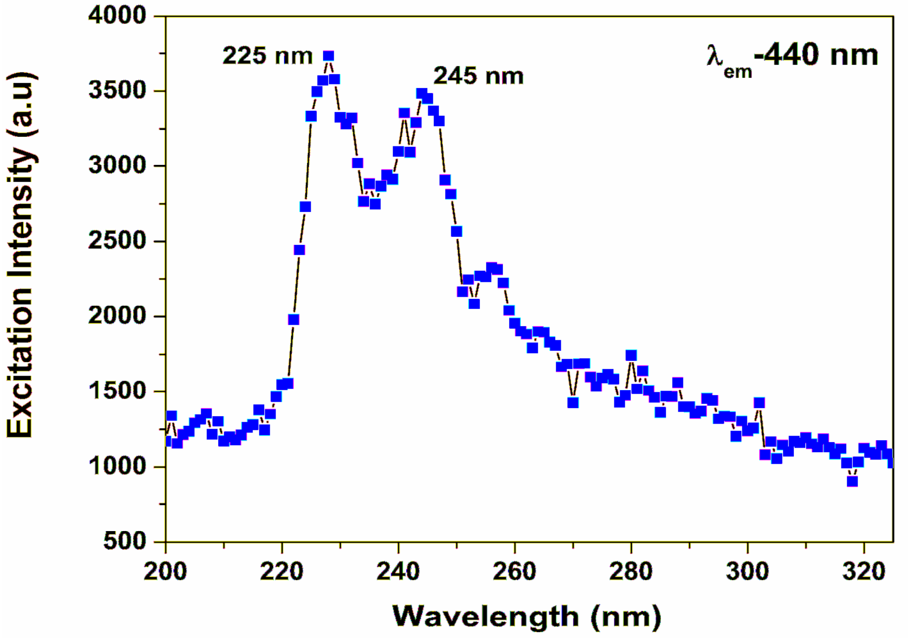

Fig. 4.1 Room temperature excitation spectrum of $MgAl_2O_4$

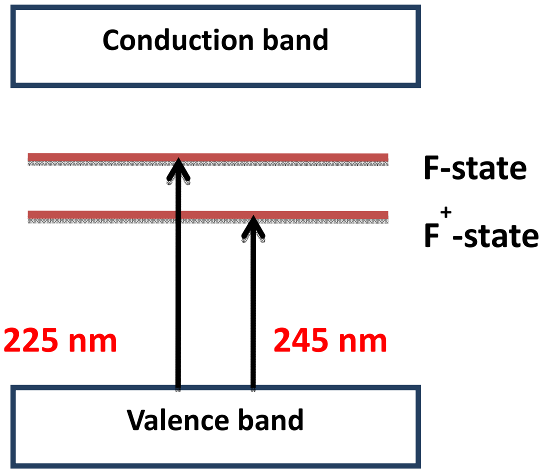

Fig. 4.2 Schematic diagram of the excitation mechanism in $MgAl_2O_4$

4.3.2. Emission spectroscopy

In order to determine the emission spectrum, the wavelength of maximum absorption (usually the same as the excitation maximum) is determined and the compound is excited at that wavelength. To scan the fluorescence emission intensity over the entire series of emission wavelengths, a monochromator is used. At various wavelengths, the relative intensity of the fluorescence is measured to plot the emission spectrum.

Figure 4.3 depicts the emission spectrum for undoped and carbon doped $MgAl_2O_4$ powder sample. Observed photoluminescence (PL) spectra are basically identical to each other irrespective of the excitation energy (225 or 245 nm), showing the common PL peak energy at 460 nm (2.7 eV). This strongly suggests that the photoexcitation of the F and F^+ centres eventually results in the same radiative relaxation channel. The PL intensity is substantially reduced when these samples are post-annealed in air at 1200^oC for 15 h. This allows to assume that oxygen vacancies are responsible for the 460 nm (2.7 eV) PL band. It can be seen from the emission spectra that doping carbon by electron gun method does not lead to substantial change in the emission characteristics compared to undoped sample. In contrast, incorporation of carbon thermo-chemically using graphite furnace (GF) (sample B) leads to enhancement in PL emission peak and also changes the peak position to lower wavelength value. Apparently, doping carbon thermo-chemically using graphite furnace leads to creation of more defects, mainly anion vacancies, which are responsible for enhanced PL emission in GF sample (B). It also increases the band gap of the $MgAl_2O_4$ and this explains the tremendous blue shift in the emission spectra.

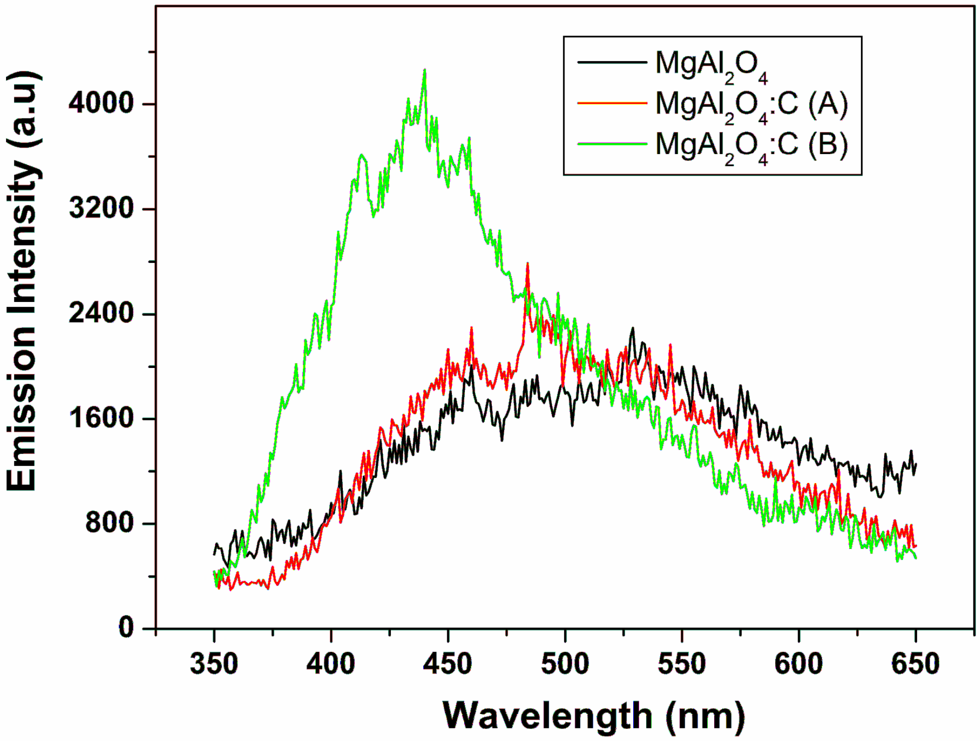

Fig. 4.3 Emission spectra for undoped and carbon doped (A and B) $MgAl_2O_4$ powder samples.

4.3.3. Probing the type of defects: Luminescence decay and EPR studies

Sample B (GF) was subjected to the decay studies in order to understand the lifetime behaviour. A typical PL decay profile measured for the ~460 nm PL band is given in Fig.4.4. The PL signal decays non-exponentially on the time scale of several tens of microseconds. It was found that the decay profile is well-fitted to a triple exponential function with time constants of 2.3, 7.9 and 51.3 µs. Such a highly non-exponential decay behavior implies that the relevant emission process experiences multiple trapping and detrapping events before the radiative recombination process eventually occurs **[143, 144, 147]**. Average lifetime is observed to be 4.83 µs which is typical of defect related emission **[128, 129]**.

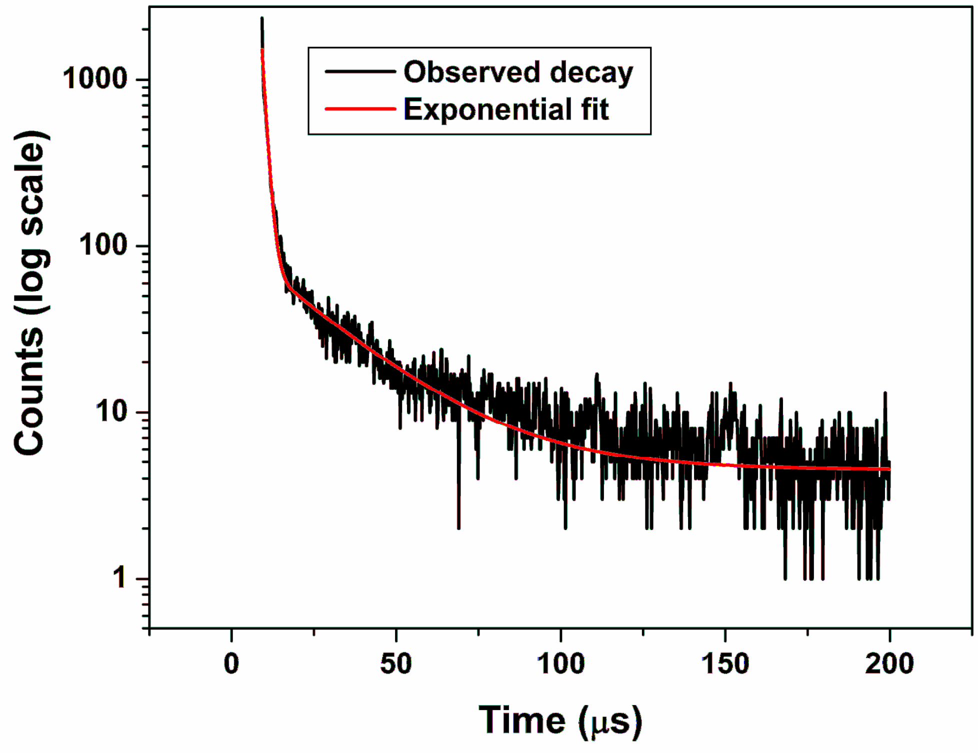

Fig. 4.4 Room temperature decay curves for carbon doped $MgAl_2O_4$ (B) sample

4.3.3.1. EPR studies

The presence of point defect is further confirmed by EPR technique, which can detect holes trapped in cation vacancy (V-center), and one electron trapped oxygen vacancies (F^+-center) and two electrons trapped oxygen vacancies (F-center). The ESR spectrum of the powder carbon doped $MgAl_2O_4$ sample B is shown in Fig. 4.5.

In Electron Paramagnetic Resonance, the resonant absorption of microwave radiation by the paramagnetic system in the presence of an applied magnetic field occurs. When an atomic or molecular system with unpaired electrons is subjected to a magnetic field, it generates discrete orientation. This orientation difference is physically equivalent to a separation of energy levels. The magnitude of the splitting of energy levels is dependent on the strength of the applied magnetic field. When the applied microwave energy exactly matches the energy level separation, resonance absorption of electromagnetic radiation (microwave energy) occurs. The degree of absorption is proportional to the number of free electrons in the material.

In the applied magnetic field, energy level separation, **ΔE** can be expressed as

$$\Delta E = \boldsymbol{h\nu} = \boldsymbol{g_e \mu_B B_0}$$

Where h is the Planck constant, v is the applied microwave frequency, g_e is the gyromagnetic ratio of the electrons (the ratio of the magnetic dipole moment to the angular momentum of an elementary particle or atomic nucleus), μ_B is the Bohar Magneton, and B_0 is the magnetic field applied.

To detect unpaired electrons or free radicals in various systems, electron paramagnetic resonance (EPR) has been identified as a powerful tool. It has found applications in different research fields, including physics, chemistry, and biology. An electron paramagnetic resonance peak was first recorded by Zavoisky (1945) **[145, 146]** at low magnetic field, 4.76 mT, with a frequency of 133 MHz, from a Cupric chloride crystal and the Zeeman factor 'g' was observed to be 2.0. Later on interpretation of Zavoisky's results of paramagnetic resonance absorption spectra was done by Frenkel (1945) **[147]**. The advantages of the use of high microwave frequencies were understood by later experiments.

In $MgAl_2O_4$:C (B), EPR spectra (Fig 4.5) exhibits one broad signal at the g-tensor component of 2.002 indicating that extrinsic defect centers were introduced into the spinel lattice due to the thermochemically controlled carbon doping employing a graphite furnace.

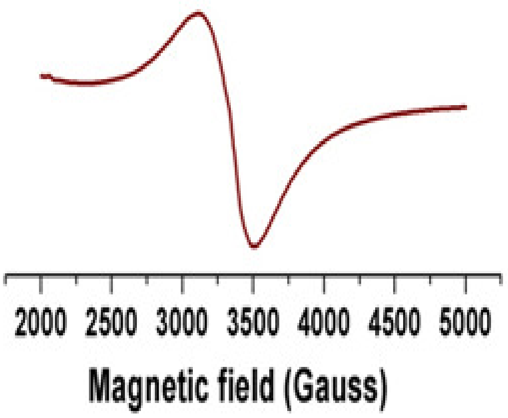

Fig. 4.5 EPR spectrum of carbon doped $MgAl_2O_4$ sample B

4.3.4 Chromaticity

W. David Wright and John Guild, in the 1920s, independently conducted a series of experiments on human sight. Their aim was to determine the colors in human vision, and give it a mathematical basis. The eye reacts to the three primaries Red, Blue and Green (RGB) separately, and the colors we see are just sensations these wavelengths cause in us. A color space maps a range of physically produced colors to color sensations registered in the eye. For that tristimulus values were used. Two light sources made up of different mixtures of various wavelengths may appear to be same color to an observer when they produce same tristimulus values. Imaginary primary colors and corresponding color matching functions have been formulated as tristimulus values to have one component that describes the perceived brightness and to avoid negative RGB values **[148, 149]**. In 1931, CIE (International Commission on Illumination) mathematically determined a color space called the CIE XYZ 1931 color space based on the results of the CIE RGB version of the human eye. The CIE XYZ color space contains all color sensations that an average person can experience.

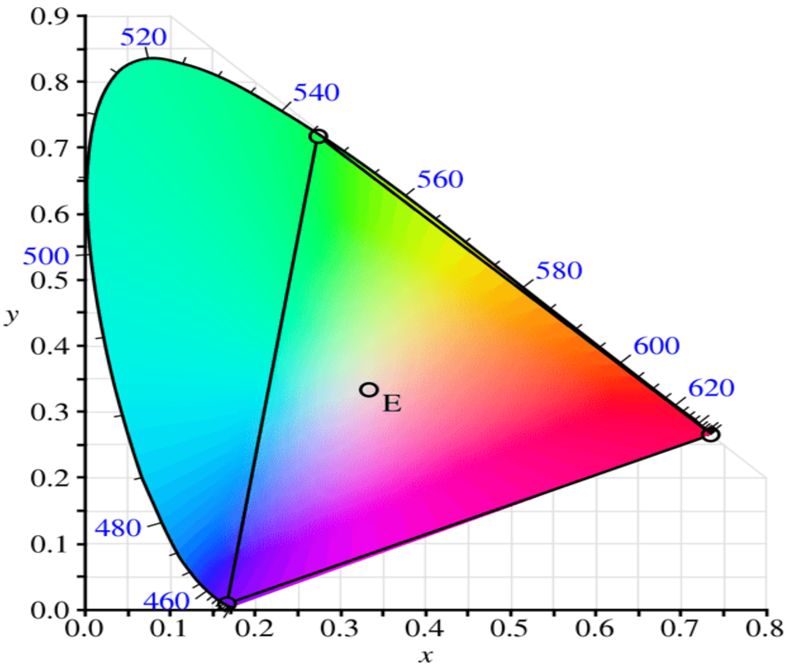

Fig. 4.6 A representative chromacity diagram

In the above chromacity diagram, the colored area is the CIE XYZ 1931 color space. The white is at the 'center'and the edges are each color at the maximum saturation. The triangle is CIE RGB and the total color space of the human eye is greater than the experimental results of CIE RGB. The extrapolations of RGB created mathematically are X, Y and Z. These are to avoid negative numbers and are called Tristimulus values. X is a mix of cone response curves chosen to be orthogonal to luminance and non-negative, Y means luminance and Z is somewhat equal to blue. In CIE xyY, Y is the luminance. The small x and y represents the chrominance values derived from the tristimulus values X, Y and Z in the CIE XYZ color space and used to draw the chromacity diagram of the CIE XYZ color space. It is another way to represent CIE XYZ. Even if the chromacity diagram looks two-dimensional, it is three dimensional. It is possible to calculate the CIE chromaticity co-ordinates of phosphor materials using the photo luminescence data.

4.3.4.1. Chromaticity coordinates calculation

To evaluate the material performance on color luminescent emission, CIE chromaticity coordinates were evaluated for carbon doped $MgAl_2O_4$ sample B (the one which gives maximum output) adopting standard procedures. The corrected spectrum with respect to source, monochromator and detector response is considered while calculating CIE indices. The values of *x* and *y* coordinates of the system were calculated to be 0.231 and 0.227, respectively. This is represented as the point '*' in the CIE diagram shown in Fig. 4.8. It is clear from these values that, carbon doped magnesium aluminate, gives a 'bluish' emission.

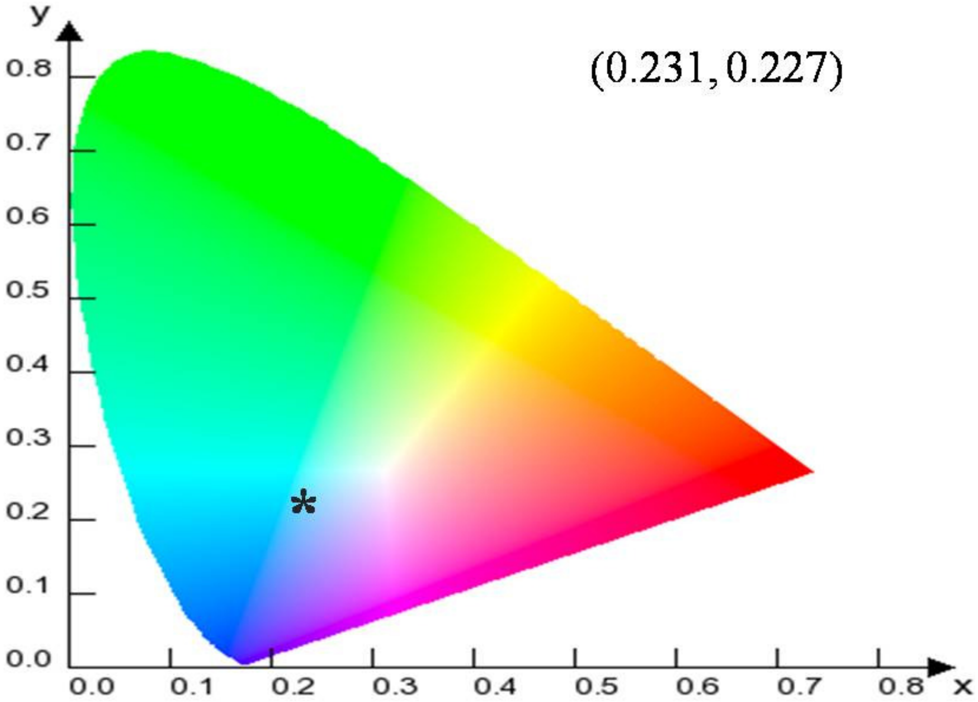

Fig. 4.7 CIE chromaticity diagram showing the emission colors for carbon doped $MgAl_2O_4$ sample B

4.4 Conclusions

Pure $MgAl_2O_4$ was synthesized by gel combustion process and the spinel phase was obtained by heating at 1100ºC for 10 hours. Carbon doping was performed by two methods which included targeting the sample with electron beam in graphite furnace and heating the sample at very high temperatures (2100ºC) in graphite furnace. The carbon-doping could introduce defect centres (mainly vacancy-related defects) which were characterised using photoluminescence spectroscopy and EPR spectroscopy. While the excitation spectra did not differ much for the carbon-doped samples prepared by two methods, the emission spectra of the graphite furnace-heated sample showed much enhanced intensity as well as blue shift in the emission band. Blue light emitting phosphors are important because it is easier to make a white LED light using blue LED. Engineers use a blue LED to excite the fluorescent component in the bulb and that converts the blue light to white light. This is an important result directed towards research on chemically and structurally robust blue-emitting phosphors based on $MgAl_2O_4$ spinel.

Chapter 5

Origin of visible photoluminescence in combustion synthesized α-Al_2O_3: Effect of thermal treatment

5.1 Introduction

Recently, a lot of focus has been diverted to synthesizing luminescent material without any rare-earth doping because of the cost and toxicity associated with it. China has almost controlled the business of rare-earths because it supplies more than 95% of the worldwide production of pure rare earth metals **[150]**. The ever growing demand for advanced phosphors with high lumen output has motivated the scientific community to look beyond lanthanide activated phosphors. Most of the luminescence materials used worldwide are activated using lanthanide ions wherein depending upon the energy levels of the host and guest, the emission colors can be tuned. Gd^{3+}activated phosphors emit in ultraviolet (UV) region **[151]**, trivalent Eu, Sm, Tb and Dy activated phosphors emit in visible region **[152, 153]** and trivalent Nd, Er and Yb activated phosphors emit in infra-red region **[154 155]**. Some of the materials also exhibit self-assisted luminescence due to charge transfer transition such as molybdates **[156]**, tungstates **[157]**, and cerates **[158]** etc. Other class of compounds which have gained significant attention recently is the defect induced luminescence materials. Although it started three decades ago; a remarkable growth has been achieved since Sailor *et al.* reported the white emission from a silicate-carboxylate sol–gel precursor **[159, 160]**. Since then defect induced emission without any dopant ion has been the thrust area of research and lot of focus has been diverted to strategies directed at replacement of conventional rare-earth based phosphors. In this direction defect induced luminescence has contributed immensely. There have also been recent studies wherein defect induced emission has been explored in simple oxides system like MgO **[161]**, ZnO **[162]**, ThO_2 **[118]**, ZrO_2 **[163]** and CeO_2 **[164]** etc. These defects can be of any kind such as cation/anion vacancy, vacancy at interstitial site, oxygen related defects etc. Identification of such defects is very important because in addition to controlling the behaviour of material under study, they also help to develop the understanding behind the defect-property correlation that can be utilized to develop advanced materials.

Alumina is an important refractory material with high melting point (~2000 ^{o}C) and hardness. Along with these properties, an excellent thermal shock resistance makes it an ideal candidate for various applications such as space applications in satellite, capacitor, cutting tools, bullet proof jacket, bio-medical and catalysis etc. **[165]**. As far as luminescence in undoped alumina is concerned there exist quite a few reports in literature. Du *et al.* **[166]** and Chen *et al.* **[167]** have carried out photoluminescence studies on porous alumina membranes (PAM) whereas Zhang *et al.* **[168]** carried out similar studies on amorphous alumina nanoparticles (AAN) wherein both have observed blue emission. Bright bluish-white emission centered at 430 and 407 nm was also observed by Lin *et al.* **[169]**. They have attributed such visible emission to radical carbonyl defects on the pore surface.

Alumina exists in various polymorphs such as α, χ, η, δ, κ, θ, γ, ρ; which are formed during the thermal treatment although the thermodynamically stable form is α-Al_2O_3. Other crystallographic phases are metastable but can still be obtained under special condition. There are reports for existence of more than 15 other phases for aluminum oxide **[170]**.

Recently Gangwar *et al.* **[171]** have stabilized metastable θ-Al_2O_3 and reported the blue emission on UV excitation. Bilir *et al.* **[172]** have observed broad band white light emission ranging from 450-900 nm from γ-Al_2O_3 nano-powders under 803.5 nm and 975 nm laser diode excitations. Vaidya *et al.* **[173]** besides getting α-Al_2O_3 have also reported a new metastable hexagonal phase μ-Al_2O_3 which transforms to stable hexagonal λ-Al_2O_3 phase in 10 to 12 weeks.

The present work attempts to explain the origin of blue and green emission bands and study the effect of annealing temperature on their intensity. Electron Paramagnetic Resonance (EPR) and photoluminescence spectroscopy (TRES) were used to find out the defects responsible for such visible photoluminescence.

5.2. Experimental

5.2.1. Synthesis

The synthesis was carried out by self-assisted gel combustion process. Aluminum nitrate, $Al(NO_3)_3.9H_2O$ as obtained from the supplier was employed as the starting material without any further purification. Aluminum nitrate required to produce 4 g of Al_2O_3 was calculated and then dissolved in minimum amount of HNO_3. Glycine, NH_2CH_2COOH, was used as the fuel. The amount of fuel is calculated based on the principles of stoichiometric chemistry wherein the net oxidising valency (15-) of the oxidant ($Al(NO_3)_3.9H_2O$ in this case) is equated to net reducing valency (9+) of fuel (glycine). In this study, the amount of glycine required to carry out approximately 40% fuel deficient combustion was determined and weighed. The solution containing Al^{3+} was then slowly evaporated till a viscous gel was obtained. At this point, the temperature of hot plate was suddenly raised to about 200°C which led to auto-ignition and an exothermic self propagating reaction ensued resulting in the voluminous powder. The powders were then calcined at 500°C to remove any carbonaceous impurities and divided into three parts which were annealed at 1200, 1300 and 1450°C, respectively.

5.2.2. Characterisation techniques

The phase purity of the prepared alumina sample was confirmed by powder X-ray diffraction (XRD) using monochromatized Cu Kα radiation on a Panalytical Xpert Pro. Silicon was used as external standard.

Photoluminescence experiments were conducted on an Edinburgh CD-920 unit equipped with 100W μF_2 Xenon flash lamp with variable frequency (10-100 Hz) as the excitation source. The data acquisition and analysis were done by F-900 software provided by Edinburgh Analytical Instruments, UK. Time resolved emission studies (TRES) were carried out on an Edinburgh F-900 unit equipped with M 300 monochromator.

The EPR spectra were recorded on a Bruker ESP-300 spectrometer operating at X-band frequency (9.5 GHz) equipped with 100 kHz field modulation and phase sensitive detection to obtain the first derivative signal. Di phenyl picryl hydrazyl (DPPH) was used for the calibration of g-values of paramagnetic species.

5.3. Results and discussion

5.3.1. Phase purity: XRD studies

Fig.5.1 represents the powder XRD patterns of Al_2O_3 powders obtained after heating at 1200, 1300 and 1450° C. It is known that the crystal system of the α-Al_2O_3 is hexagonal (JCPDS#82-1468). Similar X-ray diffraction patterns were detected for the specimens at different annealing temperatures. The XRD patterns have been indexed on hexagonal α-Al_2O_3 lattice. This implies no phase change for the observed Al_2O_3 powders on further heating to 1450°C. Careful observation exhibits some shift in the Al_2O_3 peaks as well as variation in FWHM (Inset of Fig. 5.1) on raising the annealing temperature. The shift of the XRD peaks on increasing the temperature, however, does not follow a particular trend. The pattern shifts to lower angles upon raising the temperature from 1200 to 1300°C and then again to higher angles upon heating to 1450°C. Also, the FWHM decreases at first and then upon increasing the temperature to 1450 °C, the peaks tend to broaden again which, indeed is a little surprising. It has been reported that the phase transition temperatures in Al_2O_3 depend on powder properties of starting material **[174]** and the phase transitions are continuous rather than sharp. This suggests that even though macroscopically a particular phase was observed, the variation in external factors like temperature might bring out some rearrangements in cationic and anionic sub-lattices **[174]**. These might exist as defects in parent lattice and contribute to irregular variation in FWHM.

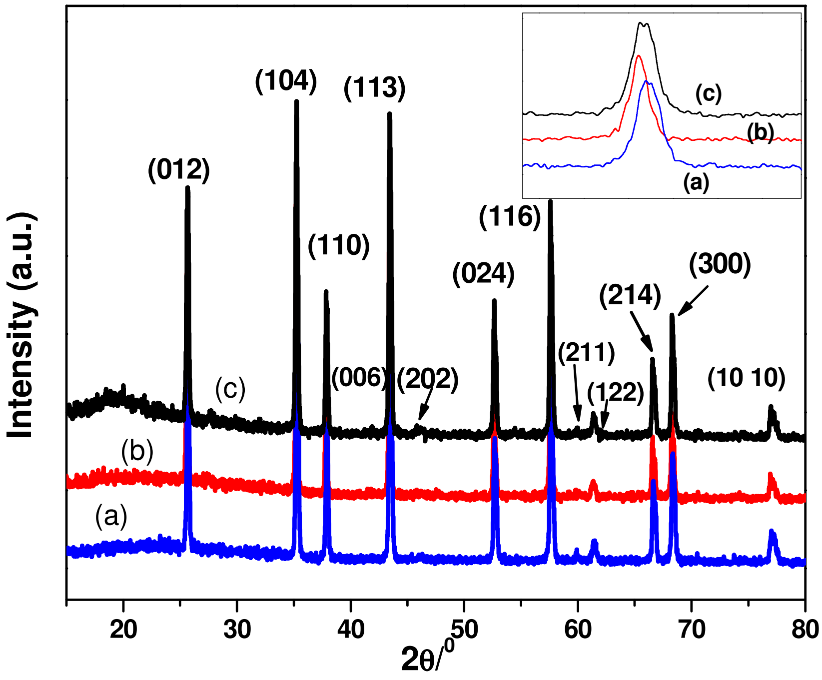

Fig. 5.1 Representative XRD patterns of Al_2O_3 annealed at (a) 1200°C, (b) 1300°C, (c) 1450°C

5.3.2. Photoluminescence

The above mentioned microstructural features make Al_2O_3 an interesting system to investigate by luminescence studies. Fig. 5.2 represents the room temperature PL spectra of as-prepared Al_2O_3 compound annealed at three different temperatures (1200,1300 and 1450°C) under excitation wavelength of 230 nm. Excitation wavelength used for recording the emission spectrum 230 nm (~ 5.39 eV) is less than the experimental band gap of bulk Al_2O_3 (~ 8.8 eV); which is indicative of the fact that certain energy levels are localized within the band gap of alumina because direct relaxation from valence band (VB) to conduction band (CB) would be forbidden in this case. In case of inorganic compounds without any activator ion; intense emissions are observed at room temperature because of local defects that arise during synthesis and thermal treatment or sometimes they are present in material inherently.

Because the existence of defects or color centers, such as oxygen vacancy, can strongly influence the electrical, optical, and thermal properties of α-Al_2O_3, it is of interest to identify such centres. It is reported that in α-Al_2O_3, photoluminescence arises mainly because of oxygen vacancies **[175, 176]**. There can be various kinds of oxygen vacancies, viz, neutral, singly ionized and doubly ionized. They are normally referred as F^+ (an oxygen vacancy occupied by single electron) and *F* (an oxygen vacancy occupied by double electrons) centers. Along with these, it is reported that additional F_2, F_2^+ and F_2^{2+} may also exist in crystalline α-Al_2O_3 phase **[177-179]**. Studies on these defect centres are relatively less because their introduction is difficult compared to F^+ and *F* centers. Interestingly in present samples, along with F-centre (~ 435 nm) there is another defect centre that emits at 520 nm which has been attributed to F_2 centre (two associated oxygen vacancies occupied by four electrons) **[180]**.

The fact that luminescence process in the present case involves Gaussian line broadening mechanism (Fig. 5.2) the emission curves of Al_2O_3 compounds in the present study were deconvoluted. After Gaussian peak fitting, the spectra were observed to exhibit three different color components (P_1, P_2 and P_3) at different wavelengths, at $\lambda_{max} \approx 440$ nm (P_1,blue), $\lambda_{max} \approx 520$ nm (P_2, green) and $\lambda_{max} \approx 570$ nm (P_3, orange-red). Such multicolor emission in visible region is typical of the system where relaxation occurs via various paths and there exists a large number of intermediate levels within the band gap

(Eg) of materials **[181]**. Blue emission (P_1) $\lambda_{max} \approx 440$ nm can be associated to F centers while the green emission at $\lambda_{max} \approx 520$ nm (P2) can be assigned to the F_2 centers. The orange-red emission $\lambda_{max} \approx 570$ nm (P3) can be assigned to F_2^{2+} centers (two associated oxygen vacancies occupied by three electrons) **[182, 183]**. This F_2^{2+} centers consists of two F^+ centers which are paramagnetic.

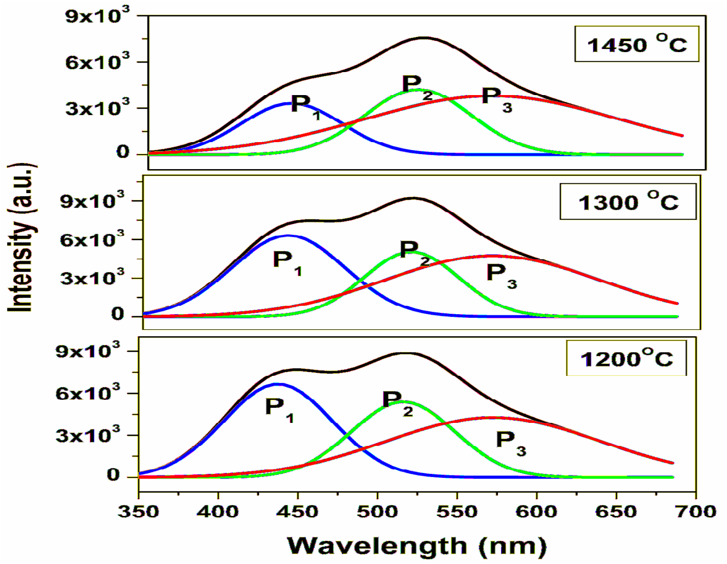

Fig. 5.2 Room temperature emission spectrum of Alumina with $\lambda_{ex} = 230$ nm.

It is obvious from Fig.5.2, that with there is a constant decrease in the P_1's intensity as the annealing temperature is increased. However, a reverse trend is being followed by P_3 peak. This is also manifested in Fig.5.3, which shows the variation in the ratio of peak areas (P_3/P_1 and P_3/P_2), obtained after deconvolution of the respective spectra at different annealing temperatures (as shown in Fig.5.2). This indicates that at higher annealing temperature population of F_2^{2+} centers increases. It would be interesting to observe these variations in EPR spectra at different annealing temperatures which would be discussed later.

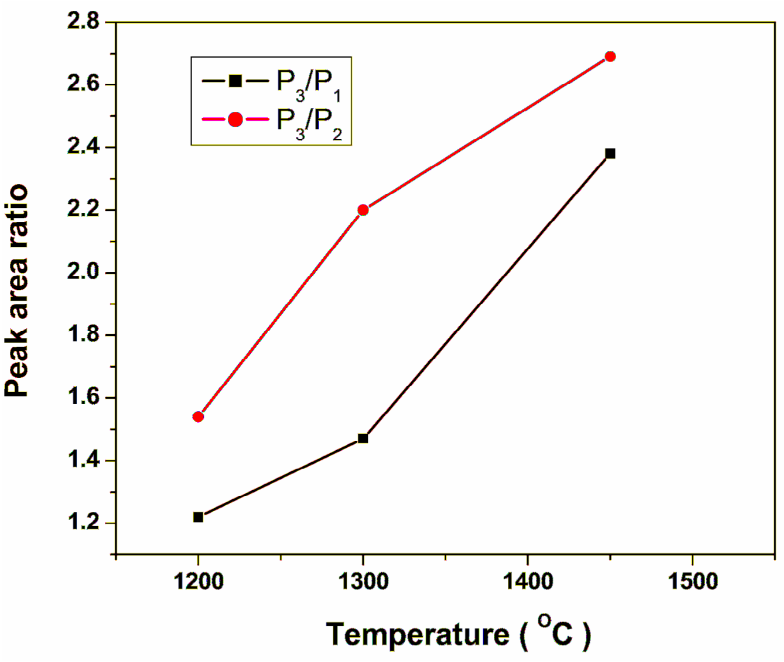

Fig. 5.3 Variation of intensity ratio of peak P_3 to P_1 and P_3 to P_2 with annealing temperature

In order to get further insight into the temperature effect on defect chemistry, time resolved emission studies were performed and PL lifetimes were recorded at various temperatures. The lifetime values are tabulated in Table 5.1. Fig.5.4 shows the luminescence decay profile of the 1200°C annealed Al_2O_3 sample under different emission wavelengths viz., λ_{em} = 440, 520 and 570 nm at an excitation wavelength of λ_{ex} = 230 nm. Since for these bands, there is an overlap with either the previous band or with the next band or by both, hence, instead of a mono-exponential decay, a multiple-exponential behaviour was observed. while monitoring the decay profiles at all the emission wavelengths i.e. at 440, 520 or 570 nm emission. Therefore the life time, which has the maximum contribution among all the lifetimes observed at a particular wavelength, can be assigned to the particular emission maxima (P_1, P_2 or P_3). The decay curves observed at different wavelengths were all found to be multi-exponential and could be fitted to a sum of two or three exponentials.

The decay curves at 440 and 570 nm were fitted using the bi-exponential decay equation 5.1 given by:

$$\mathbf{I\ (t) = A_0 + A_1\,exp\ (-t/\tau_1) + A_2\,exp\ (-t/\tau_2)} \qquad \mathbf{(5.1)}$$

While the decay curve at 520 nm was best fitted using the tri-exponential decay equation 5.2 given by:

$$\mathbf{I\ (t) = A_0 + A_1\,exp\ (-t/\tau_1) + A_2\,exp\ (-t/\tau_2) + A_3\,exp\ (-t/\tau_3)} \qquad \mathbf{(5.2)}$$

where A_0, A_1 and A_2 are scalar quantities obtained from the curve fitting, t is the time, and τ_1 ,τ_2 and τ_3 are decay time values for exponential components. The decay times (τ_1, τ_2 and τ_3) with their percentage contributions at each emission maxima; 440, 520 and 570 nm is given in Table 5.1. The decay time of paramagnetic oxygen vacancies ($\boldsymbol{V_O^{\blacksquare}}$) is reported to be around 10- 20 μs **[184]**. The $\tau_3 \approx 25$ μs at $\lambda_{em} = 570$ nm in present case is therefore attributed to paramagnetic singly ionized oxygen vacancies ($\boldsymbol{V_O^{\blacksquare}}$) or F_2^{2+} center which is nothing but a pair of F^+ centres. The longer τ_1 and τ_2 life time values compared to τ_3 value of F^+ center, can be attributed to the forbidden transition of the F center. The electronic structure of the F center can be treated as a helium atom where the ground-state configuration $(ls)^2$ corresponds to the term $^1S_0$. Excited states can be generated by promoting one electron into a 2s or a 2p state, resulting excited-state configurations 1s 2s or 1s 2p. These configurations correspond to both singlet and triplet states (^1S, ^3S, ^1P, and ^3P). The emission of F centre is due to ^3P -^1S transition which is forbidden and hence the lifetime is long **[185]**. The lower value of τ_2 in comparison to τ_1 can be explained in terms of self quenching of F_2 centres. These three different lifetimes values i.e. τ_1, τ_2 and τ_3 observed at respective emission wavelengths, recorded at different annealing temperatures are included in Table 5.2. From Table 5.2 it is clear that the percentage of contribution of τ_1 decreases at higher annealing temperature whereas those of $\tau 2$ and $\tau 3$ increase. This supports our observed emission data as shown in Fig. 5.3.

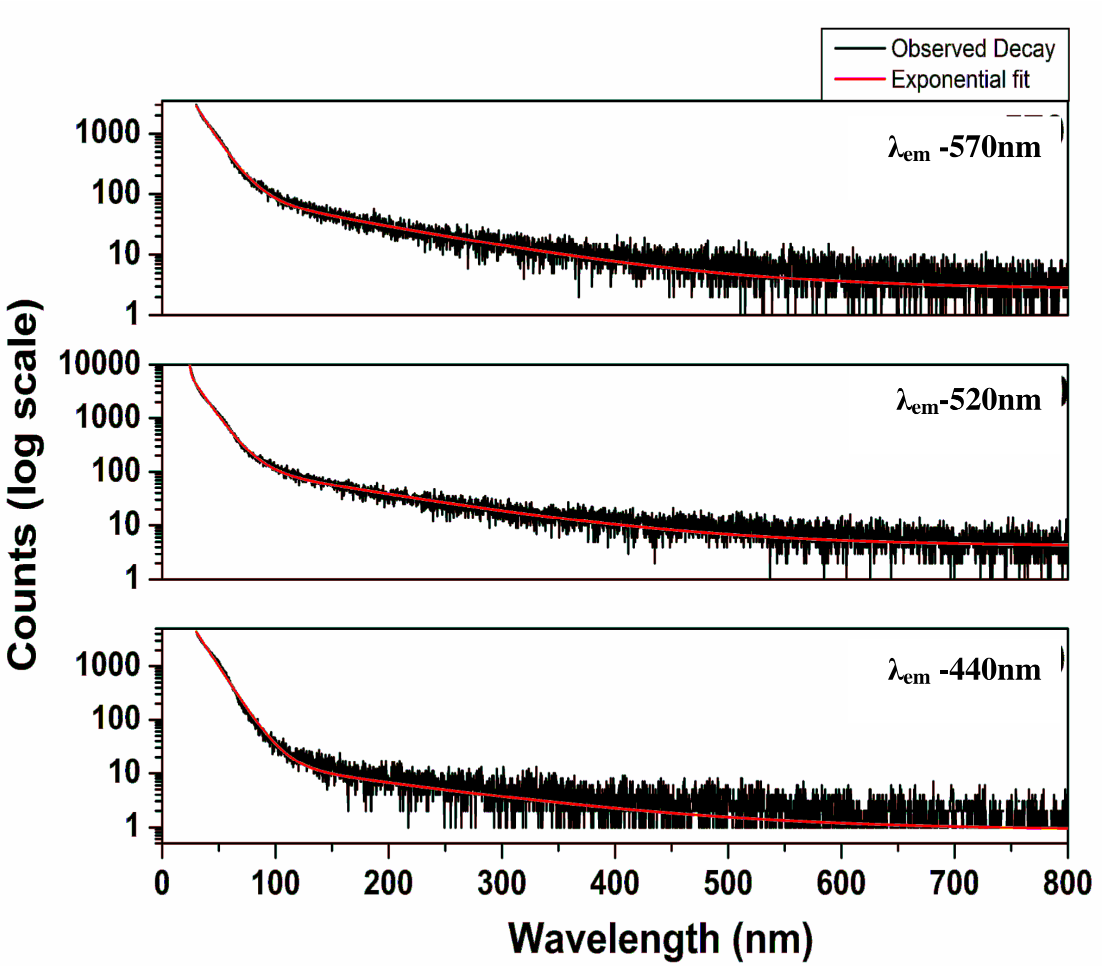

Fig. 5.4 PL decay profile of Al_2O_3 sample at different emission maxima

Table 5.1 Lifetime Values of Al_2O_3 (1200°c) at different emission wavelengths

λ_{em} (nm)	τ_1 (μs)	τ_2 (μs)	τ_3 (μs)	χ^2
440	172 (84 %)	153 (16 %)	-	1.11
520	171 (11 %)	150 (68%)	27 (21 %)	1.19
570	-	151 (27 %)	25 (73 %)	1.23

Table 5.2 Lifetime Values of Al_2O_3 at different annealing temperatures

T_{ann}	τ_1 (μs) (at λ_{em} = 440 nm)	τ_2 (μs) (at λ_{em} = 520 nm)	τ_3 (μs) (at λ_{em} = 570 nm)	χ^2
1200	172 (84 %)	150 (68 %)	25 (73 %)	1.11
1300	173 (73 %)	146 (71%)	27 (76 %)	1.19
1450	172 (66 %)	145 (77 %)	25 (83 %)	1.23

5.3.3. EPR study

Fig.5.5 shows the EPR spectra of Al_2O_3 after annealing at different temperatures. All the compounds showed an asymmetric signal at $g \approx 2.023$. Since Al^{3+} cations do not contribute to EPR due to absence of any unpaired electron, these strong intense resonance signals must be due to some type of intrinsic defects, such as oxygen vacancies. Oxygen vacancies can exist in different possible states as represented by Kroger–Vink notation. Firstly, the doubly positively charged vacancies without any trapped electron, which are assigned as $\boldsymbol{V_O^{2+}}$ or $V_O^{\cdot\cdot}$ (or F^{2+} center) and are diamagnetic, since no unpaired electron is left there. Therefore F^{2+} centers are not observed by EPR technique. Secondly the singly positively charged vacancies with one trapped electron, which are assigned as $\boldsymbol{V_O^X}$ or $V_O^{\cdot}$ (or F^+ center). They are paramagnetic and hence EPR sensitive. This defect center is same like F^+ center in alkali halides and is formed when the F^{2+} centers traps an electron from the conduction band. These F^+ centers may also exist as an aggregate such as F_2^{2+} which is nothing but consists of two F^+ centers. Hence they are also paramagnetic. Finally the singly charged centers ($\boldsymbol{V_O^{\blacksquare}}$) may become a neutral centre by capture of another electron forming the neutral F or $\boldsymbol{V_O^X}$ center. However, it must be noted that the introduction of the F^{2+} or F^{+} center must be accompanied by simultaneous introduction of some negatively charged centers such as negatively-charged cationic vacancies V_{Al}'''. These F^{2+} center can trap one or two electrons from nearest negatively-charged cationic vacancies (V_{Al}''') leading to the formation of F^{+} (oxygen vacancies occupied by one electron) and F centers (oxygen vacancies occupied by two electrons). If the spin of two trapped electrons in F or $\boldsymbol{V_O^X}$ center somehow compensates each other, the F center will be a diamagnetic one, and if they do not, the existence of a triplet state may be expected, which is EPR active and will show two fine transitions. In the present case, only one fine transition is observed in all Al_2O_3 samples annealed at different temperatures, which suggests that the resonance signal must be due to paramagnetic F^{+} or F_2^{2+} centers. From Fig.5.5, it is also clear that, there is an increasing trend of EPR signal intensity as the annealing temperature increased. Since our PL data does not reveal the presence of F^{+} centers, which show emission at lower wavelength with $\lambda_{max} \approx 330$ nm this resonance signal cannot be attributed to the single F^{+} centers. However as PL spectra show emission of paramagnetic F_2^{2+} centers with $\lambda_{max} \approx 570$ nm and the intensity trend with annealing temperature is matching with that of EPR spectra, the resonance signal at $g \approx 2.023$ can be assigned to the F_2^{2+} centers (which are infact F^{+} centers in aggregate form).

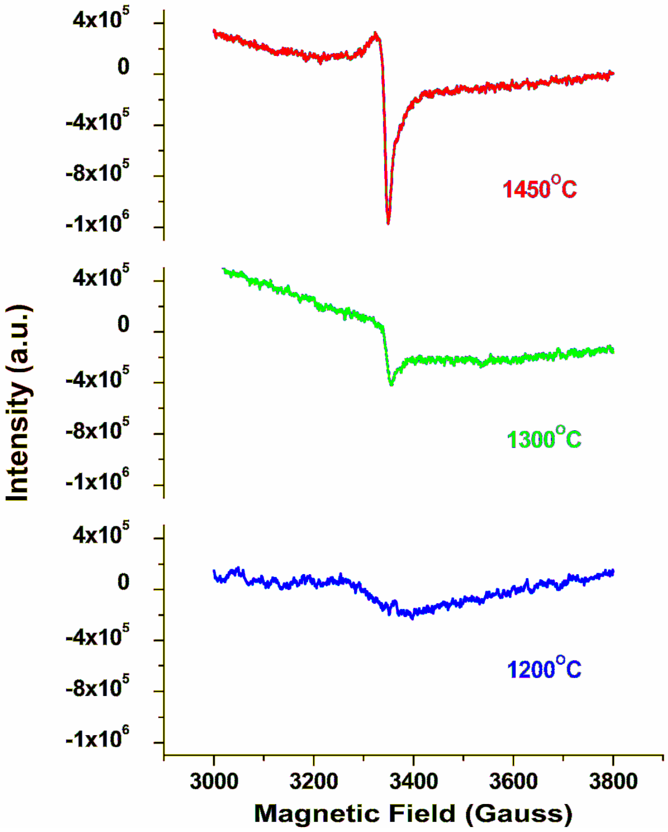

Fig.5.5 The EPR spectra for the Al_2O_3 samples as a function of annealing temperatures

It would be interesting to find a possible explanation for the observed trend of F_2^{2+} centers shown by both PL and EPR data recorded on Al_2O_3 samples treated at different annealing temperatures. There could be thermal ionization of the F_2 and F centers as follow:

$$F_2 + \Delta \leftrightarrow F_2^{2+} + 2e^-$$

$$F + \Delta \leftrightarrow F^+ + e^-$$

$$F^+ + F^+ \leftrightarrow F_2^{2+}$$

The second probability is that at very high temperature there may occur distortion around the AlO_6 octahedra followed by formation of oxygen vacancy around Al-octahedra. Kim et al. **[186]** have reported emission of red band in $ZnGa_2O_4$, which was attributed to paramagnetic single oxygen vacancies (V_O°) associated with the distorted octahedral [O_h] sites as confirmed by EPR spectroscopy **[187]**.

α-Al_2O_3, the most stable phase of alumina, known as corundum, has a rhombohedral structure in which Al^{3+} ions occupy 2/3 of the octahedral interstitial sites in hexagonal closed packed sub-lattice formed by the oxygen ions. It should be noted that in the corundum structure only octahedral Al atoms are present. The δ structure is tetragonal and can be considered as a spinel super structure built by piling up three spinel units, the Al^{3+} ions occupying (13+1/3) out of the 16 octahedral sites and all the eight tetrahedral sites of the conventional spinel structure. θ-alumina has a monoclinic structure which is isomorphic to β-Ga_2O_3 with the oxygen atom distribution close to a FCC lattice and the cations distributed in equal number on octahedral and tetrahedral sites. The structure of δ-alumina is close to that of γ-Alumina. Recently Boumaza *et al.* **[187]** have investigated phase transition of alumina under different heat treatment. They have shown that as the annealing temperature increases from 1123 K to 1323K, there is a phase transformation from $\gamma \rightarrow \delta \rightarrow \theta$. Finally, for samples prepared at higher temperature 1573K, α-Al_2O_3 is formed. Therefore, the transformation of θ into α-alumina phase is associated with the migration of ions in both sub-lattices. There will also be a modification of sub-lattice of oxygen ion from an FCC lattice structure to a hexagonal one, and the tetrahedral Al^{3+} ions will vanish and transform to only AlO_6 octahedral units. It may be noted that γ, δ and θ-Al_2O_3 phases are thermodynamically metastable. Hence, tetrahedral Al^{3+} ions in the θ phase will eventually be converted into α-alumina phase as the temperature in increased to 1573 K, and co-ordination around Al^{3+} ions will be ≤ 6. Hence the Al atoms which are placed at the octahedral sites in α-Al_2O_3 will not have perfectly octahedral symmetry, or in other words some of them will have distorted octahedral symmetry as the co-ordination of Al will be ≤ 6. This concludes that some oxygen vacancy will always be associated with the Al^{3+} ions at O_h sites in the temperature range 1000-1500 K unless and until the entire Al atoms in α-Al_2O_3 will have perfectly octahedral symmetry.

Therefore as the annealing temperature is increased from 1200°C to 1450°C, the percentage of Al atom having distorted octahedral co-ordination will also be increased which is manifested in the increase in intensity of resonance signal at $g \approx 2.023$ in the EPR spectra, since the oxygen vacancy associated with the octahedral Al atom will trap one electron and form F^+ center. At higher annealing temperature these F^+ centers may form aggregate such as F_2^{2+}, which is manifested as the increase in intensity of the P_3 peak in the PL spectra.

5.4 Conclusions

The Al_2O_3 nanopowders were synthesized by a fuel-deficient gel combustion synthesis employing glycine as a fuel and were annealed at different temperatures with the aim of introducing different defect nature/concentration and their effect on luminescence. Powder XRD studies revealed the crystallization of α-Al_2O_3 at all the three temperatures investigated. The emission spectra of all the three samples showed broad bands albeit with different shapes which on deconvolution yielded three components. This indicated the presence of three types of defects which were also characterised by time resolved emission studies. The lifetimes of different traps have been correlated to the transitions involved. This work contributes to understanding of nature of the defects occurring in Al_2O_3 as the manifestation of variation in annealing temperatures.

Chapter 6

Summary and the future scope of the work

6.1 Exploring the use of carbon doped magnesium aluminate ($MgAl_2O_4$:C) as a phosphor for radiation dosimetry

The successful application of dosimeters in various areas have helped the active development of thermoluminescence dosimetry and optically stimulated luminescence. It has been mainly employed in the area of personnel monitoring, environmental monitoring, retrospective dosimetry and radiation therapy. Studies on the properties of materials which are already being used as TL detectors have helped in the development of new materials with same or improved properties for the successful application in TL dosimetry **[8]**. However the requirements are very stringent for commercial TL/OSL dosimeters. α-Al_2O_3 has become an important material for radiation dosimetry due to its relatively low effective atomic number, excellent chemical as well as thermal stability. Doping carbon in reducing environment has enhanced its radiation sensitivity significantly. The F and F^+ centres have been found responsible for the sensitivity enhancement which are formed due to oxygen vacancies produced during carbon doping.

Like alumina, $MgAl_2O_4$ possesses a rare combination of valuable properties such as high strength at elevated and normal temperatures, thermal shock resistance, high chemical inertness **[76]**. The un-doped $MgAl_2O_4$ synthesized by gel combustion method was not TL/OSL sensitive. However, its TL study had shown the prospects of existence of high temperature deeper traps. But, carbon doping in $MgAl_2O_4$ under reducing atmosphere could bring a significant increase in TL/OSL intensity. The carbon doping has been achieved in two ways. First was done by using electron gun and then by heating in graphite furnace. Both the carbon doped samples show the TL glow peak position at almost similar temperatures with similar TL sensitivity. However, observed TL sensitivity in electron gun sample is more and the TL glow peaks are relatively better resolved in graphite furnace sample. The TL peak observed for both is a combination of various peaks. The TL glow curve parameters were resolved using a computerized curve de-convolution analysis (CCDA) for all TL peaks **[98]**. In terms of integral TL area under the peak, fourth TL glow peak is more prominent. The other TL peaks are relatively less intense. The thermal trapped depths also showed a wide variation. The TL peaks at lower temperatures are having lower half lives, hence these TL peaks are expected to show post irradiation fading. However, the TL peaks at higher temperature are having longer half-lives and thermally stable at room temperature during post irradiation storage. Thus, these peaks can be used as stable TL dosimetric peaks for radiation dosimetric applications.

The defect centres (mainly vacancy-related defects) introduced by carbon doping were characterised using photoluminescence spectroscopy and EPR spectroscopy. Observed photoluminescence (PL) spectra showed common PL peak energy at 460 nm (2.7 eV). This strongly suggests that the photoexcitation of the F and F^+ centers eventually results in the same radiative relaxation channel. The intensity of photoluminescence is substantially reduced when these samples are post-annealed in air at 1200 ^{o}C for 15 h. This leads to the assumption that oxygen vacancies are responsible for the 460 nm (2.7 eV) PL band. X-ray diffraction studies of both types of carbon doped and un-dopped $MgAl_2O_4$ have not shown any significant difference. For understanding the difference in carbon concentration profile as a function of depth (from surface) in these two types of samples techniques like electron energy loss spectroscopy (EELS) **[188]** or focused ion beam can be used. Accordingly the heating temperature and duration of doping can be optimised for both the techniques and dosimetric TL/ OSL defects in $MgAl_2O_4$:C can be engineered. The present study establish that $MgAl_2O_4$:C is superior to Al_2O_3:C in terms of dynamic range of dose linearity. Al_2O_3:C shows dose linearity only upto 10Gy where as $MgAl_2O_4$:C showing dose linearity upto 100Gy. This interesting result opens up the possibility of developing a new dosimeter based on $MgAl_2O_4$:C for a wide range of radiation doses. Therefore, there exists a great scope of further studies and after optimising the synthesis parameters of carbon doping in $MgAl_2O_4$, it can be made suitable for various fields of radiation dosimetry. These studies will be undertaken.

6.2. Defect-induced blue emission on $MgAl_2O_4$:C

It can be seen from the emission spectra that doping carbon by electron gun method does not lead to substantial changes in the emission characteristics compared to undoped sample. The emission spectra of the graphite furnace-heated sample showed much enhanced intensity with a blue shift in the emission band. Blue light emitting phosphors are important because blue LED is used to excite the fluorescent material in a bulb that converts the blue light to white light. The observations of blue emission from $MgAl_2O_4$:C is an important result and research has to be done for further development on blue-emitting phosphors based on $MgAl_2O_4$ spinel. There is a need to develop suitable methods for coating $MgAl_2O_4$:C on appropriate substrates.

6.3. Effect of thermal treatment on combustion synthesized α-Al_2O_3

Most of the luminescent materials used worldwide are activated using lanthanide ions. As the cost and toxicity associated with rare-earth doping is high, lots of research have been initiated to synthesise of luminescencent materials without any rare-earth doping.

In the present work Al_2O_3 was synthesised by self-assisted gel combustion synthesis followed by annealing at different temperatures. The alumina samples heated at different temperature exhibited qualitatively similar broad luminescence spectra. Deconvolution yielded different emissions with a systematic trend in intensity with annealing temperature and it could be assigned to defect centres such as F, F_2 and F_2^{2+} centres. The nature of defects generated due to synthesis and differential temperature treatment has been investigated using photoluminescence and EPR spectroscopy. The work also holds significance in context of exploring rare-earth free luminescent materials. There is a need to further process Al_2O_3 into suitable flexible composites with polymers. This work will also be undertaken separately as it was out of scope of present thesis.

References

References

1. O. Annalakshmi, *PhD Thesis*, HBNI, 2013.
2. L. B. Jensen*, PhD Thesis*, University of Copenhagen, 1999.
3. M. J. Aitken, *Academic Press.*1985, 3.
4. M. S. Kulkarni, *BARC Newsletter,* 2009, 2, issue no 308.
5. S.W.S. McKeever, M. Moscovitch, P. D. Townsend, *Thermoluminescence dosimetry materials: properties and uses,* Nuclear Technology Pubications, 1995 (Book).
6. B. Pajot, B. Clerjaud, *Optical absorption of impurities and defects in semiconducting crystals,* 2013 (Book), Springer Publications.
7. R. A. Johnson, A. N. Orla, *Physics of radiation effects in crystals*, 1986 (Book), Elsevier science publications.
8. E. I. Grigoriev, L. I. Trakhtenberg, *Radiation- Chemical processes in solid phase theory and application,* 1996 (Book), CRC press.
9. L. B. Jensen, Risu, *Radiat. Meas.,* 1997, 749-768.
10. P. Szuromi, D. Clery*, Science,* 1998, 281, 939.
11. V. Kortov, *Radiat. Meas.,* 2007, 42, 576-581.
12. M. S. Akselrod, V. S. Kortov, D. J. Kravetsky, Gotlib, *Radiat. Prot.Dosim.* 1990, 33, 119-122.
13. L. Trinkler, A. J. J. Bos, P, Winkelman, N. Christiansen, N. Agersnap Larsen, B. Berzinia, *Radiat.Prot. Dosim.*, 1999, 84, 207-210.
14. P. D. Townsend, C. D. Clark, P. W. Levy, *Phys.Rev*, 1967, 155, 908
15. T. Nakajima, Y. Maruyama, T. Matsuzawa, A. Koyano, *Nucl.Instum.Meth.*, 1978, 157, 155- 162.

16. R. J. Ginther, R. G. Kirk, *Report of Progress (7th edition), U.S. Naval Research Laboratory,* 1956*,* p. 12.
17. M. Topaksu, A.N. Yazici, Nucl Instrum Methods Phys. Res. B 2007, 264(2), 293-301.
18. K. P. Muthe, *PhD Thesis*, Mumbai University, April, 2012.
19. H. O. Albrecht, C. E. Mandeville, *Phys Rev.,* 1956, 101, 1250-1251.
20. P. Braunlich, D. Schafer, A. Scharmann, *Stanford: Proc International Conf on Lum Dosim*, *USAEC*; 1967, 57-73.
21. E. N. Sanborn, E. L. Beard, *Stanford: Proc International Conf on Lum Dosim, USAEC,* 1967, 183-191.
22. D. J. Huntley, D. L. Smith, M. L. Thewalt, *Nature,* 1985, 313, 105-107.
23. B. G. Markey, L. E. Colyott, S. W. Mckeever, *Radiat Meas.*, 1995, 24, 457-463.
24. C. R. Rhyner, W. G. Miller, *Health Phys*, 1970, 18, 681-684.
25. E. Tochlin, N. Goldstein, W. G. Miller, *Health Phys*, 1969, 16, 1-7.
26. R. Bernhardt, L.Herforth, *Proc 4th Int Conf Lum Dsim;* 1974, 1091-104.
27. A. S. Pradhan, K. Ayyangar, *Int J Appl. Radiat. Isoptopes,* 1977, 28, 534-535.
28. A. S. Pradhan, R. C. Bhatt, *Phys. Stat. Solid,* 1981, 68, 405-411.
29. A. S. Pradhan, B. Chandra, R. C. Bhatt, *Radiat. Prot. Dosim*, 1983, 5, 159-162.
30. L. Oster, S. Druzhyna, Y. S. Horowitz, Phys. Res.A., 2011, 648, 261-265.
31. M. S. Akselrod, N. Agersnap Larsen, V. H. Whitley, S. W. S. McKeever, *J. Appl. Phys.,* 1998, 84, 3364–3373.
32. L. Bøtter-Jensen, K. J. Thomsen, M. Jain, *Radiat. Meas*., 2010. 45, 253- 257.
33. C. A. Perks, G. Le Roy, B. Prugnaud, *Radiat. Prot. Dosim*., 2007, 125, 220-223.
34. D. Zhou, E. Semones, R. Gaza,S. Johnson., N. Zapp, M. Weyland, R. Rutledge, T. Lin, *Acta Astronaut*. 2009, 64, 437-447.

35. T. Berger,S. Burmeister, J. Labrenz, P. Bilski, T. Horwacik, A.Twardak, M. Hajek, J. K. Palfalvi, J. Szabo, I. Ambrozova, F. Vanhavere, V. Cauwels, R. Gaza, E. G. Yukuhara, E. R. ,Benton, Y. ,Uchihori, S. Kodarira, S. Kitamura, M. Boehme, G. Reitz, *Long term dose monitoring on board the European Columbus Laboratory off International space station in the year 2009-2013.,*2014.
36. D. Lovelock, S. Lim, T. LoSasson, *Med. Phys*., 2012, 39, 3604.
37. L. B. Jensen, S. W. McKeever, A. G. Wintle, *Elsevier Science: BV Publication*, 2003.
38. E. Aguirre, A. Spector, J. Hoe, I. T. Russell, M. Knapp, R. T. Woods, M. Orrell, *Trials.* 2010, 11, 46.
39. S. Y. Lee, K. J. Lee, *Appl Radiat Isotopes*., 2001, 54, 675-685.
40. E. G. Yukihara, G. O. Sawakuchi, S. Guduru, S. W. McKeever, R. Gaza, E. R. Benton, et al. *Radiat. Meas*, 2006, 41, 1126-1135.
41. L. B. Jensen, *Development of Optically Stimulated Luminescence Techniques using Natural Minerals and Ceramics, and their Application to Retrospective Dosimetry.* Risø-R-1211(EN), 1999.
42. E. G. Yukihara, S. W. McKeever, S. Mark, M. S.Akselrod, *Radiation Meas.,* 2014, 71, 15-24.
43. P. A. Jursinic, *Med. Phys.,* 2007, 34(2) 4594-4604.
44. A. S. Pradhan, J. I. Lee, J. L. Kim, *J Med Phys* 2008, 33, 85-99.
45. A. Akselrod, S. W. Mckeever, *Radiat. Prot. Dosim*, 1999, 81, 167-175.
46. E. Bulur, *Radiat. Meas.,* 1996, 26, 701-709.
47. K. J. Thomsen, L. B. Ztter-Jensen, M. Jain, P. M. Denby, A. S. Murray, *Radiat. Meas*., 2008, 43, 414 – 421.

48. E. Bulur, H. Y.Goeksu, *Radiat. Meas.,* 1998, 29, 639-650.

49. L. E. Colyott, S. W. Mckeever, M. S. Akselrod, *Radiat. Prot. Dosim*, 1999, 85, 309-312.

50. S. D. Miller, G. W. Endres, J. C. McDonal, K. L. Swinth, *Radiat. Prot. Dosim*, 1988, 25, 201-206.

51. A. S. Pradhan, *Radiat. Prot. Dosim*, 1989, 29, 213-215.

52. A. S. Pradhan, P. K. Dash Sharma, V. K. Shirva, *Radiat. Prot. Dosim*, 1996, 64, 227-231.

53. M. S. Kulkarni, D. R. Mishra, K. P. Muthe, A. Singh, M. Roy, S. K. Gupta et al. *Radiat Meas.,* 2005, 39, 277-282.

54. K. P. Muthe, M. S. Kulkarni, N. S. Rawat, D. R. Mishra, B. C. Bhatt, A. Singh et al. *J. Lumin.* 2008, 128, 445-450.

55. C. X. Zhang, Q. Tang, L. B. Bin, D. L. Luo, *Radiat. Prot. Dosim*, 2006, 119, 402-407.

56. B. C. Bhatt, P. S. Page, N. S. Rawat, D. R. Mishra, M. S. Kulkarni, *Netherlands: 15th SSD Conference Delft University*, 2007, 19, 2-09.

57. W. G. West, K. J. Kearfott, S. M. Bernal, *Radiat. Prot. Dosim*, 2006, 119, 344-349.

58. A. E. Akselrod, M. S. Akselrod, *Radiat. Prot. Dosim.*, 2002, 100, 271-220.

59. E. G. Yukihara, S. W. McKeever, *Radiat. Prot. Dosim*, 2006, 120, 354-357.

60. E. G. Yukihara, R. Gaza, S. W. McKeever, C. G. Soares, *Radiat. Meas.,* 2004, 38, 59-70.

61. G. Busuoli, L. Lembo, R. Nanni, I. Sermenghi. *Radiat. Prot. Dosim.,* 1983, 6, 317-320.

62. P. Gill, *Electrical power equipment maintenance and testing, second edition*, 2008 (Book), CRC Press.
63. J. C. Mittani, M. Prokic, E. G. Yukihara, *Radiat. Meas.*, 2008, 43, 323-326.
64. A. J. Bos, M. Prokic, J. C. Brouwer, *Radiat. Prot. Dosim*, 2006, 119, 130-133.
65. J. C. Mittani, M. Prokic, E. G. Yukihara, *Radiat. Measurement,* 2008, 43, 323-326.
66. N. M. Masson, A. J. Bos, C. W. V. Eijk, C. Furetta, J. P. Chaminade, *Radiat. Prot. Dosim.*, 2002, 100, 229-234.
67. N. M. Masson, A. J. Bos, A. J. Winkelman, C. W. V. Eijk, *IEE Trans. Nucl. Sc.,* 2001, 48, 1143-1147.
68. C. Dotzler, G. V. Williams, U. Rieser, A. Edgar, *Appl. Phys. Lett.,* 2007, 91, 121910.
69. N. M. Masson, A. J. Bos, Z. Czapla, J. C. Brouwer, C. W. V. Eijk, *Radiat Prot. Dosim.,* 2004, 110, 319-323.
70. Y. Douguchi, H. Nanto, T. Sato, A. Imai, S. Nasu, E. Kusano, et al., *Radiat. Prot. Dosim.,* 1999, 84, 143-147.
71. J. E. Geusic, H. M. Marcos, L. G. V. Uitert, *Appl. Phys. Lett.*, 1964, 4, 182.
72. M. S. Kulkarni, K. P. Muthe, N. S. Rawat, D. R. Mishra, M. B. Kakade, S. Ramanathan, S. K. Gupta, B. C. Bhatt, J. V. Yakhmi, D. N. Sharma, *Radiat. Measurements*, 2008, 43, 492-496.
73. E. H. Haskell, *Radiat Prot Dosim.*1993, 47, 297–303.
74. J. I. Lee, J. L. Kim, A. S. Pradhan, B. H. Kim, J. S. Kim, *Transactions of the Korean Nuclear society spring meeting*, Gyeongju, Korea, 2008.
75. R. Ianos, R. Lazou, *Mater. Chem. Phys.,* 2009, 115, 645-648.

76. E. Alagu Raja, S. N. Menon, B. Dhabekar, N. S. Rawat, T. K. Gundu Rao*, J. Lumin,* 2009, 129, 829-835.

77. A. Ibarra, F. J. Lopez, M. Jimenez de Castro, Phy. Rev. B 1991, 44, 7256.

78. S. S. Manoharan, K. C. Patil, *J. Amer. Ceram. Soc.*, 1992, 75, 1012.

79. J. J. Kingsley, L. R. Pederson, *Mater. Lett.*1993, 18, 89.

80. Y. Zhang, G. C. Stangle, *J. Mater. Res.*1994, 9, 1997.

81. S. Bhaduri, S. B. Bhaduri, E. Zhou, *J. Mater. Res.*,1998, 13, 156.

82. L.A. Chick, L.R. P. ederson, G.D. Maupin, J.L. Bates, L.E. Thomas, G.J. Exarhos, *Mater. Lett.*1990, 10, 6-12.

83. S. R. Jain, K. C. Adiga, V. R. P.Verneker, *Combust. Flame.* 1981, 40, 71-79

84. C. Păcurariua, I. Lazăua, Z. Ecsedia, R. Lazăua, P. Barvinschib, G. Mărgineanc, *J. Eur. Ceram.*, 2007, 27, 707-710.

85. J. G. Li , T. Ikegami, J. H. Lee, T. Mori, Y. Yajima, *J. Eur. Ceram.*, 2001, 21, 139-148.

86. V. Grover, *PhD Thesis*, Mumbai University, 2006.

87. K. H. Lee, J. H. Crawford, *Appl. Phys. Lett.*, 1978, 33, 273.

88. L. E. Colyott, M. S. Akselrod, S. W. S. McKeever, *Radiat. Prot. Dosim., 1996,* 65, 263-266.

89. X. B. Yang, H. J. Li, Q. Y. Bi, Y. Cheng, Q. Tang, J. Xu, *J. Appl. Phys.*, 2008, 104, 123112.

90. K. P. Muthe, S. K. Gupta, J. V. Yakhmi, M. S. Kulkarni, D. R. Mishra, N. S. Rawat, D. N. Sharma, *Homibhabha centenary year, BARC News letter*, 2009, *3,* issue no 308.

91. P. Ratna, P. Chaudhury, N. P. Gaikwad, D. N. Sharma, *J. Med. Phys.*, 2006, 31, 200.

92. M. S. Kulkarni, A. Soni, N. S. Rawat, D. R. Mishra, D. N. Sharma, *Proc. of the National Conference On Luminescence and its Applications, CGCRI, Kolkata*, 2009, O88-O99.

93. S.K. Gupta, *PhD Thesis,* HBNI, November, 2014.

94. G. P. Summers, G. S. White, K. H. Lee, J. H. Crawford, Jr., *Phys. Rev. B*, 1980, 21, 2578.

95. A. Ibarra, D. Bravo, F. J. Lopez, F. A. Garner, *J. Nucl. Mater.* 2005, 336, 156-162.

96. M. S. Akselrod, V. S. Kortov, D. J. Kravetsky, V. I. Gotlib, *Radiat. Prot. Dosim.,* 1990, 32, 15-20.

97. V. S. Kortov, I. I. Milman, V. I. Kirpa, J. Lesz, *Radiat. Prot. Dosim.*, 1994, 55 (4), 279- 283.

98. X. Yang, J. Xu, H. Li, H. Tang, Q. Bi, Y. Cheng, Q. Tang, *J. Phys. D: Appl. Phys.,* 2009, 42, 145411.

99. B. Dhabekar, S. N. Menon, E. A. Raja, A. K. Bakshi, A. K. Singh, M. P. Chougaonkar,Y. S. Mayya, *Nucl. Instrum. Method. Phys. Res. B*, 2011, 269, 1844-1848.

100. B. C. Bhatt, A. Soni, G. S. Polymeris, D. K. Koul, D. K. Patel, S. K. Gupta, D. R. Mishra, M. S. Kulkarni. *Radiat. Meas.*, 2014, 64, 35-45.

101. E. M. Yoshimura, E. G. Yukihara, *Radiat. Meas.*, 2006, 41, 163-169.

102. J. E. Sheehan, J. Sigalovsty, J. S. Haggerdy, J. R. Porter, *Ceram. Eng. Sci. Proc.*, 1993, 14, 660-670.

103. G. Baudim, R. Martinez, P. Pene, *J. Am. Ceram. Soc.*, 2009, 78 (7), 1857-1862.

104. H. S. Tripathi, B. Mukherjee, S. Das, M. K. Haldar, S. K. Das, A. Ghosh. *Int. Ceram.,* 2003, 29, 915-918.

105. V. Paris, S. Hayan, M. P. Dariel, N. Frange, E. Zaretsky, *AIP conference proceedings,* 2009, 1195, 1003-1006.

106. D. Mohapatra, D. Sarkar., *J. Mater. Sci.,* 2007, 42, 7286-7293.

107. C. Kinoshita, H. Abe, S. Maeda, K. Fukumoto, *J. Nucl. Materi*, 1995, 219, 152-160.

108. V. T. Gritsyna, Y. G. Kazarinov, V. A. Kobyakov, I. E. Reimanis, *Nul. Inst. Method in Physics Research B*, 2006, 250, 342-348.

109. V. T. Gritsyna, I. V. A. Charkin, Y. G. Kazarinov, K. E. Sickafus, *Nul. Inst. Method in Physics Research B*, 2004, 218, 264-270.

110. T. Kim , H. Kang , J. Woo, K. Chung, H. Choe, H. Jang , C. Whang, *J. Korean hysical Society,* 1999, 34(4), 385-389.

111. R. Chen, Y. Kirish, *Analysis of Thermally Stimulated Processes,* 1981(Book), Oxford: Pergamon Press.

112. G. Kitis, J. M. Gomez-Ros, J. W. N. Tuyn, *J. Phys. D: Appl. Phys.* 1998, 31, 2636-2641.

113. D. Afouxenidis, G. S. Polymeris, N. C. Tsirliganis, G. Kitis, *Radiat. Prot. Dosim.*, 2011, 149, 363-370.

114. H. G. Balian, N. W. Eddy, *Nucl. Instrum. Methods,* 1977, 145, 389-395.

115. D. R. Mishra, A. Soni, N. S. Rawat, M. S. Kulkarni, B. C. Bhatt, D. N. Sharma, *Radiat. Meas.,* 2011, 46, 635-642.

116. R. Cook, M. Kochis, I. Reimanis, H. J. Kleebe, Proc. SPIE 5786, *Window and Dome Technologies and Materials IX*, 41, June 22, 2005.

117. P. J. Hing, *J. Mater. Sci.*, 1976, 11, 1919-1926.

118. J. A. Wollmershauser, B. N. Feigelson, S. B. Qadri, G. R. Villalobos, M. Hunt, M. A. Imam, *Scr. Mater.* 2013, 69, 334-337.

119. K. Morita, B. N. Kim, K. Hiraga, H. Yoshida, *Scr. Mater.*, 2008, 58, 1114-1117.

120. C. Baudin, R. Martinez, P. Jena, *J. Am. Ceram. Soc.*, 1995, 78, 1857-1862.

121. M. Y. Nassar, I. S. Ahmad, I. Samir, *Spectrochim. Acta A*, 2015, 131, 329-334.

122. M. J. Iqbal, B. Ismail, C. Rentenberger, H. Ipser, *Mater. Res. Bull.*, 2011, 46, 2271-2277.

123. T. Shiono, K. Shiono, K. Miyamoto, G. Pezzotti, *J. Am. Ceram. Soc*, 2000, 83, 235-237.

124. M. Krishnan, B. Tiwari, S. Seema, N. Kalra, P. Biswas, K. Rajeswari, M. B. Suresh, R. Johnson, N. M. Gokhale, S. R. Iyer, S. Londhe, V. Arora, R. P. Tripathi, *J. Mat. Sci: Mat. Med.*, 2014, 25, 2591-2599.

125. Y. Yang, C. Zhang, Y. Song, J. Gou, L. Zhang, Y. Meng, H. Zhang, Y. Ma, *Nucl. Instrum. Methods Phys. Res., Sect. B*, 2014, 326, 260-263.

126. I. Reimanis, H. J. Kleebe, *J. Am., Ceram. Soc.*, 2009, 92, 1472-1480.

127. Y. M. Chiang, D. P. Birnie, W. D. Kingery, *Physical Ceramics: Principles for Ceramic Science and Engineering,* Wiley, New York, NY, 1996.

128. S. K. Gupta, P. S. Ghosh, A. Arya, V. Natarajan, *RSC Advances*, 2014, 4, 51244-51255.

129. S. K. Gupta, N. Pathak, M. Sahu, V. Natarajan, *Adv. Powder Technol.*, 2014, 25, 1388-1393.

130. S. K. Gupta, P. Ghosh, N. Pathak, A. Arya, V. Natarajan, *RSC Advances,* 2014, 4, 29202-29215.

131. S. W. S. McKeever, *Nucl. Instrum. Methods Phys. Res., Sect. B*, 2001, 184, 29-54.

132. E.G. Yukihara, S. W. S. McKeever, *J. Appl. Phys.,* 2006, 100, 083512.

133. T. Uchino, D. Okutsu, *Phys. Rev. Lett.,* 2008, 101, 117401.

134. T. Uchino, D. Okutsu, R. Katayama, S. Sawai, *Phys. Rev. B.*, 2009, 79, 165107

135. Y. Uenaka, T. Uchino*, Phys. Rev. B.*, 2011, 83, 195108.

136. P. K. Bandyopadhyay, G. P. Summers, *Phys. Rev. B.,* 1985, 31, 2422-2426.

137. L. S. Cain, G. J. Pogatshnik, Y. Chen, *Phys. Rev. B.,* 1988, 37, 2645.

138. K. E. Sickafus, J. M. Wills, N. W. Grimes, *J. Am. Ceram. Soc.* 1999, 82, 3279-3292.

139. S. A. T. Redfern, R. J. Harrison, H. St. C. O'Neill, D. R. R. Wood, *Am. Mineral.* 1999, 84, 299-310.

140. B. P. Uberuaga, D. Bacorisen, R. Smith, J. A. Ball, R. W. Grimes, *Phys. Rev. B*, 2007, 75, 104116.

141. J. R. Albani, *Principles and applications of flurescence spectroscopy*, 2007 (book), Blackwell Publishing Company.

142. G. P. Summers, G. S. White, K. H. Lee, J. H. Crawford, Jr., *Phys. Rev. B*, 1980, 21, 2578.

143. M. S. Minsky, S. Watanabe, N. Yamada, *J. Appl. Phys.*, 2002, 91, 5176-5181.

144. T. Onuma, S. F. Chichibu, A. Uedono, T. Sota, P. Cantu, T. Katona, J. F. Keading, S. Keller, U. K. Mishra, S. Nakamura, S. P. DenBaars, *J. Appl. Phys.* 2004, 95, 2495-2504.

145. B. Gallez, R. Swartz, *Biomed. 2*004, 17, 223–225.

146. A. L. Barra, L. C. Brune, J. B. Robert, *Chem. Phys. Lett.*1990; 165, 107–109.

147. G. Schreckenbach, T. Ziegler,. *J. Phys. Chem. A.* 1997, 101, 3388–3399.

148. *CIE Technical report*, CIE 15, 2004 3rd Edition

149. Z. W. Sherin, R. Cheu, P. Tan, G. Kortemeyer, *Am. J. Phys.,* 2016, 84, 369.

150. *Ionic Liquids Today,* Issue 2-11, 2011, 19th September.

151. S. K. Gupta, V. Grover, R. Shukla, K. Srinivasu, V. Natarajan, A. K. Tyagi, *Chem. Eng. J.,* 2016, 283, 114-126.

152. S. K. Gupta, S. Nigam, A. K. Yadav, M. Mohapatra, S. N. Jha, C. Majumder, D. Bhattacharyya, *New J. Chem.*, 2015, 39, 6531-6539.

153. S. K. Gupta, R. M. Kadam, V. Natarajan, S. V. Godbole *Mater. Sci. Engg. B*, 2014, 183, 6-11.

154. M. K. Ekmecki, M. Erdem, A. S. Basak, *Dalton Trans.*, 2015, 44, 5379-5385.

155. L. Sun, Y. Qiu, T. Liu, H. Zhang, L. Shi, *ACS Appl. Mater. Interfaces.*, 2013, 5, 9585-9593.

156. S. K. Gupta, M. Sahu, P. S. Ghosh, D. Tyagi, M. K. Saxena, R. M. Kadam, *Dalton Trans.*, 2015, 44, 18957.

157. C. Shivakumara, R. Saraf, S. Behera, N. Dhananjaya, H. Nagabhushana, *Mater. Res. Bull.*, 2015, 6, 422-432.

158. S. K. Gupta, M. Sahu, K. Krishnan, M. K. Saxena, V. Natarajan, S. V. Godbole, *J. Mater. Chem. C*, 2013, 1, 7054-7063.

159. S. Angelov, R. Stoyanova, R. Dafinova, K. Kabasanov, *J. Phys. Chem. Solids*, 1986, 47, 409-412.

160. W. H. Green, K. P. Le, J. Grey, T. T. Au, M. J. Sailor, *Science*, 1997, 276, 1826-1828.

161. J. K. Salem, I. M. El-Nahhal, T. M. Hammad, S. Kuhn, S. A. Sharekh, M. El-Askalani, R. Hempelmann, *Chem. Phys. Lett.*, 2015, 636, 26-30.

162. H. Zeng, X. Ning, X. Li, *Phys. Chem. Chem. Phys.*, 2015, 17, 19637-19642.

163. D. Manoharan, A. Loganathan, V. Kurupati, V. J. Nesamony, *Ultrason. Sonochem.*, 2015, 23,174-184.

164. M. M. Khan, S. A. Ansari, D. Pradhan, D. H. Han, J. Lee, M. H. Cho, *Ind. Eng. Chem. Res.,* 2014, 53, 9754-9763.

165. K. Davis, *European Union. J.*, 2010, 2, 109-114.

166. Y. Du, W. L. Cai, C. M. Mo, J. Chen, D. Zhang, X. G. Zhu, *Appl. Phys. Lett*., 1999, 74, 2951.

167. J. H. Chen, C. P. Huang, C. G. Chao, T. M. Chen, *Appl. Phys. A: Mater. Sci. Process*, 2006, 84, 297-300.

168. W. J. Zhang, X. L. Wu, J. Y. Fan, G. S. Huang, T. Qiu, P. K. Chu, *J. Phys.: Condens. Matter*, 2006, 18, 9937-9942.

169. C. K. Lin, M. Yu, Z. Y. Cheng, C. M. Zhang, Q. G. Meng, J. Lin, *Inorg. Chem*., 2008, 47, 49-55.

170. J. M. Andersson, *PhD Thesis*, Dissertation No-987, Linkoping University, Sweden.

171. J. Gangwar, B. K. Gupta, P. Kumar, S. K. Tripathi, A. K. Srivastava, *Dalton Trans*. 2015, 43, 17034-17043.

172. G. Bilir, J. Liguori, *J. Lumin*. 2014, 153, 350-355.

173. S. N. Vaidya, C. Karunakaran, S. N. Achary, A. K. Tyagi, *High Pressure Res*., 1999, 16, 265-278.

174. I. Levin, D. Brandon, *J. Am. Ceram. Soc.* 1998, 81, 1995-2012.

175. K. H. Lee, J. H. Crawford, *Phys. Rev. B*, 1977, 15, 4065-4070.

176. B. G. Draeger, G. P. Summers, *Phys. Rev. B,* 1979, 19, 1172-1177

177. M. J. Springs, J. A. Valbis, *Phys. Stat. Sol. B*., 1984, 123, 335-343.

178. L. S. Welch, A. E. Hughes, G. P. Pells, *J. Phys. C,* 1980, 13, 1805-1816.

179. B. D. Evans, M. Stapelbroek, *Solid State Comm*., 1980, 33, 765-770.

180. M. Itou, A. Fujiwara, T. Uchino, *J. Phys. Chem. C*, 2009, 113, 20949-20957.

181. V. M. Longo, L. S. Cavalcante, A. T. De Figueiredo, L. P. S. Santos, E. Longo, J. A. Varela, J. R. Sambrano, A. C. Hernandes, *Appl. Phys. Lett.,* 2007, 90, 091906.

182. S. Ikeda, T. Uchino, *J. Phys. Chem. C*, 2014, 118, 4346-4353.

183. B. D. Evans, *J. Nucl. Mater*. 1995, 219, 202-223.

184. N. Pathak, S. K. Gupta, P. S. Ghosh, A. Arya, V. Natarajan, R. M. Kadam, *RSC Adv. 2015,* 5, 17501-17513.

185. K. H. Lee, J. H. Crawford, *Phys. Rev. B,* 1979, 19, 3217.

186. J. S. Kim, H. I. Kang, W. N. Kim, J. I. Kim, J. C. Choi, H. L. Park, *Appl. Phys. Lett*., 2003, 82, 2029-2031.

187. A. Boumaza, L. Favaro, J. Ledion, G. Sattonnay, J.B. Brubach, P. Berthet, A. M. Huntz, P.Roy, R. Tetot , *J. Solid State Chem*. 2009, 182, 1171-1176.

188. H. Mullejans, J. Bruley. *J. Phys. Colloq*, 1993, 03, 2083-2092.